Università degli Studi di Napoli Federico II

FACOLTÀ DI INGEGNERIA AEROSPAZIALE
Corso di Laurea Magistrale in Ingegneria Aerospaziale

Tesi di Laurea Magistrale

Development of a Vortex Lattice Method for Unsteady Potential Flows with Free Wake

Candidato:
Guido Lazzerini
Matricola M53000614

Relatori:
Dr. Kiran Ramesh
Prof.-Dr. Carlo de Nicola
Dr. Paolo Caccavale

Anno Accademico 2018-2019

CONTENTS

INTRODUCTION 1

1 THEORETICAL BACKGROUND 7
1.1 Principles of Aerodynamics . . . 7
1.2 Reference Frames . . . 8
1.3 Forces Acting on a Lifting Surface . . . 9
1.4 Derivation of the Laplace Equation . . . 10
1.5 Basic Solutions and Singularity Elements . . . 21
1.6 Vortons Formulation . . . 26
1.7 Kutta's Condition . . . 27
1.8 The Bernoulli Equation . . . 28
1.9 Panel Methods . . . 30
1.10 Extension to Unsteady Incompressible Potential Flow . 39
1.11 Aerodynamic Loads . . . 42

2 DEVELOPMENT AND IMPLEMENTATION 47
2.1 Development . . . 48
2.1.1 Steady Vortex Lattice Method . . . 49
2.1.2 Unsteady Vortex Lattice Method . . . 59
2.2 Unsteady Method Implementation . . . 73
2.2.1 Airfoil Geometry . . . 75
2.2.2 Wing Geometry . . . 78
2.2.3 Kinematics Input . . . 80
2.2.4 Discretization and Vortex Lattice Creation . . . 81
2.2.5 Simulation Settings . . . 83
2.2.6 Aerodynamic Influence Matrix . . . 83
2.2.7 Time Stepping Procedure . . . 83
2.2.8 Vortons Wake Model Implementation . . . 85

3 VALIDATION AND RESULTS 87
3.1 Lift coefficient and Polars . . . 87
3.2 Taper Ratio Effect on Loads . . . 93
3.3 Sweep Angle Effect on Loads . . . 95
3.4 Curvature of Camber-Line Effect on Loads . . . 97
3.5 Sudden Acceleration . . . 98
3.6 Convergence of Steady-State Values . . . 101
3.7 Steady-State Values . . . 101
3.8 Periodic Motion . . . 103
3.9 Results for Vortons Wake Model and Comparison . . . 107
3.10 Conclusions . . . 112
3.11 Future Developments . . . 112

A APPENDIX A : INPUT FILES FORMATS 113
A.1 Airfoil Geometry Input File 113
A.2 Wing Geometry Input File 114

BIBLIOGRAPHY 115

LIST OF FIGURES

Figure 1 Physical-Mathematical aerodynamic models hierarchy . . . 3
Figure 2 An example of a conventional and an unconventional architecture aircraft. . . . 8
Figure 3 Wind and Body reference frames (Reproduced from [13]) . . . 9
Figure 4 Logical Balance Equation . . . 15
Figure 5 The two different specifications of a flow field 17
Figure 6 Quadrilater doublet and its vortex-ring equivalent (Reproduced from [9]) . . . 23
Figure 7 Vortex line segment (Reproduced from [9]) . . 25
Figure 8 Vortex ring (Reproduced from [9]) . . . 25
Figure 9 Domain for Green's third identity formulation 31
Figure 10 Lifting surface modelled by a single vortex line (Reproduced from [9]) . . . 37
Figure 11 Example of discretization of a wing and a wake model (Reproduced from [9]) . . . 38
Figure 12 Choice of reference frames for an unsteady motion (Reproduced from [9]) . . . 40
Figure 13 Example of the application of Kutta's condition in an unsteady vortex lattice method (Reproduced from [9]) . . . 42
Figure 14 Steady and unsteady vortex lattice methods overview 48
Figure 15 Image of the right-hand side of a symmetric wing model (Reproduced from [9] with modifications) . . . 49
Figure 16 Example of a vortex-ring (Reproduced from [9] with modifications) . . . 51
Figure 17 Example of trailing vortex segments (Reproduced from [9]) . . . 52
Figure 18 Definition of the vortex-ring normal . . . 53
Figure 19 Right-hand side semi-wing vortex-rings arrangement . . . 54
Figure 20 Collocation points scanning procedure (Reproduced from [9]) . . . 55
Figure 21 Kutta's condition for the steady wake model (Reproduced from [9] with modifications) . . . 57
Figure 22 Unsteady vortex-lattice method scheme for the first two time-steps (Reproduced from [9]) . . 60
Figure 23 Linear and angular velocities vectors in the IRF and BRF . . . 61

Figure 24 Sequence of the Euler angles rotations from X, Y, Z to x, y, z (Reproduced from [13] with modifications) 63
Figure 25 Right-hand side semi-wing vortex-rings arrangement for UVLM 66
Figure 26 Example of wake shedding (Reproduced from [9] with modifications) 67
Figure 27 Simplified algorithm of UVLM 74
Figure 28 NACA 2412 airfoil geometry (*Matlab*) 76
Figure 29 Boeing BACXXX airfoil geometry (*Matlab*) . . 77
Figure 30 Wing geometry (*Matlab*) 79
Figure 31 Example of Kinematics time histories (*Matlab*) 80
Figure 32 Panelling on the wing of fig.30 with LE zoom (*Matlab*) 81
Figure 33 Vortex lattice on the wing of fig.30 with $M = 8$ and $N_i = 1$ for each segment (*Matlab*) 82
Figure 34 Rotation of the normals due to the curvature of NACA 2412 airfoil (*Matlab*) 82
Figure 35 Wing and wake panels' chords 84
Figure 36 Scheme for vortex-rings to vortons conversion 86
Figure 37 $C_L - \alpha$ curves generated by the VLM for $\mathcal{R}$ = 4, $\mathcal{R}$ = 8, $\mathcal{R}$ = 16 and comparison with lifting line theory results (*Matlab*) 88
Figure 38 $C_L - \alpha$ curves generated by the VLM for $\mathcal{R}$ = 32, $\mathcal{R}$ = 64, $\mathcal{R}$ = 128 and comparison with lifting line theory results (*Matlab*) 89
Figure 39 C_{L_α} - $\mathcal{R}$ curves and comparison with lifting line theory results (*Matlab*) 90
Figure 40 $C_L - C_{D_i}$ curves generated by the VLM for $\mathcal{R}$ = 4, $\mathcal{R}$ = 8, $\mathcal{R}$ = 16 and comparison with lifting line theory results (*Matlab*) 91
Figure 41 $C_L - C_{D_i}$ curves generated by the VLM for $\mathcal{R}$ = 32, $\mathcal{R}$ = 64, $\mathcal{R}$ = 128 and comparison with lifting line theory results (*Matlab*) 92
Figure 42 Wing properties and discretization (*Matlab*) . . 93
Figure 43 Loads distribution generated by the VLM for $\mathcal{R}$ = 7.28, $\lambda = 0.4$, $M = 4$ $N = 40$, and comparison with [9] (*Matlab*) 94
Figure 44 Wing properties and discretization ($\Lambda = +45°$) (*Matlab*) 95
Figure 45 Loads distribution generated by the VLM for $\mathcal{R}$ = 4, $M = 4$ $N = 20$, and comparison with [9] (*Matlab*) 96
Figure 46 Loads distribution generated by the VLM and comparison with *Xfoil* (*Matlab*) 97

Figure 47 Sudden acceleration kinematics zoomed in the range $[0, 1]\,\tau$ (*Matlab*) 99
Figure 48 Lift coefficient generated by the UVLM for a sudden acceleration, and comparison with [9] (*Matlab*) 99
Figure 49 3-D view of a rectangular wing with $\mathcal{R} = 4$ undergoing sudden acceleration (*Matlab*) . . . 100
Figure 50 Drag coefficient generated by the UVLM for a sudden acceleration, and comparison with [9] (*Matlab*) 100
Figure 51 Convergence of lift and drag coefficients generated by the UVLM for a sudden acceleration, and comparison with results of lifting-line theory's results (*Matlab*) 102
Figure 52 Steady-state values of lift and drag coefficients generated by the UVLM, and comparison with results of lifting-line theory's results (*Matlab*) . 102
Figure 53 $C_L - 2\pi\frac{t}{T}$ curves generated by the UVLM for a periodic motion with **k = 0.25**, and comparison with results of Theodorsen theory's results (*Matlab*) 104
Figure 54 $C_L - h$ curve generated by the UVLM for a periodic motion with **k = 0.25**, and comparison with results of Theodorsen theory's results (*Matlab*) 104
Figure 55 $C_L - 2\pi\frac{t}{T}$ curves generated by the UVLM for a periodic motion with **k = 0.50**, and comparison with results of Theodorsen theory's results (*Matlab*) 105
Figure 56 $C_L - h$ generated by the UVLM for a periodic motion with **k = 0.50**, and comparison with results of Theodorsen theory's results (*Matlab*) . 105
Figure 57 $C_L - 2\pi\frac{t}{T}$ curves generated by the UVLM for a periodic motion with **k = 0.75**, and comparison with results of Theodorsen theory's results (*Matlab*) 106
Figure 58 $C_L - h$ curve generated by the UVLM for a periodic motion with **k = 0.75**, and comparison with results of Theodorsen theory's results (*Matlab*) 106
Figure 59 3-D view of a rectangular wing with $\mathcal{R} = 4$ undergoing sudden acceleration, vortons wake model (*Matlab*) 108

Figure 60 Lift coefficient generated by the UVLM for a sudden acceleration, and comparison with [9] (*Matlab*) 109
Figure 61 Drag coefficient generated by the UVLM for a sudden acceleration, and comparison with [9] (*Matlab*) 110
Figure 62 $C_L - 2\pi\frac{t}{T}$ curves generated by the UVLM for a periodic motion, and comparison with results of Theodorsen theory's results (*Matlab*) 111

INTRODUCTION

OUTLINE

The thesis has been divided into 3 chapters :

1. The first chapter includes the theoretical background underneath the unsteady vortex lattice method.

2. The second chapter shows the development of an unsteady vortex lattice method in MATLAB scripting environment.

3. The third chapter consists of the validation and peculiar results for steady and unsteady motion, general geometries with respect to analytical solutions and other numerical solutions.

MOTIVATION

During some phases of aerodynamic design the necessity of a fast and reliable determination of properties of lifting surfaces via numerical methods (Computational Fluid Dynamics) makes potential flow numerical methods (e. g.panel methods) more advisable than time-consuming complete Navier-Stokes equations solvers (e. g.finite difference method, finite volume method), though it can be stated that potential model represents the lowest level on a hierarchy of approximations of Navier-Stokes equations.
Anyway the potential flow is often a close condition to the design point of many aerodynamic bodies [17].

Panel methods discretize body's surfaces into panels composed by field singularities (vortices, doublets and sources) and solve a boundary integral equation through linear algebraic systems, thus they lead to the calculation of velocity and pressure on surfaces allowing to save time from computing those quantities in the entire fluid volume [9].
The vortex lattice method is a panel method in which the singularities chosen to substitute the lifting surfaces and the wake are vortices and their velocity inductions is computed via Biot-Savart law.

OVERVIEW

The aim of this work is to investigate the capabilities of a newly developed vortex lattice method based on vortices sheets and vortex particles (vortons) in unsteady potential flows. This method can be employed for preliminary design and optimization of lifting surfaces in steady or unsteady conditions, such as in HALE (High-Altitude Long-Endurance) aircraft.

Indeed high aspect ratio aircraft are capable of longer and more efficient flights due to the benefits on induced drag and lift but they are also likely to suffer fluid-structure interaction and unsteady aerodynamics phenomena because longer wings increase flexibility.

The wing is modeled by placing vortex rings on the non-planar surface. Variations in twist angle and airfoil shape is taken into account by rotation of the normal vector of the panels.
An unlimited number of wing's segments can be modeled, each segment is defined by 6 parameters : span length, taper ratio, sweep angle, dihedral angle, root twist angle and tip twist angle.

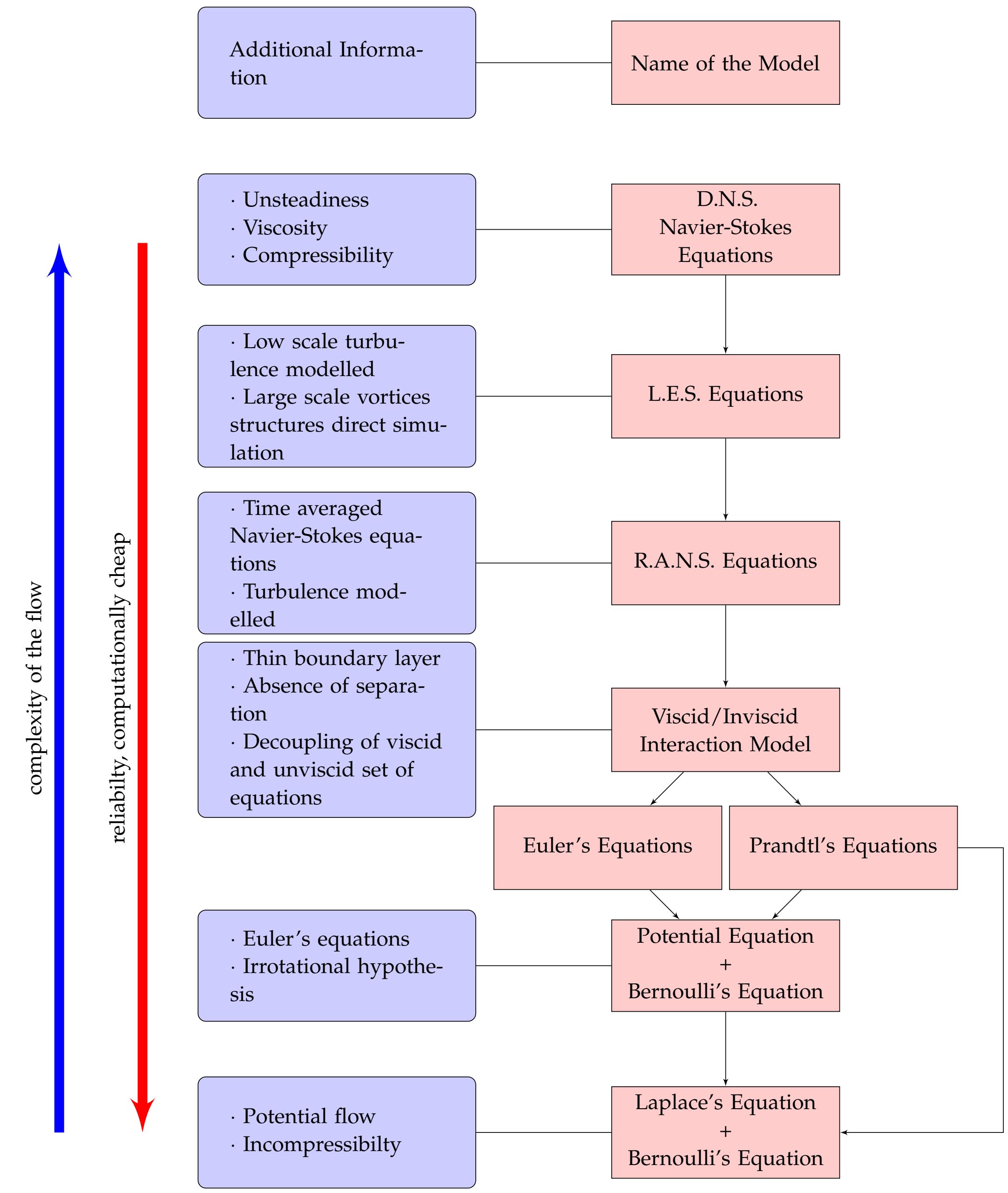

Figure 1: Physical-Mathematical aerodynamic models hierarchy

LITERATURE REVIEW

A short review of the literature consulted is here reported to show vortex lattice methods development and applications in history.

As said before, potential flow field, namely incompressible, irrotational, inviscid flow is governed by the continuity equation in the form of the Laplace equation in terms of the velocity potential Φ :

$$\nabla^2\Phi = 0 \tag{1}$$

This linear, elliptic, partial differential equation must be associated with boundary conditions on the domain of interest (typically flow tangency for impermeable bodies and velocity disturbance vanishing at infinity) and a condition which closes the circulation problem, being generally more complex to express.
Solutions of this boundary-value problems may come both from an analytical method for specific geometries (e.g. conformal transformations, Prandtl's theory) or a numerical approximated solution (e.g. panel methods).
Analytical methods to solve potential flows have been widely developed during the 20^{th} century for 2D and 3D geometries, and they represent the beginning of every rational lifting surface's analysis, thus they are described in detail in every textbook [9], [2], [17].

As mentioned before, analytical solutions of potential flows have been found for a limited number of geometries, thus approximated numerical solutions have always been of primary interest for aeronautical (and nautical) engineering applications [9], [2], [17].

The vortex lattice method is the natural extension to 3D geometries of the properties of flat plate's $\frac{3}{4}$ chord point, analysed by E.Pistolesi more than a century ago [17].

One of the first applications of steady vortex lattice method to computers was developed in FORTRAN programming language by R. J. Margason and J. E. Lamar at NASA in the year 1971 [19].
A huge collection of vortex lattice method's early literature has been made by NASA during a conference about vortex lattice method utilization in 1976 [16]. In that conference the state-of-art of vortex lattice method was established and future developments were presented.
The aim of many studies was to extend the vortex lattice method to unsteady motion, which required to take account of time-evolving wake structures and update of boundary condition in time domain. For example P.Konstandinopoulos [10] developed an unsteady vortex lattice method which showed good agreement in force and moments evaluation and so did A.Sakurai [1] who focused his study on vortex

properties such as de-singularised cores.
Nonetheless the interest of these authors for vortices shedding in steady motion and wake evolution was lift up by slender wings which couldn't be modelled by existing steady methods.

Vortices structures properties were deeply analysed by G. S. Winckelmans and A. Leonard in their studies which also gave a mathematical-oriented point of view of the implementation and utilization of vortex particles singularities in fluid-dynamic tools [5].

Since then, the possibilities coming from increasing computer processing capabilities has lead many research institutions and universities to develop their own vortex lattice methods and to add features to those already existing.
Among the others, TORNADO, created by T.Melin [14], has been one of the first open-source vortex lattice methods implemented in MATLAB.

Recent interest in flapping flight and high-aspect ratio's flexible wings lead to unsteady applications of vortex lattice methods.
L.N. Long and T.E. Fritz used object-oriented programming accounting for general motion and very complex lifting surfaces geometries to model birds' flapping flight [12].

Another approach to the wake model is to replace the vortex-rings made by vortex-filaments with discrete vorticity particles or vortons, giving the chance to extend this method to a multi-body panel method (in fact vortons don't suffer from intersection with body panels) and decreasing significantly the time of simulations. The formulation of this method, both theoretically and numerically was developed by [5] while [3], [11] and [4] emplyed the vortons wake model in the unsteady vortex-lattice method. These methods showed very good agreement between calculations and experimental data, demonstrating the capabilities of unsteady vortex lattice methods with vortons in the wake model as fast and reliable aerodynamic tools.

Furthermore unsteady vortex lattice methods are largely employed nowadays, especially in those aeroelastic frameworks which require time-domain aerodynamic analyses, such as those developed by C. de Souza, J. Murua, R. J. Simpson, H. Hesse and J. A. Geoghegan, [23], [15], [22], [7], [6].

Current research is directed towards investigating vortices structures shedding at the leading edge in low Reynolds flows which have been demonstrated to behave in a very similar fashion to vortices shedding at the trailing edge and thus modelled in unsteady vortex lattice methods (both 2D and 3D) [4], [20], [18], [8].

1

THEORETICAL BACKGROUND

The derivation of numerical aerodynamic methods has been successfully achieved through ages of analytical and experimental studies and the help of an increasing computational power has amplified their possibilities.
Without the basic theoretical concepts of aerodynamics and its peculiar theories the utilization of a numerical method to accomplish tasks like evaluating lift and drag would be impossible.

Aerodynamics is the branch of physics that deals with the interactions between bodies and air in relative motion, and as a consequence of it, the generation of forces and moments. It is a sub-field of fluid dynamics, which more generally includes interactions between bodies and different kinds of fluid.

This chapter follows the main steps towards the solution of the unsteady, potential, incompressible flow field and the derivation of the numerical method called unsteady vortex lattice method.

1.1 PRINCIPLES OF AERODYNAMICS

When a body and air are in relative motion, forces and moments are generated on the surfaces of the body, namely the aerodynamic force and aerodynamic moment.
These forces and moments depend upon flight conditions, such as height, flight speed, and body attitude w.r.t velocity vector and on body configuration, its actual geometry [17].

The aim of aerodynamic studies is to evaluate aerodynamic forces and moments in every phase of a flight mission of an aircraft.

If we restrict our analysis to flying bodies heavier than air, called aerodynes, we can generally assume a common shape made of a fuselage, containing loads, the lifting surface or wing, generating the aerodynamic force essential to fly, stability and control surfaces, which let the pilot steer the aircraft and keep it stable and engines, which pro-

pel the aircraft.
By the way, aircraft shape is affected by state-of-art technology and sometimes the geometry is unconventional, such as the "flying wings" in which the fuselage and the wing are integrated.

(a) Dassault Falcon 2000

(b) Northrop B2 Spirit

Figure 2: An example of a conventional and an unconventional architecture aircraft.

We are interested in evaulating the aerodynamic force and moment, thus we need to specify a cartesian reference frame in which these quantities can be more easily calculated and have peculiar meanings.

1.2 REFERENCE FRAMES

The body reference frame (BRF) is fixed to the aircraft, centered in its mass center, with the x axis along the fuselage, the y axis in the lateral direction, and z upward.

The wind reference frame (WRF) is fixed to the aircraft, centered in its mass center but the axis lays on the direction of the undisturbed relative velocity vector $\underline{V}_\infty$, the z axis is the intersection between the vertical plane that contains $\underline{V}_\infty$ and the orthogonal plane to velocity vector passing through the mass center (G) , and the y axis complete the orthogonal triad.

The attitude of the aircraft in terms of the BRF with respect to the WRF determines its aerodynamic behaviour; two angles give the attitude of the BRF, the angle of attack α and the side-slip angle β. The angle of attack is the angle between x_w and its projection onto the BRF plane (x_b - y_b) while the side-slip angle is the angle between x_w and its projection onto the BRF plane (x_b - z_b) as shown in fig. 3.

1.3 FORCES ACTING ON A LIFTING SURFACE

Thus we define the lift (L), the drag (D), and side force (Y) as the projection of the aerodynamic force respectively onto the z_w, x_w, y_w axes of the WRF.
In the simplest but effective model of an aircraft as a mass point, it is immediately clear that lift is what counteracts weight (W) and possibly pushes the aircraft up, but drag must be overcome to go forward, so the necessity of engines which produce thrust (T).

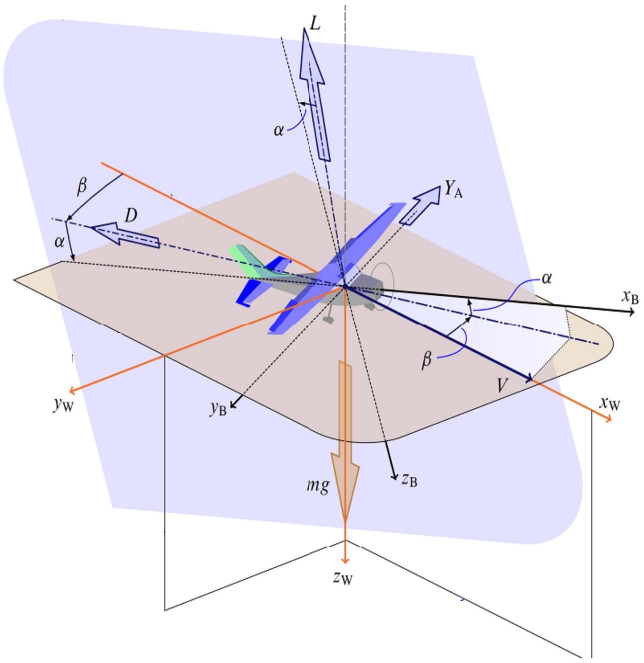

Figure 3: Wind and Body reference frames (Reproduced from [13])

The nondimensionalization of lift and drag in terms of lift and drag coefficient is

$$C_L = \frac{L}{\frac{1}{2}\rho_\infty V_\infty^2 S} \tag{2}$$

$$C_D = \frac{D}{\frac{1}{2}\rho_\infty V_\infty^2 S} \tag{3}$$

where ρ_∞ is the freestream dynamic pressure, V_∞ is the freestream velocity and S is the chosen reference surface.

As regards the wide and complex discipline of aerodynamic design, it is necessary to calculate a big amount of data describing the aerodynamic effects generated by interaction between a body and air in relative motion.
Some of these data can be nondimensional and have a simple formulation, such as those global coefficients which depends on independent variables, others are more complex and distributed over surfaces,

such as thermodynamic quantities, and they require a lot of effort in calculation.

1.4 DERIVATION OF THE LAPLACE EQUATION

This section describes the derivation of the Laplace equation through the application of the balance equations.
As many others analytical models, the system derived from Laplace's equation is well-suited for a limited number of physical phenomena and it should be integrated with more complex analyses to get a full knowledge of the actual flow field (e. g. boundary layer equations for the viscous phenomena).

Fluids properties

It is now necessary to introduce the basic properties of fluids before presenting the formulation of the equations which model fluid-dynamic phenomena.
Fluids are substances which cannot react to shear stress, or similarly have zero shear modulus.
When a force is applied tangential to a fluid, the fluid will start to flow, with a velocity depending on its viscosity.
We conclude that there must be a relationship between the tangential force (shear force) applied and the velocity of deformation of the fluid.

Viscosity

Viscosity is the property of fluids which relates the shear stress to the velocity of deformation, and it can be seen as the aptitude of fluid layers to flow on each other and/or onto a solid surface. It is ineherently related to the chemical composition of the fluid and its temperature.
For Newtonian fluids the relationship between shear stress on a unit area and velocity of deformation is [21]

$$\tau = \mu \frac{\partial u_x}{\partial y} \tag{4}$$

where $\tau\left[N/m^2\right]$ is the shear stress, $\mu\,[kg/m\ s]$ is the viscosity coefficient and $\dfrac{\partial u_x}{\partial y}$ is the rate of change of x velocity of deformation along y direction.

This formula models the one-dimensional motion with variation of velocity along the perpendicular direction.

Taking into account all the 3-dimensional velocities and their derivatives, the dissipative stress tensor is obtained as follows

$$\underline{\underline{\tau}}_d = 2\mu \left(\underline{\nabla V}\right)_0^s \tag{5}$$

or extended

$$\begin{bmatrix} \sigma_x & \tau_{x\,y} & \tau_{x\,z} \\ \tau_{y\,x} & \sigma_y & \tau_{y\,z} \\ \tau_{z\,x} & \tau_{z\,y} & \sigma_z \end{bmatrix} = \mu \begin{bmatrix} 2\frac{\partial u}{\partial x} & \frac{\partial u}{\partial y} + \frac{\partial v}{\partial x} & \frac{\partial u}{\partial z} + \frac{\partial w}{\partial x} \\ \frac{\partial v}{\partial x} + \frac{\partial u}{\partial y} & 2\frac{\partial v}{\partial y} & \frac{\partial v}{\partial z} + \frac{\partial w}{\partial y} \\ \frac{\partial w}{\partial x} + \frac{\partial u}{\partial z} & \frac{\partial w}{\partial y} + \frac{\partial v}{\partial z} & 2\frac{\partial w}{\partial z} \end{bmatrix} - \frac{2}{3}\mu \left(\frac{\partial u}{\partial x} + \frac{\partial v}{\partial y} + \frac{\partial w}{\partial z} \right) \begin{bmatrix} 1 & 0 & 0 \\ 0 & 1 & 0 \\ 0 & 0 & 1 \end{bmatrix} \tag{6}$$

From this formulation of the stresses generated by viscosity of fluids we get the following result: if we consider that shear stress can't assume infinite values, they tell us that viscosity *smoothen* velocity field discontinuities, and when a fluid is in relative motion with a solid surface there is still a region, close to the surface, where the fluid is not moving, the so-called boundary layer[3].

It is now clear that if we want to evaluate the shear stress, i. e. the friction of the fluid onto a solid surface, we must take into account the viscosity of the fluid.
Solutions of the boundary layer equations are the only rigorous physical processes able to evaluate drag that is generated by friction.

Reynolds number

We are interested in evaluating the effects of viscosity through a simple formula which would tell us the relation between viscous stresses and inertial forces.
The Reynolds number, used for the non-dimensionalization of the Equilibrium equation (see sect.), contains the information about the geometry, the kinematics and the thermodynamics, relative to the viscous effects, of the fluid-dynamic phenomenon we are modelling.

$$Re = \frac{\rho_{ref} V_{ref} L_{ref}}{\mu} \tag{7}$$

where ρ_{ref} is the reference density, V_{ref} is the reference velocity, L_{ref} is the reference length and μ is the viscosity.
The use of a reference length ties Reynolds number to the extension of the flow field of our interest. This point is fundamental to understand what the Reynolds number tells us about the effects of viscosity.
If we consider the flow field around a 3-D solid body moving in a still fluid, we use one of its dimension as reference length and we get a Reynolds number bigger than the threeshold for a non-viscous flow field, we may say that the viscous effects are negligible compared to the convection of momentum (pressure) and inertial forces. In fact, close to the surface of the solid body there is a region in which the velocity goes to zero because of viscosity, and the reference length to use in the Reynolds number is the distance from the solid surface.
This leads to the analysis of the boundary layer, which can be accounted for with a set of equations, namely Prandtl equations.

Thermodynamic properties

Let's assume that the fluid of our interest is continuous, that means the matter is distributed uniformly all over the field and there are no empty spaces: The inertial, kinematic and thermo-dynamic properties of matter are continuous functions of spatial coordinates [3].
This assumption is true if the fluid is enough dense, that is the number of molecules contained in the volume of the flow-field is sufficiently high. This is expressed in the formula:

$$\rho = \lim_{\mathrm{d}V \to \mathrm{d}V_0} \frac{\mathrm{d}m}{\mathrm{d}V} \tag{8}$$

where the density $\rho \left[Kg/m^3\right]$ is defined as the derivative of mass m times the volume V which tends to the the smallest volume V_0 for which we can consider the fluid continuous.

A continuous fluid is characterized by density, temperature $T\,[K]$ and pressure $p\,\left[N/m^2\right]$.
Temperature and pressure are two macroscopic properties which *measure* microscopic effects, the first one being proportional to the average kinetic energy of the random miscrospic motions and the latter being proportional to the force generated by collisions of particles in the fluid.

Density, temperature and pressure are phenomenologically related, and the analytical formulation of this relationship, namely the equation of state, depends upon the fluid of our interest. We can assume that air is an ideal gas, thus the equation of state is

$$p = \rho R T \tag{9}$$

where $R = 287.26 J/kgK$ is the gas constant for air and depends on chemical composition of the fluid.

Following the ideal gases properties, the relationship between energy and temperature is then

$$e = c_v(T)\,T \tag{10}$$

where $c_v(T)\,[J/K]$ is the specific heat at constant volume of the ideal gas, that is how many Joule of heat we need to increase the temperature of a gram of substance of one Kelvin at constant volume.

The ratio between specific heat at costant pressure and specific heat at costant volume is function of the temperature as

$$\gamma(T) = \frac{c_p}{c_v} \tag{11}$$

Mach number

As it has been made for viscosity, the phenomenon of density (or volume) variations, namely the compressibility, can be expressed with a non-dimensional number:

$$M = \frac{V_{\mathrm{ref}}}{a} \tag{12}$$

where V_{ref} is the reference velocity, and a is the speed of sound.

Indeed the compressibility, that is the capability of a fluid of reducing its volume (increasing its density) when pressure is applied to it, is related to the speed of sound.
The volume V decreases of a quantity ΔV proportional to the initial volume and the pressure applied, converseley the density ρ increases of a quantity $\Delta\rho$:

$$\Delta V = -a_c V \Delta p \tag{13}$$

$$\Delta\rho = a_c \rho \Delta p \tag{14}$$

where a_c is the compressibility coefficient(conventionally positive). The sound is the propagation of small density disturbances through waves, this can be easily experienced making a thin layer of metal

vibrate and noticing that the sound is generated by pressure waves that change the density of the fluid in which they move [3].
The speed of sound is obtained through eq. 14 for infinitesimal volumes,

$$a^2 = \frac{\partial p}{\partial \rho} \left[\frac{m^2}{s^2} \right] \tag{15}$$

when eq. 15 is evaluated for isoentropical variations of pressure, a is the laplacian speed of sound and it can be substituted in Mach number.

It has been stated that sound propagates through small pressure disturbances waves, conversely small pressure disturbances move at the speed of sound, hence using reference dynamic pressure $p_{\mathrm{ref}} = \frac{1}{2}\rho V_{\mathrm{ref}}^2$, eqs. 15 and 12 show that the square of Mach number is an indicator of the compressibility effects in terms of relative density variations,

$$\Delta\rho = \frac{\Delta p}{a^2} \simeq \frac{1}{2}\rho\frac{V_{\mathrm{ref}}^2}{a^2} \Rightarrow \frac{\Delta\rho}{\rho} \simeq \frac{1}{2}M^2 \tag{16}$$

The limit condition of $M = 0$, obtained when $a \to \infty$, means that the fluid is incompressible so its density does not vary through the flow field. In aerodynamics the fluid is considered incompressible when $M \ll 1$, for example if $M = 0.3$ relative density variations due to compressibility are smaller than 5%.

It is again remarked that the reference velocity should be carefully chosen and deductions from Mach number can lead to wrong conclusions, such as when the reference velocity of a body makes Mach number smaller than 0.3 , but expansion on its surface lead to much higher velocity regions of the flow field with relevant compressibility effects.

General specifications of balance equations

The actual aerodynamic event needs to be interpreted through physical laws expressed in analytical equations to solve for the requested quantities. In aerodynamics, we search for a set of equations in which the kinematic and thermodynamic variables are related and it is possible to reach for approximated or numerical solutions.

It is fundamental to shape the domain in which these laws have to be applied, namely the physical system where the aerodynamic phenomenon takes place.
Unlike typical mechanical problems in which the system is usually solid, in aerodynamics the volume of the system is fluid and, because of that, can change its shape in time.

If we apply a logical balance to evaluate the variation in time of the quantity G in the volume V we can observe that the quantity may vary either through an exchange across the surface of the volume or by production or distruction inside the volume.

$$\boxed{\text{Variation in time}} = \boxed{\text{External interaction}} + \boxed{\text{Internal production}}$$

Figure 4: Logical Balance Equation

The analytical tool that evaluates the variation in time of a general quantity G between two sides of a surface is the flux, defined analytically as a vector by the formula:

$$\underline{\phi}_G \cong g^+ \underline{V} \tag{17}$$

where g^+ is the density per unit volume of the quantity G and $\underline{V}$ is the velocity vector, hence the dimension of a flux is

$$\left[\underline{\phi}_G\right] = \frac{[G]\,[L]}{[L]^3\,[t]} \tag{18}$$

The quantity G in the volume V can be produced or destroyed in time because of internal causes, and we call this production $\dot{g}^+$ which has the dimensions of the quantity G per volume, per time unit, or

$$\left[\dot{g}^+\right] = \frac{[G]}{[L]^3\,[t]} \tag{19}$$

We are going to express the fundamental laws in a fixed volume V, enclosed by the outer surface S_0 through integrals extended to the finite volume of the domain.

We remark that physical quantities like density, momentum and energy are costant in the smallest volume for which the continuous fluid hypothesis is valid, namely the infinitesimal volume $\mathrm{d}V$.

Then we evaluate the total amount of the quantity G in the volume of our interest as the integral

$$G_t = \int_V g^+ \mathrm{d}V \tag{20}$$

and its variation per time unit is the derivative $\dfrac{\mathrm{d}G_t}{\mathrm{d}t}$.
Similarly the total production $\dot{G}$ can be evaluated as

$$\dot{G} = \int_V \dot{g}^+ \mathrm{d}V \tag{21}$$

which is positive if the quantity is created, negative if the quantity is destroyed.

The external exchange of the quantity is taken into account through the flux $\underline{\phi}_G$ which is defined on the outer surface S_o with normal vector $\underline{n}$, and its total flow is

$$\int_{S_o} \left(\underline{n} \cdot \underline{\phi}_G\right) \mathrm{d}S_o \tag{22}$$

which is positive if the quantity is going out, negative if the quantity is coming in.

The general global form of a balance equation is then

$$\frac{\mathrm{d}}{\mathrm{d}t}\left[\int_V g^+ \mathrm{d}V\right] = -\int_{S_o} \left(\underline{n} \cdot \underline{\phi}_G\right) \mathrm{d}S_o + \int_V \dot{g}^+ \mathrm{d}V \tag{23}$$

It is useful to express the same balance equation for the infinitesimal volume, hence we apply the Gauss theorem to obtain the local formulation of the balance equation, valid under the hypothesis of continuity of the function inside the integral

$$\int_V \left[\frac{\partial g^+}{\partial t} + \underline{\nabla} \cdot \underline{\phi}_G - \dot{g}^+\right] \mathrm{d}V = 0 \tag{24}$$

The local formulation of the balance equation is

$$\frac{\partial g^+}{\partial t} + \underline{\nabla} \cdot \underline{\phi}_G = \dot{g}^+ \tag{25}$$

The global (eq.23) and local (eq.25) formulations of the balance equation have been obtained considering the domain V fixed in an inertial reference frame, this process is called *Eulerian* specification of the flow field [21].

If the balance equations are evaluated following the particles of fluid and the mass M is fixed, instead of considering the phenomena

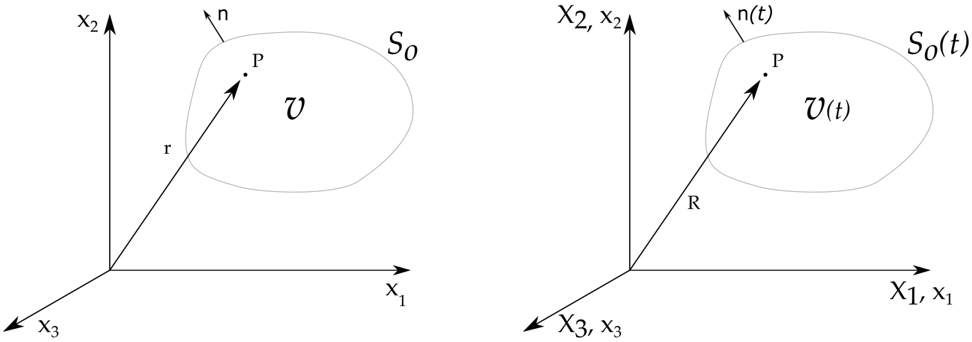

(a) Eulerian Approach (b) Lagrangian Approach

Figure 5: The two different specifications of a flow field

restricted to a fixed volume, we obtain a different specification of the flow field called *Lagrangian* [21].

In a *Lagrangian* flow field the balance equations are evaluated in a fixed mass M, defined as the domain, which can generally vary in motion, volume and shape with respect to the inertial reference frame.

The infinitesimal particles of the domain mass M in which the same domain is virtually decomposed are defined as dM and their center of mass is given by the vector $\underline{R}$ pointing to their position P at the starting time. The configuration of the system varies and at some time t the particles have moved and a new position vector is defined as $\underline{r}$ pointing to the new point p.

The evolution of the system as a function of the starting positions of the particles $\underline{R}$ is then expressed by the formula:

$$\underline{r} = \underline{r}\left(\underline{R}, t\right) \tag{26}$$

and as we stated before the next formula is valid

$$\underline{r} = \underline{r}\left(\underline{R}, t_0\right) = \underline{R} \tag{27}$$

and the inverse transformation is

$$\underline{R} = \underline{r}\left(\underline{r}, t\right) \qquad \underline{R}\left(\underline{r}, t_0\right) = \underline{r} \tag{28}$$

These transformations are valid since any region of the mass domain doesn't vanish nor become infinite and there isn't compenetration between separate region of the volume (continuity hypothesis).

In the lagrangian specification the quantity G is expressed as

$$G = \underline{G}\left(\underline{R}, t\right) \tag{29}$$

Any derivative obtained considering the lagrangian specification of the system, such as when $\underline{R}$ remains constant, is called substantial derivative and is defined as follows

$$\frac{\mathrm{D}G}{\mathrm{D}t} = \left(\frac{\partial G}{\partial t}\right)_{\underline{R}=\mathrm{const.}} \tag{30}$$

Following the derivatives chain rules and the transformation of eq.26 the substantial derivative is calculated as

$$\frac{\mathrm{D}G}{\mathrm{D}t} = \left(\frac{\partial G}{\partial t}\right)_{x_i=\mathrm{const.}} + \sum_{i=1}^{3}\left[\left(\frac{\partial G}{\partial x_i}\right)\cdot\left(\frac{\partial x_i}{\partial t}\right)\right] \tag{31}$$

or introducing the velocity vector $\underline{V}$ of the particle defined by the vector $\underline{r}$

$$\frac{\mathrm{D}G}{\mathrm{D}t} = \frac{\partial G}{\partial t} + \underline{V}\cdot\underline{\nabla}G \tag{32}$$

The general lagrangian balance equation is

$$\frac{\mathrm{d}}{\mathrm{d}t}\left[\int_{V_m(t)} g^{+}\,\mathrm{d}V_m\right] = -\int_{S_{o,m}(t)}\left(\underline{n}\cdot\underline{J}_G\right)\mathrm{d}S_{o,m} + \int_{V_m(t)} \dot{g}^{+}\,\mathrm{d}V_m \tag{33}$$

where the control volume and surface are now functions of time (the mass particles are fixed), and the flux is only diffusive since the domain doesn't exchange mass with the environment.

When the properties of substantial derivatives are applied and using the same process that leads to eq.25 we get a new expression for the local balance equations:

$$\rho\frac{\mathrm{D}g}{\mathrm{D}t} + \underline{\nabla}\cdot\underline{J}_G = \rho\dot{g} \tag{34}$$

where the quantity per unit mass g has replaced the the quantity per unit volume g^{+}.

Mass, momentum and energy equations

Summarizing the basic physical aspects (fluids properties, dynamics and thermodynamics) of the problem, the following laws lay the foundations of fluid dynamics

- Conservation of mass
- Momentum equation (Newton's law)
- Conservation of energy

The Lagrangian formulation (following a particle of fluid), neglecting gravitational effects, is [17]

$$\frac{D\rho}{Dt} + \rho\left(\underline{\nabla} \cdot \underline{V}\right) = 0 \tag{35}$$

$$\rho\frac{D\underline{V}}{Dt} - \left(\underline{\nabla} \cdot \underline{\underline{\tau}}\right) = 0 \tag{36}$$

$$\rho\frac{DE}{Dt} + \underline{\nabla} \cdot \left(\underline{J}_{ter} - \underline{\underline{\tau}} \cdot \underline{V}\right) = 0 \tag{37}$$

where $\underline{V}$ is the velocity field, ρ is the density, E is the total energy, $\underline{\underline{\tau}}$ is the stress tensor and $\underline{J}_{ter}$ is the internal energy diffusive flow.

The derivatives of density, velocity vector field and total energy are *substantial* derivatives, hence they take into account both the diffusive and convective variation of these quantities.
$\underline{\underline{\tau}}$ is composed by the pressure tensor and the stress deviator tensor $\underline{\underline{\tau}} = -p\underline{\underline{U}} + \underline{\underline{\tau}}_t$, the second one being related to friction and the dissipation of momentum.

The approximations are obtained through non-dimensionalization, introducing into the equations the already defined Reynolds number, Mach number and Prandtl number $Pr = c_p\mu/\lambda$,

$$\frac{D\rho}{Dt} + \rho\left(\underline{\nabla} \cdot \underline{V}\right) = 0 \tag{38}$$

$$\rho\frac{D\underline{V}}{Dt} + \underline{\nabla} \cdot p = \frac{1}{Re_\infty}\underline{\nabla} \cdot \underline{\underline{\tau}}_d \tag{39}$$

$$\rho\frac{DH}{Dt} = (\gamma - 1) M^2{}_\infty \frac{\partial p}{\partial t} - \frac{1}{Re_\infty}\left\{\underline{\nabla} \cdot \left[\frac{\underline{J}_{ter}}{Pr} - (\gamma - 1) M^2{}_\infty \underline{\underline{\tau}}_d \cdot \underline{V}\right]\right\} \tag{40}$$

Potential flow field and Laplace's equation

The equation presented above are very complex and their solution, even by numerical methods, is difficult for many practical applications. Anyway, large regions of the flow field are often capable of being modelled with less complex equations, in which small terms

are neglected .
In this case we are interested in the lowest level of approximation of Navier-Stokes equation, namely the potential flow field.
If the domain is inviscid $1/Re_{\infty} = 0$, the flow doesn't conduct heat $\lambda = 0$ and Crocco's theorem ensures vorticity is null, we get the potential equation, which can be further simplified into the Laplace equation when compressibility is neglected ($M_{\infty} = 0$),

$$\nabla^2 \Phi = 0 \tag{41}$$

where $\underline{V} = \nabla \Phi$ is the potential scalar function of the velocity vector field, and the Laplace operator, namely the divergence of the gradient of a function, is defined as follows

$$\nabla^2 f = \sum_{i=1}^{N} \frac{\partial^2 f}{\partial x_i^2} \tag{42}$$

The equation 41 is a second order partial differential equation and its non-trivial solutions are called *harmonic* functions.

The linearity of Laplace's equation allows the application of the superposition principle, namely any linear combination of harmonic functions is an harmonic function itself or mathematically,

$$\Phi = \sum_{i=1}^{N} c_i \Phi_i \tag{43}$$

In Cartesian coordinates the eq.41 becomes

$$\nabla^2 \Phi\,(x, y, z) = \frac{\partial^2 \Phi}{\partial x^2} + \frac{\partial^2 \Phi}{\partial y^2} + \frac{\partial^2 \Phi}{\partial z^2} = 0 \tag{44}$$

Boundary conditions

As in any other mathemathical model of a physical phenomena, the solution to the problem requires additional conditions to be specified on the borders of the domain of interest, namely the boundary conditions.

In the case of Laplace's equation applied to a volume, the boundary conditions must be imposed on every surface enclosing the domain. In the case of a solid body included in the volume of interest, the boundary conditions will be specified on the surface of the body as well.

As we can notice from the absence of time dependencies in Laplace's equation the unsteadiness of the flow field can be taken into account introducing time functions in the boundary conditions.

Considering an infinite domain, one of the boundary condition will be specified at infinity, which is the surface where all the disturbances caused by bodies in the flow field vanish, also known as far field boundary condition,

$$\Phi(P) \to \Phi_\infty \quad when \quad P \to \infty \tag{45}$$

where

$$\frac{\partial \Phi_\infty}{\partial x} = U_\infty \quad ; \quad \frac{\partial \Phi_\infty}{\partial y} = V_\infty \quad ; \quad \frac{\partial \Phi_\infty}{\partial z} = W_\infty \tag{46}$$

The boundary condition on internal boundaries between the domain and any body included in the volume of interest models the physical properties of the interaction between a fluid and a solid.
Then the tangential velocity on the body surface, namely the component of the velocity parallel to the surface, is null when the flow field is viscid as we stated in the viscosity section.
For a potential flow field we cannot assume any variation of the tangential velocity in the proximity of a solid body, so the fluid will slip on the surface, then the normal component of velocity is imposed on the surfaces, which can have a known value of mass flow velocity $h(S)$ on the surface S,

$$\underline{V} \cdot n = \underline{\nabla}\Phi \cdot \underline{n} = h(S) \quad \text{on} \quad S \tag{47}$$

If the body is solid and there is no mass flow through the surface then the normal velocity is null and the fluid flows tangential to the surface,

$$\underline{V} \cdot n = \underline{\nabla}\Phi \cdot \underline{n} = 0 \quad \text{on} \quad S \tag{48}$$

In this type of boundary condition we assign the value of the velocity potential function, namely the velocity gradient, hence we call it a *Neumann*'s condition, while when the velocity value is assigned directly the condition is called a Dirichlet condition.

1.5 BASIC SOLUTIONS AND SINGULARITY ELEMENTS

The analytical properties of Laplace's equation and the corresponding boundary value problem shown in the previous section demonstrated

that it is still possible to obtain a solution, also called an harmonic function, with a linear combination of two or more elementary solutions, i. e. the principle of superposition.
These elementary solutions are called singularities since their velocity inductions becomes singular approaching to their position in the flow field.
Once their *influence*, i. e. their induced potential and velocity, at an arbitrary point is calculated, these quantities replace the unknown terms in the analytical or numerical boundary integral equation.

The vortex lattice method, and its unsteady extension, both employ 3-D vortex-rings to solve the potential flow around lifting surfaces.

It is necessary to clarify that the numerical solution found in 106 doesn't directly include vortices, but only sources and doublets, yet it is possibile to show that doublet elements are equivalent to vortex elements of one order of polynomial approximation lower.

Polynomial function

A polynomial first order function, that is a solution to Laplace's equation, is often employed for the free stream potential, as it models the constant velocities of undisturbed flow.

Velocity potential is in general

$$\Phi(x, y, z) = U_\infty x + V_\infty y + W_\infty z \tag{49}$$

and the velocity increment, now called $\underline{q}$ to avoid confusion with its component v, is

$$\underline{q} = (u, v, w) = \nabla\Phi = (U_\infty,\ V_\infty,\ W_\infty) \tag{50}$$

Quadrilater doublet

The simplest 3-D elements have a quadrilater geometry with a constant strength singularity.

The quadrilater doublet shown in fig.6 have corners 1, 2, 3, 4 and a constant strength μ, its potential induction on a point $P(x, y, z)$, which coordinates are expressed in a local reference frame, is developed using the point elements distributed on the surface S, obtaining [9]

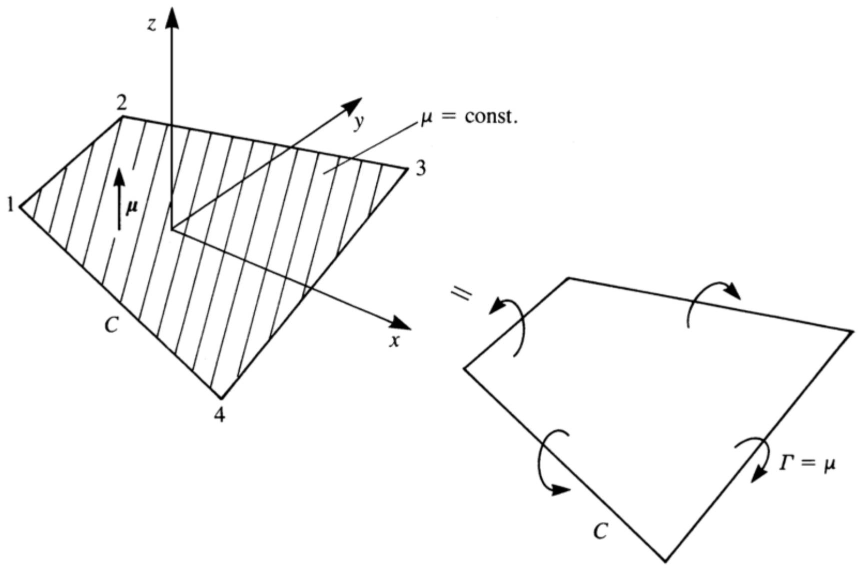

Figure 6: Quadrilater doublet and its vortex-ring equivalent (Reproduced from [9])

$$\Phi(x,y,z) = \frac{-\mu}{4\pi}\int_S \frac{z\mathrm{d}S}{\left[(x-x_0)^2+(y-y_0)^2+z^2\right]^{\frac{3}{2}}} \tag{51}$$

or in a simpler fashion,

$$\Phi(x,y,z) = \frac{-\mu}{4\pi}\int_S \frac{z\mathrm{d}S}{r^3} \tag{52}$$

where $r = \left[(x-x_0)^2+(y-y_0)^2+z^2\right]^{\frac{1}{2}}$.

The velocity increment can be obtained through

$$\underline{q} = (u,v,w) = \left(\frac{\partial\Phi}{\partial x}, \frac{\partial\Phi}{\partial y}, \frac{\partial\Phi}{\partial z}\right) \tag{53}$$

hence we get

$$\underline{q} = \frac{-\mu}{4\pi}\int_S \nabla\frac{z}{r^3}\mathrm{d}S = \frac{\mu}{4\pi}\int_S \left[\underline{i}\,\frac{\partial}{\partial x_0}\frac{z}{r^3} + \underline{j}\,\frac{\partial}{\partial y_0}\frac{z}{r^3} - \underline{k}\,\left(\frac{1}{r^3}-\frac{3z^2}{r^5}\right)\right]\mathrm{d}S \tag{54}$$

Quadrilater doublet and vortex-ring equivalence

As shown in fig.6, C represents the curve bounding the panel, so we consider a vortex filament of circulation Γ along C.

From Biot-Savart law we obtain the velocity increment induced by the filament as

$$\underline{q} = \frac{\Gamma}{4\pi}\int_C \frac{d\underline{l} \times \underline{r}}{r^3} \tag{55}$$

and for $d\underline{l} = (dx_0, dy_0)$ and $\underline{r} = (x - x_0, y - y_0, z)$ we get

$$\underline{q} = \frac{\Gamma}{4\pi}\int_C \{\underline{i}\,\frac{z}{r^3}dy_0 - \underline{j}\,\frac{z}{r^3}dx_0 - \underline{k}\,\left[\frac{(y-y_0)}{r^3}dx_0 - \frac{(x-x_0)}{r^3}dy_0\right]\} \tag{56}$$

Using Stokes' theorem on eq.56 as in [9] we get

$$\underline{q} = \frac{\Gamma}{4\pi}\int_S \left[\underline{i}\,\frac{\partial}{\partial x_0}\frac{z}{r^3} + \underline{j}\,\frac{\partial}{\partial y_0}\frac{z}{r^3} - \underline{k}\,\left(\frac{1}{r^3} - \frac{3z^2}{r^5}\right)\right] dS \tag{57}$$

Once the differentiation has been performed we get the same velocity as the doublet panel if $\Gamma = \mu$.

This simplified derivation of equivalence can be generalized to doublet distributions corresponding to vortex distributions of one order less plus a vortex-ring whose strength is equal to the edge value of the doublet distribution [9].

Constant strength vortex line segment

Following Biot-Savart's law a vortex line segment starting from point 1 and ending to point 2 as shown in fig.7, the velocity at an arbitrary point P can be obtained from

$$\Delta\underline{q} = \frac{\Gamma}{4\pi}\frac{d\underline{l} \times \underline{r}}{r^3} \tag{58}$$

where $\Delta\underline{q}$ is the increment for the infinitesimal segment on the line $d\underline{l}$, then we get the total induction

$$\underline{q} = \frac{\Gamma}{4\pi}\,\frac{\underline{r}_1 \times \underline{r}_2}{\|\underline{r}_1 \times \underline{r}_2\|^2}\,(\underline{r}_1 - \underline{r}_2)\cdot\left(\frac{\underline{r}_1}{r_1} - \frac{\underline{r}_2}{r_2}\right) \tag{59}$$

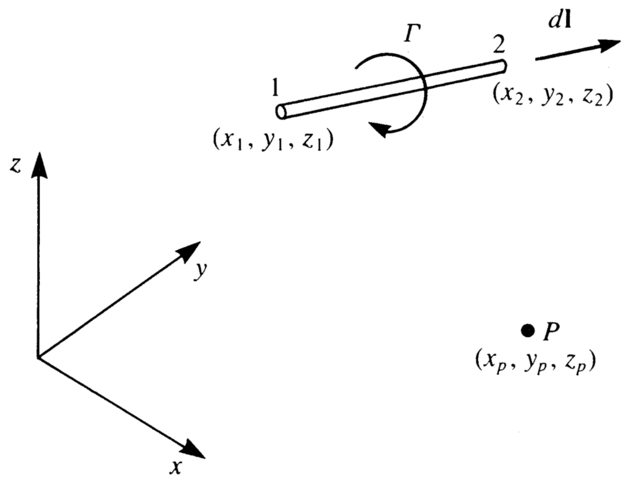

Figure 7: Vortex line segment (Reproduced from [9])

Vortex-ring

A vortex-ring is a combination of 4 vortex line segments in a quadrangle as shown in fig.8.

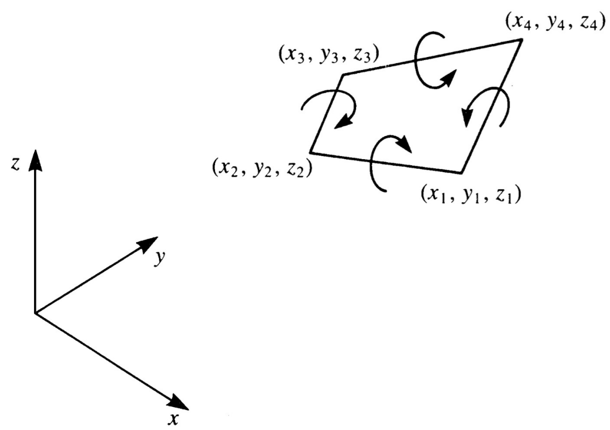

Figure 8: Vortex ring (Reproduced from [9])

The velocity induced by a vortex-ring can be calculated as the sum of the components induced by its 4 sides as follows,

$$\underline{q} = \sum_{i=1}^{4} \underline{q}_i = \begin{pmatrix} u \\ v \\ w \end{pmatrix} = \begin{pmatrix} u_1 \\ v_1 \\ w_1 \end{pmatrix} + \begin{pmatrix} u_2 \\ v_2 \\ w_2 \end{pmatrix} + \begin{pmatrix} u_3 \\ v_3 \\ w_3 \end{pmatrix} + \begin{pmatrix} u_4 \\ v_4 \\ w_4 \end{pmatrix} \quad (60)$$

where the $\underline{q}_i$ components are calculated through eq.59 for each segment with the same circulation Γ.

1.6 VORTONS FORMULATION

The code implements the possibility to adopt a vortex-particles (vortons) wake model, giving the chance to extend this method to a multibody panel method (in fact vortons don't suffer from intersection with body panels) and decreasing significantly the time of simulations (every vortex-ring, composed by 4 vortex vertices, is converted into a single vorton).

Since the vortex-particles employed in a vorton method are a discretization of the vorticity in the domain we need a theoretical formulation starting from the relationships between vorticity, velocity and the vector potential.

The vorticity in the domain, $\omega(\underline{r}, t)$, is defined as the curl of the velocity,

$$\omega(\underline{r}, t) = \nabla \times \underline{q} \tag{61}$$

The velocity due to the vector potential, $\underline{\Psi}$, is

$$\underline{q}_{\Psi} = \nabla \times \underline{\Psi} \tag{62}$$

Substituting the vector potential relationship into the definition of vorticity we obtain

$$\nabla^2 \underline{\Psi} = -\underline{\omega} \tag{63}$$

that is a vector Poisson equation relating the vector potential to the vorticity.
As vortex particles represent discretized elements of vorticity in the flow-field they are subjected to convection with local velocity and stretching due to the velocity gradients. This vorticity stretching is obtained recalling the equation of vorticity evolution, derived from the incompressible Euler equation, that is

$$\frac{D\underline{\omega}}{Dt} = \underline{\omega} \cdot \nabla \underline{Q} \tag{64}$$

where the term on the right hand side represents the vorticity stretching due to the gradient of the velocity field. A vortex particle in a 3-D domain is defined by the vector $\underline{\alpha}(x, y, z, t)$.
In the vorton method, the vorticity is replaced by a discretized set of vortons, so the vorticity is expressed through the linear combination of the vorticities represented by the vortons, as follows

$$\underline{\omega} = \sum_p \underline{\alpha}_p(\underline{r}, t) \tag{65}$$

while the vector potential given by Poisson's equation can be determined through

$$\underline{\Psi}_p(\underline{r}, t) = \frac{1}{4\pi} \sum_p \frac{\underline{\alpha}_p(\underline{r}, t)}{|\underline{r} - \underline{r}_p|} \tag{66}$$

where $\underline{r}$ is the distance from the vorton to the point of evaluation. A core-function ξ_ψ must be introduced to eliminate the singularity when $\underline{r} - \underline{r}_p$ approaches zero, so that if $|\underline{r} - \underline{r}_p| < r_\sigma$ the vector potential is not singular.

The velocity field induced by the set of vortons is given by the curl of the vector potential

$$\nabla \times \underline{\Psi}_p(\underline{r}, t) = \frac{1}{4\pi} \sum_p \frac{(\underline{r} - \underline{r}_p)}{|\underline{r} - \underline{r}_p|} \times \underline{\alpha}_p(\underline{r}, t) \tag{67}$$

Therefore the vorton induction decays as $\frac{1}{r^2}$ and again a core-function ξ_Q must be introduced to avoid the singularity when $|\underline{r} - \underline{r}_p| \to 0$.

Similarly the gradient of the velocity field used in the stretching term of vorticity is defined as follows

$$\nabla \left(\nabla \times \underline{\Psi}_p(\underline{r}, t) \right) = \frac{1}{4\pi} \sum_p \nabla \left(\frac{(\underline{r} - \underline{r}_p)}{|\underline{r} - \underline{r}_p|^3} \times \underline{\alpha}_p(\underline{r}, t) \right) \tag{68}$$

The core function that will be used in this implementation is defined in [5], called *high order algebraic smoothing* function and successfully employed in the methods developed in [11] and [4]. Recall that this method will suffer from the fact that the particle representation of vorticity doesn't guarantee the divergence-free field for long times of simulations, thus a relaxation scheme should be implemented to avoid un-physical augmentation of vorticity in the field.

1.7 KUTTA'S CONDITION

Once the boundary conditions at the free stream and at the surfaces of the solid bodies included in the flow field have been added to the analytical problem governed by Laplace's equation, we must ensure

that the solution we get is unique as it must resemble the physical phenomenon.
The uniqueness of the solution for a multiple connected region, i. e. the case of a 3-dimensional wing shedding a wake, is ensured when the circulation is fixed by means of a physical condition [9]. Moreover we assume that the physical condition is then related to the shape of the solid bodies, as their geometries influence the way the flow approaches, flows and then leaves their borders [3].
Kutta condition's applies to aerodynamic bodies, by definition those with a sharp trailing edge, because the fluid flowing on their surface would eventually encounter an infinite curvature, hence it would require an infinite acceleration.
The effect of viscosity decelerate the fluid in the proximities of the solid surfaces and neutralize the increasing acceleration trend at the trailing edge.

When the flow field is potential the effects of viscosity is negligible and the infinite acceleration of the fluid at the trailing edge must be treated with another condition.
The fluid velocity direction and module are fixed such that it doesn't follow the curvature but instead leaves the corner smoothly, i. e. the velocity field is continue and the module is finite.

The ways to address Kutta's condition depend on the numerical method employed in the aerodynamic analysis, but it is common to fix the amount of circulation around the trailing edge through the velocity components or directly its value.

1.8 THE BERNOULLI EQUATION

The solution to Laplace's equation and the related boundary conditions leads to the calculation of the velocity field.
To accomplish the goals of aerodynamic design we are often interested in the calculation of the pressure field, and finally to the computation of forces on the bodies, hence we need an appropriate expression obtained from the momentum equation.

From Euler equation, i. e. the inviscid compressible fluid approximation of momentum equation, we obtain the incompressible approximation,

$$\frac{\partial \underline{V}}{\partial t} + \underline{V} \cdot \nabla \underline{V} = \underline{f} - \frac{\nabla p}{\rho} \tag{69}$$

The convective acceleration term is rewritten using the vector identity,

$$\underline{V} \cdot \nabla \underline{V} = \nabla \frac{V}{2} - \underline{V} \times \underline{\zeta} \tag{70}$$

where ζ is the vorticity, twice the angular velocity,

$$\underline{\zeta} \cong 2\omega = \nabla \times \underline{V} \tag{71}$$

then the Euler equation becomes

$$\frac{\partial \underline{V}}{\partial t} + \underline{V} \times \underline{\zeta} + \nabla \frac{V^2}{2} = \underline{f} - \frac{\nabla p}{\rho} \tag{72}$$

With the additional hypothesis of irrotational flow and conservative body force we obtain

$$\nabla \left(E + \frac{p}{\rho} + \frac{V^2}{2} + \frac{\partial \Phi}{\partial t} \right) = 0 \tag{73}$$

or conversely,

$$E + \frac{p}{\rho} + \frac{V^2}{2} + \frac{\partial \Phi}{\partial t} = C\,(t) \tag{74}$$

and if the conservative body force doesn't influence the motion of particles in the flow field, that is when the gradient of forces produced by gravity are negligible, we obtain

$$\frac{p}{\rho} + \frac{V^2}{2} + \frac{\partial \Phi}{\partial t} = C\,(t) \tag{75}$$

In a potential flow field, as we can notice from eq.75 and eq. 41, the velocity field(or its potential function) and the pressure field are the only two unknown variables and they are decoupled, making it easier to develop numerical methods to obtain these quantities.

Comparing two points in the fluid, the first is arbitrary and the second is a reference point at infinity that is chosen such that $\Phi_\infty = \mathrm{const.}$ and $\underline{V}_\infty = 0$, the pressure p can be calculated from

$$\frac{p_\infty - p}{\rho} = \frac{V^2}{2} + \frac{\partial \Phi}{\partial t} \tag{76}$$

and in cartesian coordinates in an inertial reference frame,

$$\frac{p_\infty - p}{\rho} = \frac{1}{2}\left[\left(\frac{\partial\Phi}{\partial X}\right)^2 + \left(\frac{\partial\Phi}{\partial Y}\right)^2 + \left(\frac{\partial\Phi}{\partial Z}\right)^2\right] + \frac{\partial\Phi}{\partial t} \tag{77}$$

in the BRF using the chain rule the time derivative can be expressed as

$$\frac{\partial}{\partial t_{\mathrm{inertial}}} = -\left[\underline{V}_0 + \underline{\Omega} \times \underline{r}\right] \cdot \left(\frac{\partial}{\partial x}, \frac{\partial}{\partial y}, \frac{\partial}{\partial z}\right) + \frac{\partial}{\partial t_{\mathrm{body}}} \tag{78}$$

so eq. 77 becomes

$$\frac{p_\infty - p}{\rho} = \frac{1}{2}\left[\left(\frac{\partial\Phi}{\partial x}\right)^2 + \left(\frac{\partial\Phi}{\partial y}\right)^2 + \left(\frac{\partial\Phi}{\partial z}\right)^2\right] - \left(\underline{V}_0 + \underline{\Omega} \times \underline{r}\right) \cdot \nabla\Phi + \frac{\partial\Phi}{\partial t} \tag{79}$$

In the case of three-dimensional panel methods the simplest way to calculate pressure is

$$\frac{p_{\mathrm{ref}} - p}{\rho} = \frac{V^2}{2} + \frac{\partial\Phi}{\partial t} - \frac{v_{\mathrm{ref}}{}^2}{2} \tag{80}$$

where V is the modulus of the local fluid velocity and $\underline{v}_{\mathrm{ref}} = -\left[\underline{V}_0 + \underline{\Omega} \times \underline{r}\right]$ is the reference kinematic velocity.

From eq. 80 we get an expression for the pressure coefficient, that is a dimensionless quantity which relates the difference of the pressure at an arbitrary point and static pressure with a reference quantity called *dynamic* pressure,

$$C_p = \frac{p - p_{\mathrm{ref}}}{(1/2)\,\rho v_{\mathrm{ref}}{}^2} = 1 - \frac{V^2}{v_{\mathrm{ref}}{}^2} - \frac{2}{v_{\mathrm{ref}}{}^2}\frac{\partial\Phi}{\partial t} \tag{81}$$

1.9 PANEL METHODS

Laplace's equation with an appropriate set of boundary conditions can be solved through numerical methods which employs a general solution of the potential flow field through Green's third identity and its applications to harmonic functions.

In panel methods a field singularities (vortices, doublets and sources), which inherently satisfy the potential flow field analytical requirements, is employed to discretize the body geometries and this process leads to a boundary integral equation solved through a linear algebraic system for the calculation of pressure and forces directly on the bodies.

It is remarkable that panel methods are able to model a large number of physical phenomena and yet they are computationally cheaper than other numerical method, the calculation of unknown quantities being restricted to a finite number of *control* points on the surface of bodies.

In this section the derivation of the numerical methods known as panel methods will be developed through the analytical process that leads to a general solution of the incompressible, potential flow field equations and the application of the properties of field singularities.

General solution from Green's third identity

The analytical problem described by Laplace's equation and the boundary conditions set in the previous sections will be solved using Green's identities in a domain shown in fig.9 which allows us to formulate a solution on the boundaries of the domain [3].

The domain is composed by the volume of interest V bounded by the outer surface S_∞ and enclosing an arbitrary body shedding a wake surface, delimited by S_b and S_w. This domain can either be 2-dimensional or 3-dimensional.

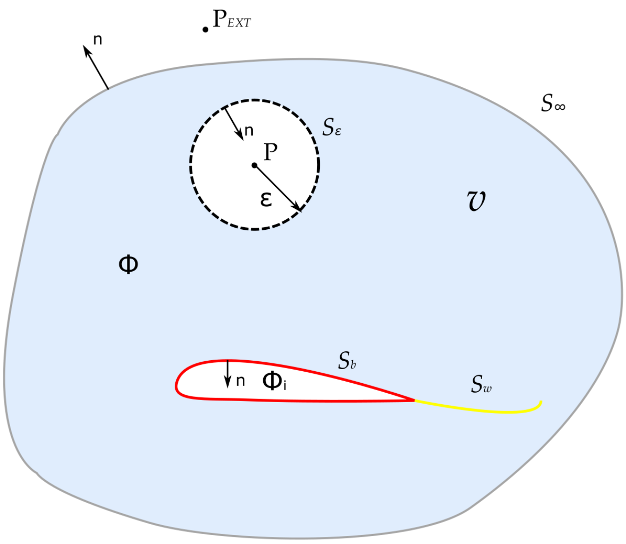

Figure 9: Domain for Green's third identity formulation

Green's second identity is obtained from the divergence's theorem as follows

$$\iint_S \underline{Q} \cdot \underline{n} \mathrm{d}S = \iiint_V \underline{\nabla} \cdot \underline{Q} \mathrm{d}V \tag{82}$$

and when $Q = \Phi_1 \underline{\nabla} \Phi_2 - \Phi_2 \underline{\nabla} \Phi_1$, where Φ_1 and Φ_2 are two scalar, continuous and differentiable functions in V,

$$\iint_S \left(\Phi_1 \underline{\nabla} \Phi_2 - \Phi_2 \underline{\nabla} \Phi_1 \cdot \underline{n}\right) \mathrm{d}S = \iiint_V \left(\Phi_1 \nabla^2 \Phi_2 - \Phi_2 \nabla^2 \Phi_1\right) \mathrm{d}V \tag{83}$$

We apply Green's second identity, eq. 83, to the volume of our interest with the functions $\Phi_1 = \dfrac{1}{r}$ and $\Phi_2 = \Phi$, where r is the distance from an arbitrary point in the volume and Φ is the velocity potential function solution of Laplace's equation in the volume V, then we obtain

$$\iint_S \left(\frac{1}{r} \underline{\nabla} \Phi - \Phi \underline{\nabla} \frac{1}{r}\right) \cdot \underline{n} \mathrm{d}S = \iiint_V \left(\frac{1}{r} \nabla^2 \Phi - \Phi \nabla^2 \frac{1}{r}\right) \mathrm{d}V \tag{84}$$

When the volume integral of eq.84 is evaluated outside the boundary S_∞ both the laplacian quantities are null (the functions are solution of Laplace's equation), hence the surface integral is null as well,

$$\iint_S \left(\frac{1}{r} \underline{\nabla} \Phi - \Phi \underline{\nabla} \frac{1}{r}\right) \cdot \underline{n} \mathrm{d}S = 0 \quad when \quad \mathsf{P}_{ext} \notin V \tag{85}$$

while inside the domain the quantity $\dfrac{1}{r}$ becomes singular when $r \to 0$, then we must subtract an infinitesimal sphere of radius ϵ from the integration volume V, and rewrite the surface as $S + S_\epsilon$, to obtain the expression,

$$\iint_{S+S_\epsilon} \left(\frac{1}{r} \underline{\nabla} \Phi - \Phi \underline{\nabla} \frac{1}{r}\right) \cdot \underline{n} \mathrm{d}S = 0 \quad when \quad \mathsf{P} \in V \tag{86}$$

The surface integral on the infinitesimal sphere is evaluated introducing a spherical coordinate system centered in the sphere so that the radius versor is opposite to the normal $\underline{n} = -\underline{e}_r$ and $\underline{n} \cdot \underline{\nabla}\Phi = -\dfrac{\partial \Phi}{\partial r}$, $\underline{\nabla}\dfrac{1}{r} = -\dfrac{1}{r^2}\underline{e}_r$ and eq. 86 becomes

$$\iint\limits_{S} \left(\frac{1}{r}\underline{\nabla}\Phi - \Phi\underline{\nabla}\frac{1}{r}\right) \cdot \underline{n} dS - \iint\limits_{S_\epsilon} \left(\frac{1}{r}\frac{\partial \Phi}{\partial r} + \frac{\Phi}{r^2}\right) dS = 0 \tag{87}$$

which can be further simplified if the potential function Φ and its derivatives are well-behaved functions in the domain [9], and considering the infinitesimal surface of the sphere as $\iint\limits_{S_\epsilon} dS = 4\pi\epsilon^2$ when $\epsilon = r$,

$$\iint\limits_{S} \left(\frac{1}{r}\underline{\nabla}\Phi - \Phi\underline{\nabla}\frac{1}{r}\right) \cdot \underline{n} dS - \iint\limits_{S_\epsilon} \left(\frac{\Phi}{r^2}\right) dS = 0 \tag{88}$$

$$\iint\limits_{S} \left(\frac{1}{r}\underline{\nabla}\Phi - \Phi\underline{\nabla}\frac{1}{r}\right) \cdot \underline{n} dS - \ 4\pi\ \Phi(P) = 0 \tag{89}$$

and finally,

$$\Phi(P) = \frac{1}{4\pi}\iint\limits_{S} \left(\frac{1}{r}\underline{\nabla}\Phi - \Phi\underline{\nabla}\frac{1}{r}\right) \cdot \underline{n} dS \tag{90}$$

Eq. 90 is Green's Third Identity when the two potential functions Φ_1 and Φ_2 are both harmonic, and it is remarkable as it can be used to evaluate the potential function $\Phi(P)$ at any point in the volume V, given the value of the potential Φ and its normal derivative $\dfrac{\partial \Phi}{\partial n}$ on the surface of the boundary S.

To obtain an expression that includes the contribution of every surface of the domain we must evaluate first the potential in the body volume, the *internal* potential, which is outside the volume V and similarly to eq.85,

$$\iint\limits_{S_b} \left(\frac{1}{r}\underline{\nabla}\Phi_i - \Phi_i\underline{\nabla}\frac{1}{r}\right) \cdot \underline{n} dS = 0 \tag{91}$$

and the complete expression for the potential becomes

$$\begin{aligned}\Phi(P) = & \frac{1}{4\pi}\iint\limits_{S_b}\left[\frac{1}{r}\underline{\nabla}(\Phi-\Phi_i)-(\Phi-\Phi_i)\underline{\nabla}\frac{1}{r}\right]\cdot\underline{n}dS + \\ & + \frac{1}{4\pi}\iint\limits_{S_\infty+S_w}\left(\frac{1}{r}\underline{\nabla}\Phi-\Phi\underline{\nabla}\frac{1}{r}\right)\cdot\underline{n}dS\end{aligned} \tag{92}$$

and if we consider the potential function at ∞ as a known function and the wake surface as a thin discontinuity such as the quantity $\frac{\partial\Phi}{\partial n}$ is continue and the value of the potential is the difference between the upper border and the lower border we obtain

$$\begin{aligned}\Phi(P) = & \frac{1}{4\pi}\iint\limits_{S_b}\left[\frac{1}{r}\underline{\nabla}(\Phi-\Phi_i)-(\Phi-\Phi_i)\underline{\nabla}\frac{1}{r}\right]\cdot\underline{n}dS + \\ & - \frac{1}{4\pi}\iint\limits_{S_w}\left[\underline{\nabla}(\Phi_u-\Phi_l)\frac{1}{r}\right]\cdot\underline{n}dS + \\ & + \Phi_\infty(P)\end{aligned} \tag{93}$$

General solution in terms of doublets and sources distributions

Eq.93 can be rewritten in terms of doublets and sources singularities, once we have introduced the following quantities,

$$-\mu = \Phi - \Phi_i \tag{94}$$

$$-\sigma = \frac{\partial\Phi}{\partial n} - \frac{\partial\Phi_i}{\partial n} \tag{95}$$

where μ is the doublet element intensity and σ is the source element intensity and the minus sign is due to the direction of the normals on the boundary surfaces, so we get

$$\begin{aligned}\Phi(P) = & -\frac{1}{4\pi}\iint\limits_{S_b}\left[\sigma\left(\frac{1}{r}\right)-\mu\underline{n}\cdot\underline{\nabla}\left(\frac{1}{r}\right)\right]dS + \\ & + \frac{1}{4\pi}\iint\limits_{S_w}\left[\mu\underline{n}\cdot\underline{\nabla}\left(\frac{1}{r}\right)\right]dS + \\ & + \Phi_\infty(P)\end{aligned} \tag{96}$$

and if we replace $\underline{n} \cdot \underline{\nabla} = \frac{\partial}{\partial n}$ we get

$$\begin{aligned} \Phi(P) = & -\frac{1}{4\pi} \iint\limits_{S_b} \left[\sigma \left(\frac{1}{r} \right) - \mu \frac{\partial}{\partial n} \left(\frac{1}{r} \right) \right] dS + \\ & + \frac{1}{4\pi} \iint\limits_{S_w} \left[\mu \frac{\partial}{\partial n} \left(\frac{1}{r} \right) \right] dS + \\ & + \Phi_\infty(P) \end{aligned} \tag{97}$$

which is the equation that allows us to calculate the velocity potential at arbitrary points given the sources and doublet distribution on the boundaries.
We notice that the potential of sources and doublets will vanish when $\underline{r} \to \infty$, hence it will inherently fulfill the boundary conditions at infinity, but even when the same set of boundary conditions are given the choice of the distribution is not unique and we need further physical considerations to find an appropriate solution for arbitrary geometries.

Numerical solution

In this section the derivation of a unique distribution of singularities for the analytical solution of eq.97 is shown for the panel method known as vortex lattice method.
We need to address the physical properties of the flow field of our interest.
First the boundary condition of zero flow normal to the surfaces known as *Neumann's condition* will be carried out.
Then the right choice of singularities and their distribution will be made.
Finally, as we have learnt from the Kutta's condition, the amount of circulation is directly linked to the properties of the flow field and the geometry of the bodies (solid bodies and wakes) therefore it requires to be fixed [9].

Based on eq.97 we have the following expression for the total velocity potential, now called Φ^*,

$$\Phi^*(x,y,z) = \frac{1}{4\pi} \int_{S_B+S_W} \mu \frac{\partial}{\partial n} \left(\frac{1}{r} \right) dS - \frac{1}{4\pi} \int_{S_B} \sigma \left(\frac{1}{r} \right) dS + \Phi_\infty \tag{98}$$

then we rewrite the boundary condition of eq.48 replacing the total velocity potential Φ^* as the sum of perturbation potential Φ and free stream velocity potential Φ_∞,

$$\underline{\nabla}(\Phi + \Phi_\infty) \cdot \underline{n} = 0 \quad \text{on} \quad S \tag{99}$$

and the condition at the outer boundaries of the domain, that is inherently fulfilled by the singularities used in this context, becomes,

$$\underline{\nabla}\Phi\,(P) \to 0 \quad \text{when} \quad P \to \infty \tag{100}$$

We use the velocity field as expressed below to met the condition of eq.99,

$$\nabla\Phi^*\,(x, y, z) = \frac{1}{4\pi}\int_{S_B+S_W} \mu\,\nabla\left[\frac{\partial}{\partial n}\left(\frac{1}{r}\right)\right]\,dS - \frac{1}{4\pi}\int_{S_B} \sigma\,\nabla\left(\frac{1}{r}\right)\,dS + \nabla\Phi_\infty \tag{101}$$

then we obtain,

$$\left\{\frac{1}{4\pi}\int_{S_B+S_W} \mu\,\nabla\left[\frac{\partial}{\partial n}\left(\frac{1}{r}\right)\right]\,dS - \frac{1}{4\pi}\int_{S_B} \sigma\,\nabla\left(\frac{1}{r}\right)\,dS + \nabla\Phi_\infty\right\} \cdot \underline{n} = 0 \tag{102}$$

This is the boundary integral equation needed to discretize the solution in a finite number of points called *collocation points*, and so to turn the analytical problem into a numerical one, that can be solved through an algebraic system in terms of the unknown singularities. Finally we need to clarify the wake properties and specify how singularities will be employed in the case of our interest.

Wake properties

An appropriate wake surface model is not only necessary to address the circulation problem and Kutta's condition but also strongly related to the characteristics of the flow field and the geometry of the bodies in the domain.

A simple model for a wake surface is developed when the body of our interest is a lifting wing discretized with one bound vortex line with the strength Γ as shown in fig.10, which according to Helmholtz theorems,

$$\frac{\partial\Gamma_x}{\partial x} = \frac{\partial\Gamma_y}{\partial y} \tag{103}$$

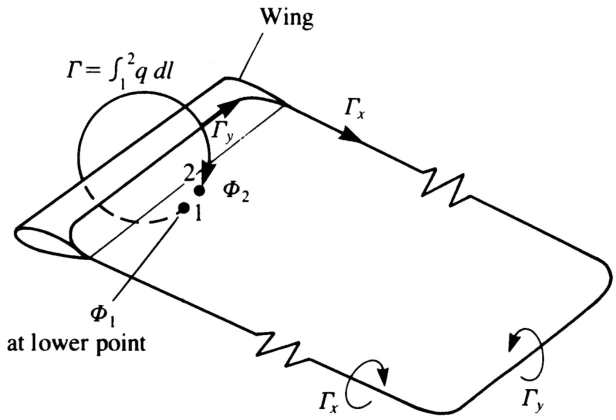

Figure 10: Lifting surface modelled by a single vortex line (Reproduced from [9])

which implies that the vortex line has constant stregth and requires to be continued beyond the wing.
The bound circulation is then calculated as follows,

$$\Gamma = \int_1^2 \underline{v} \cdot d\underline{l} \tag{104}$$

where $\underline{v}$ is the velocity field in the domain, showing that a discontinuity in the velocity potential must exist near the trailing edge.

This brief considerations show that any physical condition, required for the uniqueness of the solution, has to be addressed in relation to a wake model that will fix the strength and the shape according to it.

Wake strength and shape

As regards the strength, the Kutta's condition implies that the amount of circulation is fixed at the trailing edge to make the fluid flow smoothly.

The shape of the wake will be treated accordingly to the fact that the wake panels can't sustain any load unlike the body panels, since they are not solid surfaces.
Assuming that the wake is modelled by vortex line segments with a circulation vector $\underline{\Gamma}$ and following Kutta-Joukowski theorem the force $\underline{F}$ generated by circulation is given by

$$\underline{F} = \rho \underline{v} \times \underline{\Gamma} \tag{105}$$

where $\underline{v}$ is the local fluid velocity, hence assuming $\underline{\Gamma} \neq 0$ the force will be null if the direction of the vortex line segments are parallel to the local fluid velocity, $\underline{v} \parallel \underline{\Gamma}$.

Reduction to a set of linear algebraic equations

Once the choice of singularity elements and a wake model has been made, the bodies and the wake are discretized into panels, and the boundary condition of eq.102 can be applied to each of these elements on their *collocation points*.

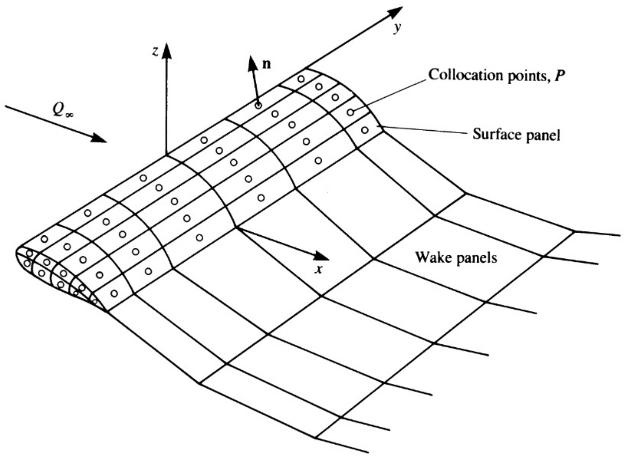

Figure 11: Example of discretization of a wing and a wake model (Reproduced from [9])

Assuming N collocation points for a discretized body and N_w for the wake as shown in fig.11, eq.102 is rewritten as follows,

$$\begin{aligned}
&\Bigg\{ \sum_{k=1}^{N} \frac{1}{4\pi} \int_{Body\ panel} \mu \, \nabla \left[\frac{\partial}{\partial n} \left(\frac{1}{r} \right) \right] \, dS \, + \\
&+ \sum_{l=1}^{N_w} \frac{1}{4\pi} \int_{Wake\ panel} \mu \, \nabla \left[\frac{\partial}{\partial n} \left(\frac{1}{r} \right) \right] \, dS \, + \\
&- \sum_{k=1}^{N} \frac{1}{4\pi} \int_{Body\ panel} \sigma \, \nabla \left(\frac{1}{r} \right) \, dS + \nabla \Phi_\infty \Bigg\} \cdot \underline{n} = 0
\end{aligned} \tag{106}$$

which means that for each collocation point P on our solid body(recall that Neumann's condition is applied to the body surface S_b), eq.106 takes account of the influence of each body panel k and each wake panel l through surface integrals.

Once the integrals are evalued numerically or analytically, if the doublets and the sources have constant strength, we obtain a numerical expression of Neumann's condition,

$$\sum_{k=1}^{N} C_k \mu_k + \sum_{l=1}^{N_W} C_l \mu_l + \sum_{k=1}^{N} B_k \sigma_k = A_k \quad \texttt{for each point} \quad \mathtt{P} \quad (107)$$

where C_k and B_k depend on the geometrical properties and shape of the body panels and the wake model, while A_k are related to the free stream potential and it's assumed that they are known quantities.

At this point the algebraic system resulting from eq.107 leads to the calculation of the unknown doublets strength μ_k once we have expressed the wake doublets μ_l in terms of the body singularities(by using a physical condition) and fixed the sources strength σ_k.

Finally we obtain a system of N equations with the N unkwown μ_k in the following form,

$$\begin{pmatrix} a_{11}, & a_{12}, & ..., & a_{1N} \\ a_{21}, & a_{22}, & ..., & a_{2N} \\ \vdots & \vdots & & \vdots \\ a_{N1}, & a_{N2}, & ..., & a_{NN} \end{pmatrix} \begin{pmatrix} \mu_1 \\ \mu_2 \\ \vdots \\ \mu_N \end{pmatrix} = \begin{pmatrix} \mathrm{RHS}_1 \\ \mathrm{RHS}_2 \\ \vdots \\ \mathrm{RHS}_N \end{pmatrix} \quad (108)$$

where the RHS's contain the information of zero normal flow of Neumann's condition and the matrix on the left side is often called *aerodynamic influence matrix*.

1.10 EXTENSION TO UNSTEADY INCOMPRESSIBLE POTENTIAL FLOW

The goal of this section is to address the modifications required by the numerical methods known as panel methods to take account of the unsteadiness in the incompressible potential flow fields.

First it should be reminded that Laplace's equation doesn't contain time-dependent derivatives, hence the unsteadiness of the flow field will be accounted for in the boundary conditions and in a more complex wake model.
Then the unsteady specification of the Bernoulli equation will be used to include the unsteady loads in the aerodynamic analysis.

It is assumed that the unsteady motion is prescribed and aerodynamic equations are decoupled from the equations of motion which determine the path and attitude of the body submerged in the fluid.

Unsteady solution

We are interested in the modifications of Neumann's boundary condition when the motion is unsteady, in the case of our interest a body submerged in a stationary fluid follows a prescribed unsteady motion path.
As shown in fig.12 the choice between the body reference frame (BRF) and the inertial reference frame (IRF) becomes very important to have a clear and simple expression of the velocity components.

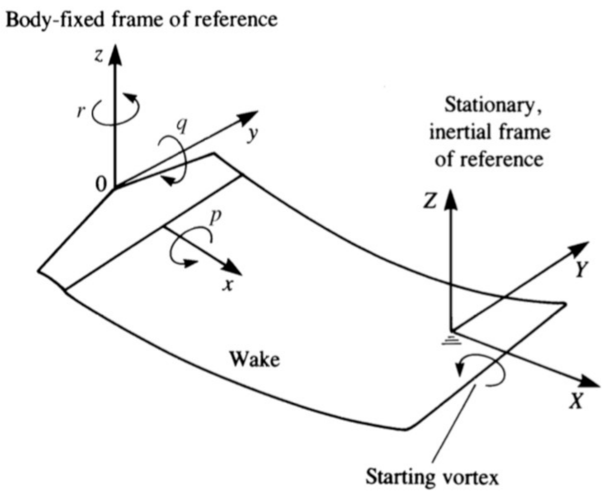

Figure 12: Choice of reference frames for an unsteady motion (Reproduced from [9])

Assuming that BRF origin moves with a velocity V_0, its angular velocity is $\Omega = (p, q, r)$, the distance from the origin of the IRF is r and an additional relative velocity $v_{rel}(x, y, z)$ with respect to the origin of the BRF is defined, we get an expression for the kinematic velocity v of the undisturbed fluid due to the BRF points motion as follows,

$$v = -\left[V_0 + \Omega \times r + v_{rel}\right] \tag{109}$$

and eq.109 can be expressed in both IRF coordinates (X, Y, Z) or BRF coordinates (x, y, z) once the transformation function between f between these reference frames has been established,

$$\begin{pmatrix} x \\ y \\ z \end{pmatrix} = f\left(X_0, Y_0, Z_0, \phi, \theta, \psi\right) \begin{pmatrix} X \\ Y \\ Z \end{pmatrix} \tag{110}$$

where the transformation takes account of the translations $(X - X_0), (Y - Y_0), (Z - Z_0)$ and attitude in terms of Euler's angles (ϕ, θ, ψ).

Finally we get an identical expression for Laplace's equation and the free stream condition, and a new Neumann's condition expression that takes account of the BRF motion,

$$\nabla\Phi^2 = 0 \tag{111}$$

$$[\underline{\nabla}\Phi - (V_0 + \Omega \times r + v_{rel})] \cdot \underline{n} = 0 \quad \text{on } S \tag{112}$$

$$\nabla\Phi \to 0 \quad \text{when } \underline{R} \ \to \ \infty \tag{113}$$

The absence of time derivatives let us apply the steady-state solution techniques in the same fashion once the time varying motion is accounted for in the momentary boundary conditions [9].

We get an unsteady expression of the numerical solution suitable for panel methods, i. e. eq.102 found in the previous section, adding the BRF kinematic velocity,

$$\left\{ \frac{1}{4\pi} \int_{S_B + S_W} \mu \, \nabla \left[\frac{\partial}{\partial n} \left(\frac{1}{r} \right) \right] \, dS - \frac{1}{4\pi} \int_{S_B} \sigma \, \nabla \left(\frac{1}{r} \right) \, dS - \underline{V}_0 - \underline{v}_{rel} - \underline{\Omega} \times \underline{r} \right\} \cdot \underline{n} = 0 \tag{114}$$

In this way we get a different algebraic system, eq.107, for each momentary boundary condition.

Unsteady Kutta's condition

Similarly to the steady case a physical condition should be developed to fix the amount of circulation at the trailing edge.
A simple way to address the unsteadiness of the wake shape is to extend the steady Kutta condition at every time step included in the calculation.

The parameters affecting the status of the extension of the steady Kutta's condition are mainly the $reducedfrequency$, $k = \omega L/2V$, where ω is a reference angular velocity, L is a reference length and V is a reference velocity, and the amplitude of the disturbances in terms of body displacement at the trailing edge and the corresponding velocities[9].

It has been demonstrated by comparisons with experiments that for attached flows in which the reduced frequency is less than 1, and the displacements are small, i. e. one order less than the reference length,

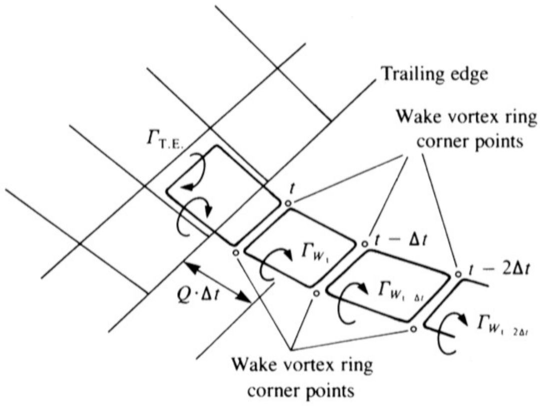

Figure 13: Example of the application of Kutta's condition in an unsteady vortex lattice method (Reproduced from [9])

the application of the steady Kutta condition leads to an appropriate calculations of aerodynamic loads, even if a certain lag could be present.

An example of the application of steady Kutta's condition in an unsteady vortex lattice method through the setting of the amount of circulation $\Gamma_{wake} = \Gamma_{T.E.}$ of the first row of wake panels is given in fig.13.

Forces evaluation

The instantaneous unsteady Bernoulli equation should be applied to calculate the pressure on the body, to take account of the unsteady loads generated by an accelerating body, as we already found in eq.80,

$$\frac{p_{ref} - p}{\rho} = \frac{V^2}{2} + \frac{\partial \Phi}{\partial t} - \frac{{v_{ref}}^2}{2} \tag{115}$$

where V and p are the local fluid velocity and pressure and $v_r ef = V_0 + \Omega \times r$ is the reference velocity due to the motion of the body.

1.11 AERODYNAMIC LOADS

Polars

A fundamental role in aerodynamic design is played by lift, drag and moments coefficients as we have already stated.
The polars are (C_D, C_L), (C_M, C_L) curves which describe global aerodynamic behaviour of the aircraft and can be used as a basis for further calculations, because of their immediate visual impact.

However they are calculated varying the flight parameters, and can give a wide knowledge of the aircraft properties in real flight conditions, for example one can consider different Mach and Reynolds numbers which are related to height, aircraft speed and dimensions. Other factors affecting the polars are the turbulence ratio (Tu), which measures the kinetic energy content associated to turbulence compared to that associated to freestream velocity, and aircraft configuration, such as deployment of control devices, spoilers and air-brakers. The amount of different polars necessary to accomplish the goals of aerodynamic design depends on the complexity of the aircraft and flight conditions.

It is also important to notice that aerodynamic data, and especially polars, are not only obtained through computational or analytical methods but also calculated from experimental data taken inside wind tunnels and flight-test campaigns.

Wing Loads

The wings are the structural parts of the aircraft that generate the biggest amount of lift, there are usually three kinds of wings on a conventional aircraft, the wing itself, the horizontal tail wing and the vertical tail wing.
Other structural parts of the aircraft such as fuselage and engines produce lift too, but the amount is often negligible compared to that of the wings and it is only considered during detailed aerodynamic design.
We can briefly synthetize the process of aerodynamic force generation as a normal stress field over the surface of the wing (mainly due to pressure) and a tangential one, which are different from the static ones: the integration of all the stresses over the entire surface gives the aerodynamic force.

When the aircraft is flying at costant altitude the global variation of momentum has a downward component, so the reaction is an upward force on the wing, namely the lift.
The lifting force is bigger than the friction tangential force of approximately one order of magnitude during most of flight conditions, therefore the lift represents well the whole aerodynamic force, unless we are dealing with particular flight maneuvers (high angles of attack).

Moreover the fact that wings are usually thin surfaces tells us that

- pressure stresses are mainly perpendicular to the direction of aircraft velocity

- tangential stresses are mainly oriented towards the direction of aircraft velocity
- hence the lift is mainly due to pressure stress field

The computation of lift on a lifting surface, that is almost equal to the whole aerodynamic force for aircraft in cruise flight, is carried out integrating the z component of the pressure difference Δp between the top and bottom part of the surface extended to the entire surface

$$L \cong \iint_S \Delta p\,(x, y)\,dxdy \tag{116}$$

$\Delta p\,(x, y)$ is the pressure distribution over the lifting surface defined on points $P(x,y,0)$ of the wing in plan-view.

Airfoil Loads

If we introduce an infinite wing which has no spanwise ending, we can section it with planes parallel to $(x,\ z)$ and call these sections "airfoils". The airfoil x-wise dimension is the length known as "chord line" c and it is usually defined as the length between the foremost and the rearest point of the airfoil [17].

Similarly to the wing load, we can assume that every airfoil generates a certain amount of lift (per span unit) $l = l(y)$ equals to the chord-wise integration of the pressure distribution

$$\mathfrak{l} \cong l\,(y) \cong \int_{c(y)} \Delta p\,(x, y)\,dx \tag{117}$$

The lift per unit span can be also non-dimensionalized as

$$C_l\,(y) = \frac{l}{\frac{1}{2}\rho_\infty V_\infty^2 c\,(y)} \tag{118}$$

$$\tag{119}$$

and this lead to the introduction of vorticity or non-dimensional airfoil load $\gamma\,(x)$,

$$C_l \cong \int_0^1 \frac{\Delta p}{\frac{1}{2}\rho_\infty V_\infty^2} d\left(\frac{x}{c}\right) = \int_0^1 \gamma d\left(\frac{x}{c}\right) \tag{120}$$

$$\gamma\left(\frac{x}{c}\right) = \frac{\Delta p}{\frac{1}{2}\rho_\infty V_\infty^2} \tag{121}$$

which can be seen as the quantity that has to be integrated over the non-dimensional chord-line to obtain the lift coefficient per unit-span.

Span-wise Loads

Total lift can be evaluated from the equation:

$$L = \int_{-\frac{b}{2}}^{+\frac{b}{2}} l\,(ydy) \tag{122}$$

and from Eq. 118 we obtain

$$L = \int_{-\frac{b}{2}}^{+\frac{b}{2}} \frac{1}{2}\rho_\infty V_\infty^2 C_l\,(y)\,c\,(y)\,dy = \frac{1}{2}\rho_\infty V_\infty^2 b^2 \int_{-1}^{1} \frac{C_l\,(y)\,c\,(y)}{2b} d\left(\frac{y}{\frac{b}{2}}\right) \tag{123}$$

And introducing the non-dimensional lift coefficient,

$$C_L = \frac{L}{\frac{1}{2}\rho_\infty V_\infty^2 S} \tag{124}$$

$$C_L = \frac{b^2}{S}\int_{-1}^{1} \frac{C_l c}{2b} d\left(\frac{y}{\frac{b}{2}}\right) = \text{Æ}\!\!\!\!R \int_{-1}^{1} \frac{C_l c}{2b} d\,(\eta) = \text{Æ}\!\!\!\!R \int_{-1}^{1} \gamma\,(\eta)\,d\eta \tag{125}$$

Where γ is the non-dimensional wing load, function of the non-dimensionalized span-wise coordinate η, and Æ is the aspect ratio of the wing.

The non-dimensional wing load is the most important quantity in aerodynamic analyses of lifting surfaces. Knowing its span-wise distribution allows to calculate many features of the aerodynamic behaviour of a lifting surface.
It gives the lift distribution over the wing, namely how loaded the η coordinate of the wing is, and it can be seen that the lift coefficient C_l and the chord length c contribute in the same proportional way to the load.

Some of the remarkable consequences of a good span-wise lift distribution are

- low induced drag
- good stall behaviour

- good load distribution on the wing structures, hence lower weights
- optimization of the configuration and integration of wing, fuselage and control surfaces

It has to be reminded that the wing load could be symmetrical or have a non-symmetrical distribution, depending on the shape of the wing and its airfoils.

2

DEVELOPMENT AND IMPLEMENTATION

The development and implementation of an unsteady vortex lattice method will be addressed following the standard sequence toward the construction of numerical solution for potential flows.

First the **type of singularity elements**, the **boundary conditions** and the **wake model** have to be considered based on the desired capability of the numerical solution to model the physical phenomenon but also on the efficiency and speed of the method. Then the process can advance to the following steps.

1. The **selection of surface singularity elements**, their distributions, order and the influence routine to calculate their velocity inductions $\Delta u, \Delta v, \Delta w$ and if necessary the potential $\Delta\Phi$.

2. The **discretization of geometry and grid generation**, that is the numerical model of an actual body submerged in the potential flow field, made by the singularities chosen before. The shape, amount and location of the singularities and their collocation points influences the convergence to a certain solution.

3. **Influence coefficients** will be calculated based on the algebraic equations obtained through the reduction of the boundary conditions. As stated in the first chapter, the influence coefficients will be gathered in an *aerodynamic influence matrix* or **AIC**.

4. The **RHS** of the matrix equations will be established based on the relative motion between the body and the fluid when the Neumann's condition is applied.

5. Once the known quantities (AIC, RHS) are calculated, the **set of equations** will be solved by standard matrix techniques.

6. The solution of the set of equations leads to the singularities strength and the velocity field, then the desired quantities such as **pressures, loads and aerodynamic coefficients** can be computed through the Bernoulli equation or via physical derivation (e. g. Kutta-Joukowski's theorem).

2.1 DEVELOPMENT

A steady vortex lattice method will be developed in this section, then the modifications required to extend the method to unsteady motion will be addressed. Indeed, as we stated in the previous chapter, the steady numerical solution can be applied to unsteady cases with the addition of a time-dependent boundary condition, an appropriate wake model and the unsteady loads.
A short overview of the main steps is shown in the diagram below.

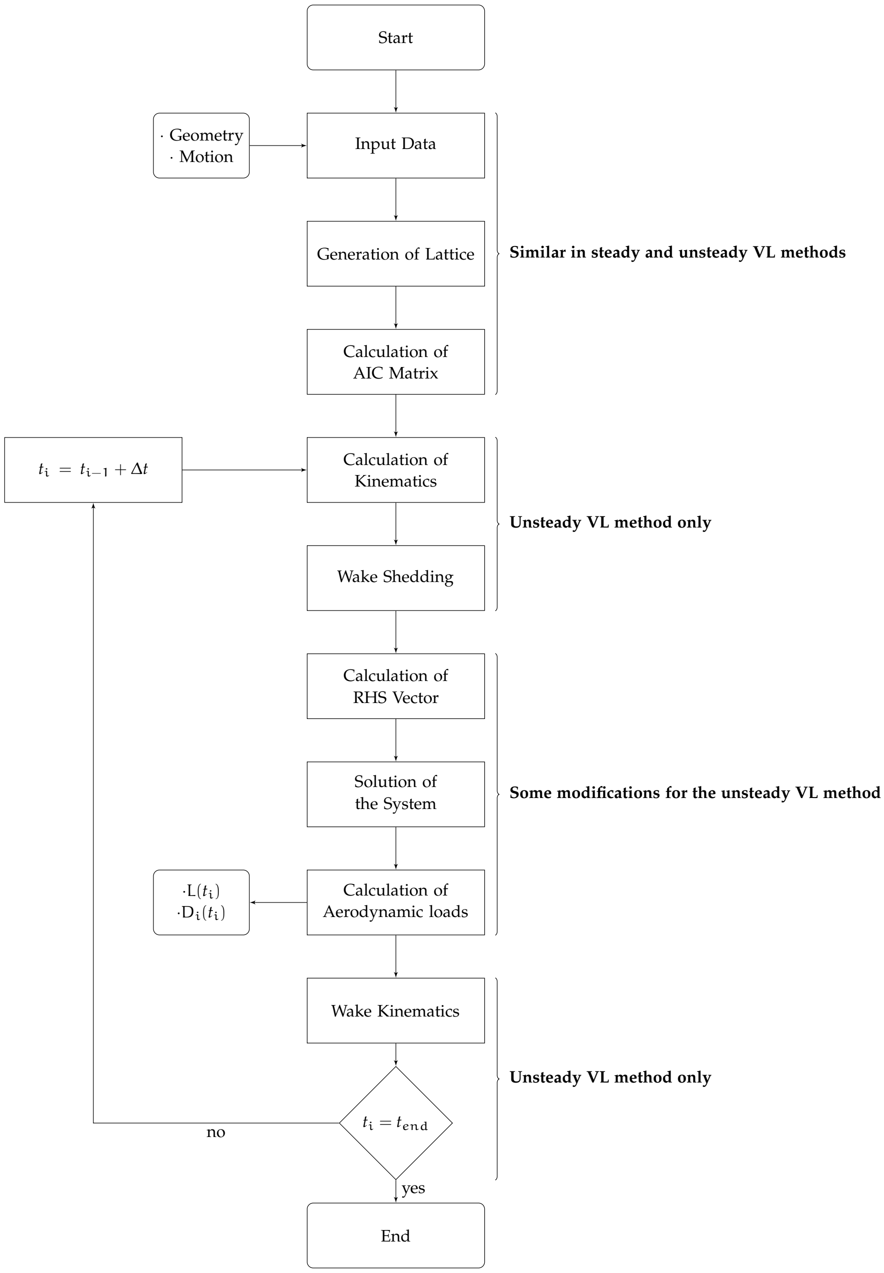

Figure 14: Steady and unsteady vortex lattice methods overview

2.1.1 *Steady Vortex Lattice Method*

The steady vortex lattice method employs the vortex-ring singularities to model the surface of a body submerged into a potential flow field to satisfy Neumann's boundary condition [9], [17], [14]. The substitution of vortex singularities into the expression of Neumann's condition of eq.97 is valid due to the equivalence of vortex distributions to doublets distribution of one order higher, demonstrated in the previous chapter.
We are interested in the aerodynamics of an arbitrary shape thin lifting-surface, that we will generally call wing, hence the choice of a vortex distribution decreases the programming effort and it is suitable as long as the effects of thickness on aerodynamic loads can be neglected.

Symmetry properties

When the wing is symmetrical and we limit our analysis to motions that generate symmetrical loads, the simplicity and the computational cost can be improved through *the method of images* [9].

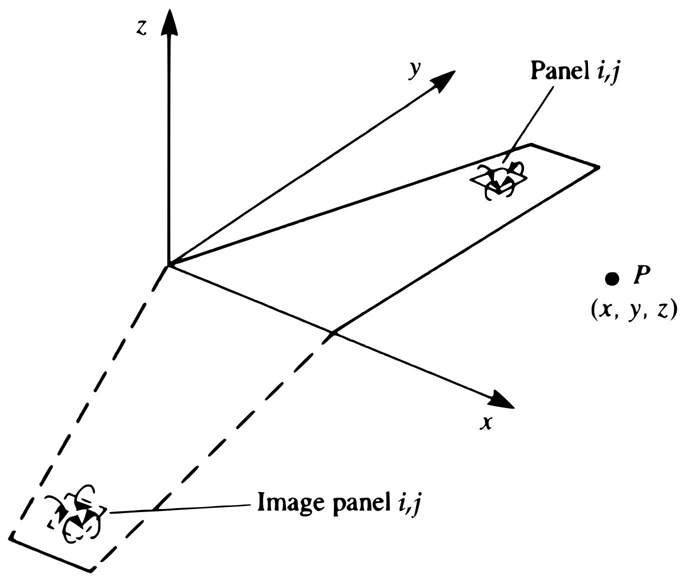

Figure 15: Image of the right-hand side of a symmetric wing model (Reproduced from [9] with modifications)

As shown in fig.15, only the right-hand side of a symmetric wing is modelled by the vortex-rings singularities and due to the fact that the corresponding singularity will have the same strength $\Gamma_{i,j}$, the influence of the left-hand side of the wing at an arbitrary point $P(x, y, z)$ will be included in the calculations evaluating the influence of the i,j panel at point P $(x, -y, z)$ and changing the sign of the v component.

When the inductions is evaluated through a routine *func_induction*, function of the point P, the singularity index i, j and strength, the velocity induced by the right-hand and left-hand sides corresponding elements at point P are

$$(u_R,\ v_R,\ w_R) = \mathit{func\_induction}\ (x,\ y,\ z,\ i,\ j,\ \Gamma_{i,\ j}) \tag{126}$$

$$(u_L,\ v_L,\ w_L) = \mathit{func\_induction}\ (x,\ -y,\ z,\ i,\ j,\ \Gamma_{i,\ j}) \tag{127}$$

and the total induction is

$$(u,\ v,\ w) = (u_R,\ v_R,\ w_R) + (u_L,\ -v_L,\ w_L) \tag{128}$$

This example shows that by applying the method of images when we evaluate the velocity induction at an arbitrary point P, we only change the y value of point P and correct the v component to take account of the left-hand side of the model, hence we reduce the number of calculations of any influence coefficient by half.

Singularity elements

The singularities employed in the current method are vortex-rings. The vortex-ring is a quadrangle with a corresponding strength Γ defined according to the right-hand rule as in fig.16, namely its circulation, that for Kelvin's theorem doesn't change along the perimeter. A normal vector $\underline{n}$ is defined in the direction of the upper surface of the wing.
The vortex-rings will form an array or lattice, over the wing, once the discretization has been established, with i and j as indexes.

The velocity induced by a vortex-ring can be calculated as the sum of the inductions of the 4 vortex-lines, shown in fig.16, as in eq.59.

First we calculate the induction for each side k of the i, j vortex-ring,

$$(u_k,\ v_k,\ w_k) = \frac{\Gamma_{i,\ j}}{4\pi} \frac{\underline{r}_{1,k} \times \underline{r}_{2,k}}{\|\underline{r}_{1,k} \times \underline{r}_{2,k}\|^2} (\underline{r}_{1,k} - \underline{r}_{2,k}) \cdot \left(\frac{\underline{r}_{1,k}}{r_{1,k}} - \frac{\underline{r}_{2,k}}{r_{2,k}} \right) \tag{129}$$

where $\underline{r}_{1,k}$ and $\underline{r}_{2,k}$ are the distances from the point $P(x,\ y,\ z)$ to the corners of the vortex-line segments, defined as follows,

$$\underline{r}_{1,k} = \left[(x - x_{1,k}),\ (y - y_{1,k}),\ (z - z_{1,k}) \right] \tag{130}$$

$$\underline{r}_{2,k} = \left[(x - x_{2,k}),\ (y - y_{2,k}),\ (z - z_{2,k}) \right] \tag{131}$$

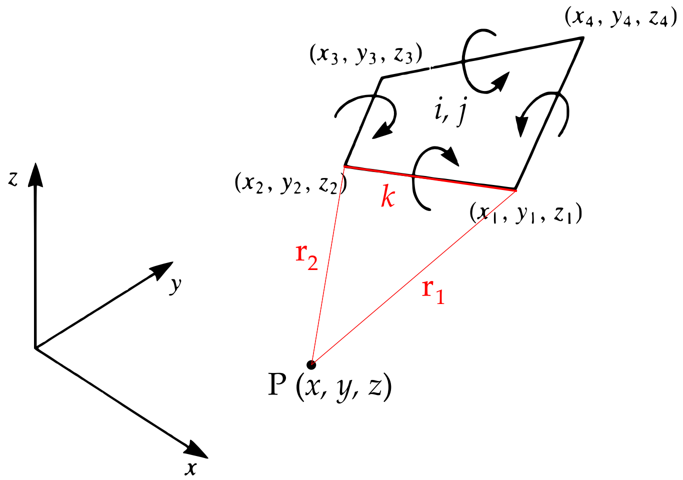

Figure 16: Example of a vortex-ring (Reproduced from [9] with modifications)

so the cross product $\underline{r}_{1,k} \times \underline{r}_{2,k}$ becomes

$$\underline{r}_{1,k} \times \underline{r}_{2,k} = \begin{bmatrix} (y - y_{1,k}) \cdot (z - z_{2,k}) - (z - z_{1,k}) \cdot (y - y_{2,k}) \\ -(x - x_{1,k}) \cdot (z - z_{2,k}) + (z - z_{1,k}) \cdot (x - x_{2,k}) \\ (x - x_{1,k}) \cdot (y - y_{2,k}) - (y - y_{1,k}) \cdot (x - x_{2,k}) \end{bmatrix} \tag{132}$$

(133)

and the dot products $(\underline{r}_{1,k} - \underline{r}_{2,k}) \cdot \underline{r}_{1,k}$ and $(\underline{r}_{1,k} - \underline{r}_{2,k}) \cdot \underline{r}_{2,k}$

$$\begin{aligned}(\underline{r}_{1,k} - \underline{r}_{2,k}) \cdot \underline{r}_{1,k} = {} & (x_{2,k} - x_{1,k})(x - x_{1,k}) + \ (y_{2,k} - y_{1,k})(y - y_{1,k}) + \\ & + (z_{2,k} - z_{1,k})(z - z_{1,k})\end{aligned} \tag{134}$$

$$\begin{aligned}(\underline{r}_{1,k} - \underline{r}_{2,k}) \cdot \underline{r}_{2,k} = {} & (x_{2,k} - x_{1,k})(x - x_{2,k}) + \ (y_{2,k} - y_{1,k})(y - y_{2,k}) + \\ & + (z_{2,k} - z_{1,k})(z - z_{2,k})\end{aligned} \tag{135}$$

then we can calculate the velocity components,

$$\begin{bmatrix} u_k \\ v_k \\ w_k \end{bmatrix} = \begin{bmatrix} K\ (\underline{r}_{1,k} \times \underline{r}_{2,k})_x \\ K\ (\underline{r}_{1,k} \times \underline{r}_{2,k})_y \\ K\ (\underline{r}_{1,k} \times \underline{r}_{2,k})_z \end{bmatrix} \tag{136}$$

where

$$K = \frac{\Gamma_{i,\,j}}{4\pi\ \|\underline{r}_{1,k} \times \underline{r}_{2,k}\|^2} \left[\frac{(\underline{r}_{1,k} - \underline{r}_{2,k}) \cdot \underline{r}_{1,k}}{r_{1,k}} - \frac{(\underline{r}_{1,k} - \underline{r}_{2,k}) \cdot \underline{r}_{2,k}}{r_{2,k}} \right] \tag{137}$$

finally we obtain the total induction of the *i*, *j* vortex-ring as a sum of the inductions of the 4 sides,

$$(u,\ v,\ w) = \sum_{k=1}^{4} (u_k,\ v_k, w_k) \tag{138}$$

These calculations can be implemented in a routine (*'func_voring'*) which will be a function of the point $P(x, y, z)$ in which we are calculating the induction, the 4 corner points of the vortex-ring (indexed and defined by the couple (i, j)) and its circulation $\Gamma_{i,\ j}$, as follows,

$$(u,\ v,\ w) = func\_voring\ (x,\ y,\ z,\ i,\ j,\ \Gamma_{i,\ j})$$

When only the velocity components induced by the trailing vortices are needed the routine to calculate the induction should implement the following expression,

$$(u,\ v,\ w)^* = (u,\ v, w)_{TRAIL.VORT.1} + (u,\ v, w)_{TRAIL.VORT.2} \tag{139}$$

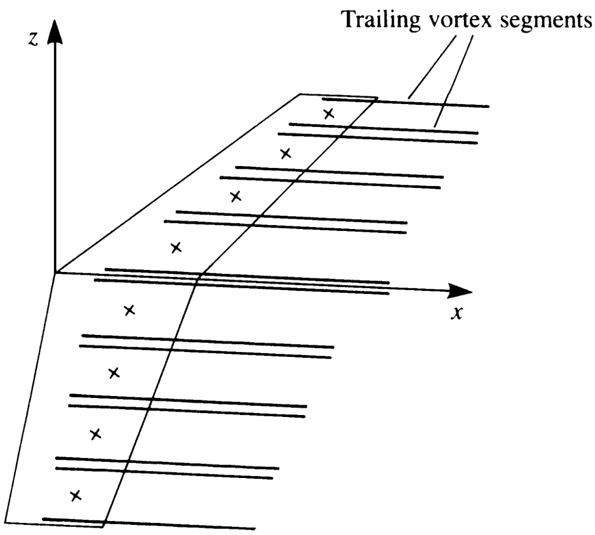

Figure 17: Example of trailing vortex segments (Reproduced from [9])

Grid generation

The leading segment of the vortex-rings is placed at 1/4 of the wing panel chord-wise length to ensure that the corresponding collocation points (CPs) are at 3/4 to satisfy the aerodynamic properties of the Pistolesi's point (neutral rear point) [17], [9]. The CPs are placed at the span-wise and chord-wise mid-point of the vortex-rings. Then the normal vector $\underline{n}$ is defined as shown in fig.18 and calculated as follows,

$$\underline{n}_{i,j} = \frac{\underline{A}_{i,j} \times \underline{B}_{i,j}}{\|\underline{A}_{i,j} \times \underline{B}_{i,j}\|} \tag{140}$$

where $\underline{A}_{i,j}$ and $\underline{B}_{i,j}$ are two vectors defining the panel opposite corners.

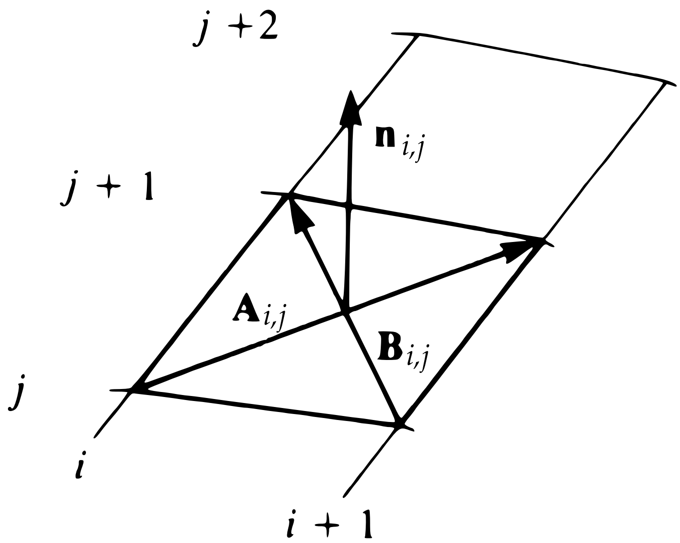

Figure 18: Definition of the vortex-ring normal

A positive Γ is defined through the right-hand rule. When computing pressure loads, recall that the local circulation is different from the circulation of the vortex-rings, being equal to the difference $\Gamma_i - \Gamma_{i-1}$. Also the Kutta condition is satisfied when the circulation at the trailing edge is canceled, hence a row of vortex-rings wake panels will be shed and their strengths will be equal to those of the last row of wing panels $\Gamma_{T.E.} = \Gamma_{wake}$.

For the right-hand side semi-wing of fig.19 the number of chord-wise divisions is $M = 4$ and the span-wise divisions is $N = 4$, investigations on the influence of the discretization on the quality of the aerodynamic analyses will be carried out in the next chapter.

Influence coefficients

At this point the aerodynamic influence matrix (AIM) must be filled with the aerodynamic influence coefficients (AIC), namely the velocity inductions on each collocation point when $\Gamma = 1$ for each bound vortex-ring. From eq.106, when the vortex-rings are the only singularities in the flow-field, we obtain the following expression for the

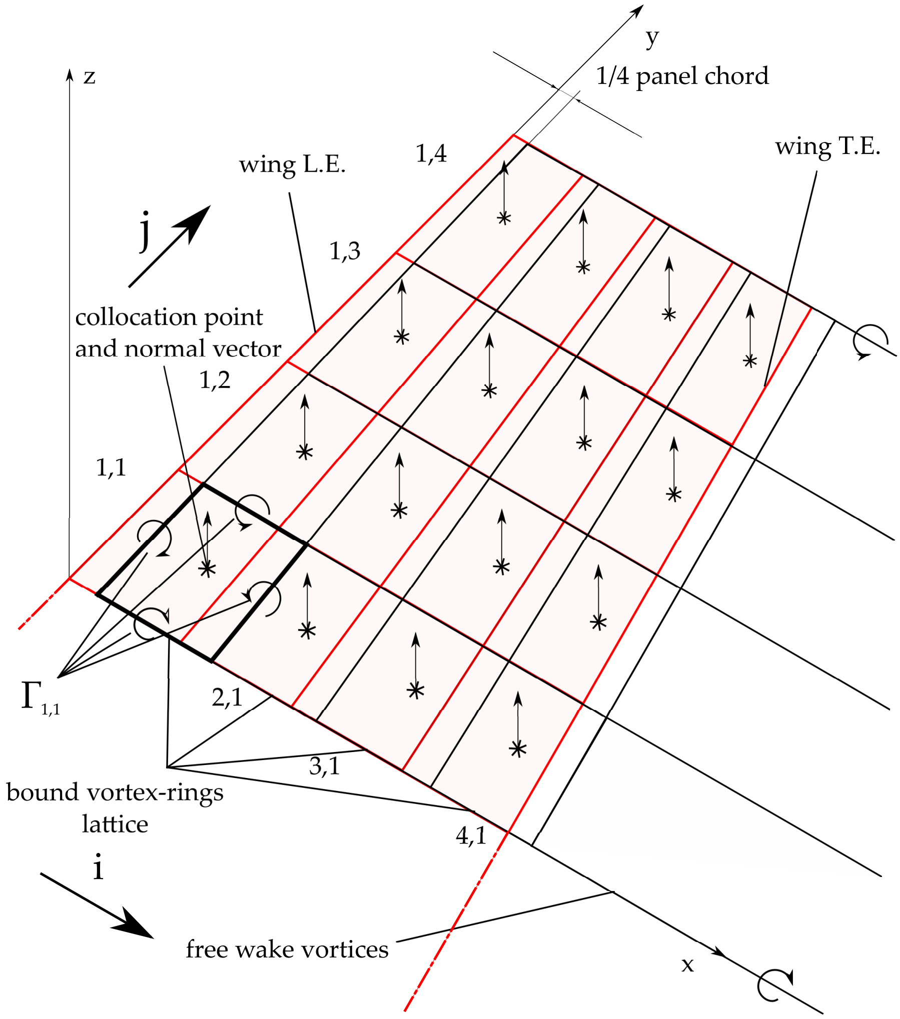

Figure 19: Right-hand side semi-wing vortex-rings arrangement

Neumann condition of no normal flow applied to the first collocation point,

$$[(u,\ v,\ w)_{11}\Gamma_1 + (u,\ v,\ w)_{12}\Gamma_2 + \cdots + \ (u,\ v,\ w)_{1m}\Gamma_m + (U_\infty,\ V_\infty,\ W_\infty)] \cdot \underline{n}_1 = 0 \tag{141}$$

where the total number of vortex-rings in the flow field is $m = M \times N$ and the strengths Γ are unknown.
The discretized form of eq.106 is

$$\begin{aligned} a_{11}\Gamma_1 + a_{12}\Gamma_2 + \cdots + \ a_{1m}\Gamma_m &= \underline{Q}_\infty \cdot \underline{n}_1 \\ a_{21}\Gamma_1 + a_{22}\Gamma_2 + \cdots + \ a_{2m}\Gamma_m &= \underline{Q}_\infty \cdot \underline{n}_2 \\ \vdots \qquad\qquad & \qquad \vdots \\ a_{m1}\Gamma_1 + a_{m2}\Gamma_2 + \cdots + \ a_{mm}\Gamma_m &= \underline{Q}_\infty \cdot \underline{n}_m \end{aligned} \tag{142}$$

hence the influence coefficients are defined as

$$a_{K,\ L} = (u,\ v,\ w)_{L,\ L} \cdot \underline{n}_K \tag{143}$$

where K and L are the loop counters of the scanning procedures defined in this section.

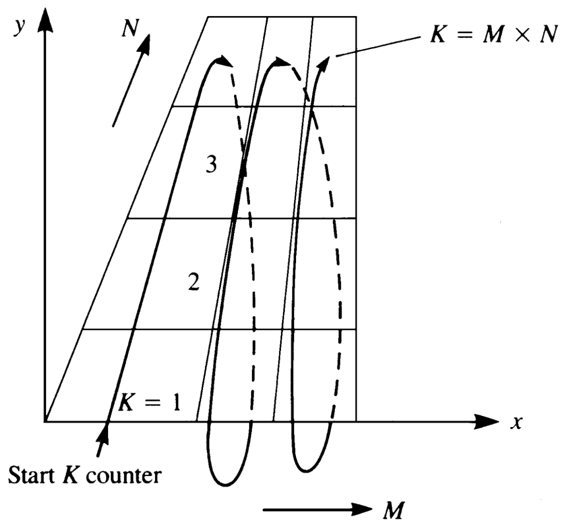

Figure 20: Collocation points scanning procedure (Reproduced from [9])

A scanning procedure, with K as sequential counter from 1 to $M \times N$, takes each collocation point, starting from the first CP(x, y, z), K = 1, of the first vortex-ring (i=1, j=1) to calculate the self-induction and the induction of the corresponding image on the left-hand side, as follows,

$$(u_R,\ v_R,\ w_R)_{11} = \mathit{func\_voring}\ (x,\ y,\ z,\ i=1,\ j=1,\ \Gamma=1.0)$$

$$(u_L,\ v_L,\ w_L)_{11} = \mathit{func\_voring}\ (x,\ -y,\ z,\ i=1,\ j=1,\ \Gamma=1.0)$$

$$(u,\ v,\ w)_{11} = (u_R,\ v_R,\ w_R)_{11} + (u_L,\ -v_L,\ w_L)_{11}$$

where the subscript $()_{11}$ represents the influence of the first vortex at the first collocation point, and both counters vary from 1 to $M \times N$. Finally the influence coefficient a_{11} is

$$a_{11} = (u,\ v,\ w)_{11} \cdot \underline{n}_1 \tag{144}$$

Another nested scanning procedure is needed to calculate the inductions of each vortex-ring of the wing surface, with a counter $L = 1 : M \times N$.
The two loops fill the matrix of eq.145,

$$[AIM] = \begin{bmatrix} a_{11}, & ..., & a_{1m} \\ \vdots & a_{KL}, & \vdots \\ a_{m,1}, & ..., & a_{mm} \end{bmatrix} \tag{145}$$

The influence coefficients for the induced downwash, obtained through the trailing vortex segments, are calculated as follows,

$$b_{11} = (u,\ v,\ w)^*_{11} \cdot \underline{n}_1 \tag{146}$$

where $(u,\ v,\ w)^*_{11}$ takes account of the trailing vortices induction.

At this point we need to clarify the influence of the wake model in the steady vortex lattice method, because we need to include the inductions of the wake panels in the calculations.

2.1.1.1 *Wake model and influence coefficients*

We fulfill the Kutta condition at the trailing edge by fixing the same circulation $\Gamma_{T.E.} = \Gamma_{wake}$ for the last row of wing panels and the corresponding wake panels.
The wake panels are defined as shown in fig.21, the first side lays on the trailing edge and the corner points correspond to those of the wing panels, while the opposite side should be as far as possible [9], [14].

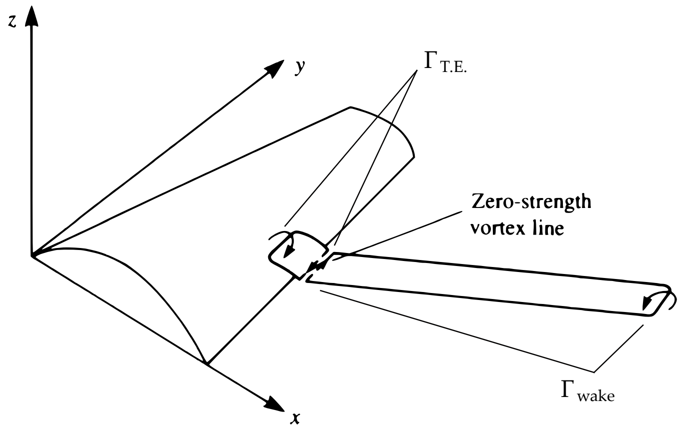

Figure 21: Kutta's condition for the steady wake model (Reproduced from [9] with modifications)

The velocity induction of the wake panels is taken into account every time the scanning procedure for the bound vortex-rings reaches the last row of wing panels, that is when $i = M$ or $L = m$, and for the first CP ($j = 1$), it is calculated as follows,

$$(u_R,\ v_R,\ w_R)_{1mW} = func\_voring\ (x,\ y,\ z,\ i = M+1,\ j = 1,\ \Gamma = 1.0)$$

$$(u_L,\ v_L,\ w_L)_{1mW} = func\_voring\ (x,\ -y,\ z,\ i = M+1,\ j = 1,\ \Gamma = 1.0)$$

$$(u,\ v,\ w)_{1mW} = (u_R,\ v_R,\ w_R)_{1mW} + (u_L,\ -v_L,\ w_L)_{1mW}$$

where $i = M + 1$ is considered to be the counter for the wake vortex-ring elements.

Finally we obtain the influence coefficient with the wake induction,

$$a_{1m} = [(u,\ v,\ w)_{1m} + (u,\ v,\ w)_{1mW}] \cdot \underline{n}_1 \tag{147}$$

RHS

The RHS vector of eq.142 is computed scanning the $M \times N$ collocation points,

$$\text{RHS}_K = -\underline{Q}_\infty \cdot \underline{n}_K \tag{148}$$

Solver

Once the AIM and the RHS vector are computed, the algebraic set of equations can be solved, and it leads to the computation of the unknown strength ΓK of the bound vortex-rings.

The set of equation is

$$\begin{pmatrix} a_{11}, & a_{12}, & ..., & a_{1m} \\ a_{21}, & a_{22}, & ..., & a_{2m} \\ \vdots & \vdots & & \vdots \\ a_{m1}, & a_{m2}, & ..., & a_{mm} \end{pmatrix} \begin{pmatrix} \Gamma_1 \\ \Gamma_2 \\ \vdots \\ \Gamma_m \end{pmatrix} = \begin{pmatrix} RHS_1 \\ RHS_2 \\ \vdots \\ RHS_m \end{pmatrix} \tag{149}$$

and it needs a matrix inversion(of order m) to be solved.

Pressure and loads

Once the $\Gamma_{i,j}$ have been calculated, the fastest way to calculate the total lift generated by the wing is to apply the Kutta-Joukowski theorem to each bound vortex segment [9].
So the increment of lift per vortex segment is

$$\Delta L_{i,\,j} = \rho V_\infty \Gamma_{i,\,j} \Delta y_{i,\,j}, \quad \text{when } i = 1 \tag{150}$$

$$\Delta L_{i,\,j} = \rho V_\infty (\Gamma_{i,\,j} - \Gamma_{i-1,\,j}) \Delta y_{i,\,j}, \quad \text{when } i > 1 \tag{151}$$

and the total lift and the corresponding lift coefficient are

$$L = 2 \times \sum_{i=1}^{M} \sum_{j=1}^{N} \Delta L_{i,\,j} \tag{152}$$

$$C_L = \frac{L}{\frac{1}{2} V_\infty^2 S_{ref}} \tag{153}$$

The pressure on every panel is

$$\Delta p_{i,\,j} = \frac{\Delta L_{i,\,j}}{\Delta S_{i,\,j}} \tag{154}$$

Similarly to the thin-lifting surface theory, and with its limitations, the drag is calculated through the downwash of the trailing vortex segments, solving the following set of equations,

$$\begin{pmatrix} w_{ind,1} \\ w_{ind,2} \\ \vdots \\ w_{ind,m} \end{pmatrix} = \begin{pmatrix} b_{11}, & b_{12}, & ..., & b_{1m} \\ b_{21}, & b_{22}, & ..., & b_{2m} \\ \vdots & \vdots & & \vdots \\ b_{m1}, & b_{m2}, & ..., & b_{mm} \end{pmatrix} \begin{pmatrix} \Gamma_1 \\ \Gamma_2 \\ \vdots \\ \Gamma_m \end{pmatrix} \tag{155}$$

so the drag increments per panel are

$$\Delta D_{i,\,j} = -\rho w_{i,\,j}\Gamma_{i,\,j}\Delta y_{i,\,j} \quad \text{when } i = 1 \tag{156}$$

$$\Delta D_{i,\,j} = -\rho w_{i,\,j}(\Gamma_{i,\,j} - \Gamma_{i-1,\,j})\Delta y_{i,\,j} \quad \text{when } i > 1 \tag{157}$$

and the total drag and the drag coefficient are

$$D = 2 \times \sum_{i=1}^{M}\sum_{j=1}^{N} \Delta D_{i,\,j} \tag{158}$$

$$C_D = \frac{D}{\frac{1}{2}V_\infty^2 S_{ref}} \tag{159}$$

2.1.2 *Unsteady Vortex Lattice Method*

The following method is based on the steady vortex lattice method solution with the modifications needed to treat unsteady motion.
The wing and the wake are modelled by the same vortex-ring elements that we used in the steady-state method. The solution is now based on a time-stepping technique, since we need to update the boundary condition (i. e. the solution of the set of equations 149) for each time step included in the calculation. We assume a prescribed kinematics time history of the wing, between the starting time $t = 0$ to an arbitrary final time $t = t_{fin}$. We also assume that the wing standed still before the first time step $t = \Delta t$ and only the $m = M \times N$ bound vortex-rings are present.
A solution to the system 149 doesn't require any additional condition since we apply the boundary condition on the corresponding m collocation points to calculate a vector of m strengths Γ_t (the physical condition is the Kelvin condition and it is inherently satisfied by the geometry of the vortex rings).
A wake model has to be implemented during the second time step $t = 2\Delta t$, as the wing moves on its flight path and a row of wake vortex-rings is shed at the trailing edge, adding N Γ_{wake} new unknown strengths. In the case of our interest the shedding procedure assing the strength $\Gamma_{wake} = \Gamma_{T.E.,t-1}$, that is the steady Kutta condition extension to unsteady motion. The system 149 has still m unknown strengths Γ_t and the velocity induction of the N wake vortex-rings has to be calculated.
The scheme of the first two time-steps is shown in fig.22.

This time-stepping technique can be applied until the final time has been reached, and at each time step the wake can be moved according to the velocity induced on the corner points of the wake vortex-rings introducing a *wake roll-up* routine.

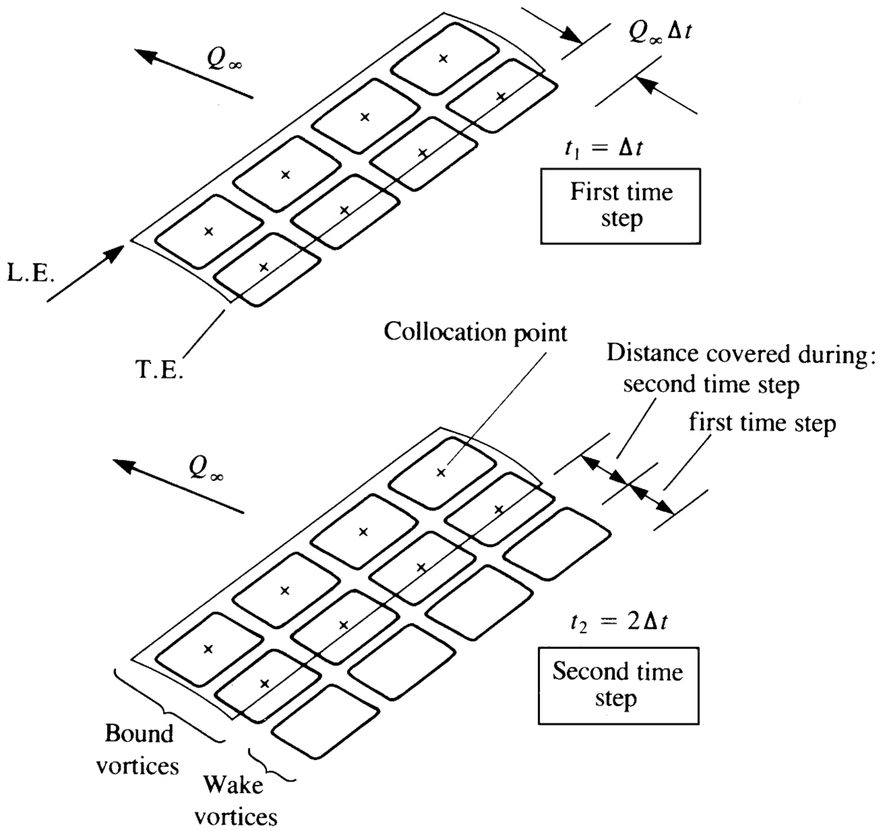

Figure 22: Unsteady vortex-lattice method scheme for the first two time-steps (Reproduced from [9])

Symmetry properties

As it was shown in fig.15, once again only symmetrical geometry can be modelled due to the limitations of the the method of images, with the advantage of reducing the number of calculations of influence coefficients and velocity inductions by half.
Being based on the hypothesis that any vortex ring modelling the right-hand side of the wing has the same circulation strength Γ of the corresponding vortex-ring on the left-hand side, the method of images can be applied only when the motion generates a symmetrical distribution of circulation and, as a consequence of it, of pressures and loads.

The linear velocities in the inertial reference frame (IRF), U, W, and the angular velocity in the body reference frame (BRF) q shown in blue in fig.23) only generate symmetrical distribution of circulation, hence we will assume that the other velocities (shown in red in fig.23) are null.

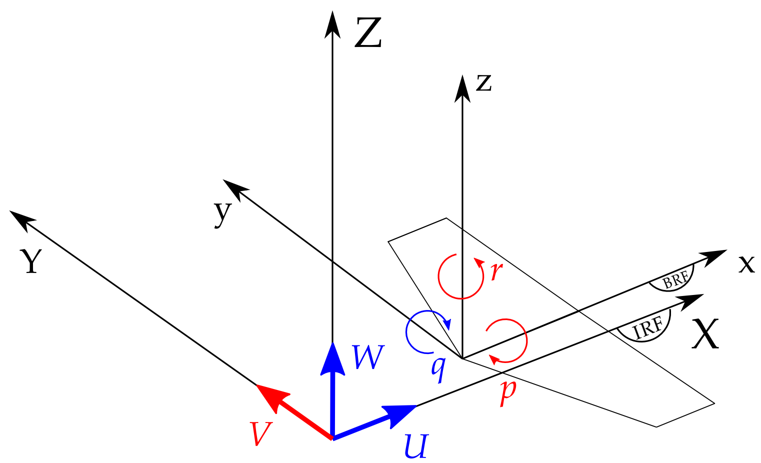

Figure 23: Linear and angular velocities vectors in the IRF and BRF

Singularity elements

The singularity elements used in the unsteady vortex-lattice method are the same vortex-rings employed in the steady method.
The vortex-rings are defined by the four corner points coordinates, a corresponding strength Γ defined according to the right-hand rule and the normal vector $\underline{n}$ in the direction of the upper surface of the

wing.

The velocity induced by a vortex-ring can be still calculated through the velocities induced by the four vortex-segments composing the quadrangle (as in eq.s 129 and 136), obtaining the sum

$$(u,\ v,\ w) = \sum_{k=1}^{4} (u_k,\ v_k, w_k) \tag{160}$$

hence the sum of eq.60 can be implemented in a routine ('*func_voring*') that will be employed to calculate the induction of a vortex-ring defined by the couple (i, j)) and the strength $\Gamma_{i,\,j}$ on the point $P(x, y, z)$, as follows,

$$(u,\ v,\ w) = \mathit{func\_voring}\ (x,\ y,\ z,\ i,\ j,\ \Gamma_{i,\,j})$$

When only the velocity components induced by the trailing vortices are needed the routine to calculate the induction should implement the following expression,

$$(u,\ v,\ w)^* = (u,\ v, w)_{TRAIL.VORT.1} + (u,\ v, w)_{TRAIL.VORT.2} \tag{161}$$

Kinematics

First we define a stationary inertial frame of reference (IRF) and a body reference frame (BRF) attached to the wing, with the origin at the intersection between the leading-edge and the axis of symmetry of the wing. At the initial time the IRF and the BRF origins and directions overlap.
The prescribed flight path, which define the kinematics of the wing, can be accounted for in terms of the linear velocities in the IRF and the angular velocities in the BRF.

Considering the hypothesis of symmetrical distribution of loads, as it was shown in fig.23, the velocities time histories that must be given as an input are

$$U(t) = \frac{\mathrm{d}X(t)}{\mathrm{d}t}, \quad W(t) = \frac{\mathrm{d}Z(t)}{\mathrm{d}t} \tag{162}$$

which are the two components of the velocity of the origin of the BRF with respect to the IRF, in the IRF, and $q(t)$ which represents the velocity of the rotation of the BRF around its y axis.

At this point we define a transformation between the IRF and BRF coordinates systems, that is necessary when the Neumann condition is expressed in the BRF, hence the velocity components are expressed in the x, y, z coordinates system. Following the calculations developed in [13] the coordinates of a vector expressed in the IRF (v_X, v_Y, v_Z) can be transformed into the BRF coordinates (v_x, v_y, v_z) with a transformation matrix (also called direction cosine matrix) involving the three Euler angles, ϕ, θ, ψ,

$$\begin{pmatrix} v_x \\ v_y \\ v_z \end{pmatrix} = \begin{bmatrix} C_\theta C_\psi & C_\theta S_\psi & -S_\theta \\ S_\phi S_\theta C_\psi - C_\phi S_\psi & S_\phi S_\theta S_\psi + C_\phi C_\psi & S_\phi C_\theta \\ C_\phi S_\theta C_\psi + S_\phi S_\psi & C_\phi S_\theta S_\psi - S_\phi C_\psi & C_\phi C_\theta \end{bmatrix} \begin{pmatrix} v_X \\ v_Y \\ v_Z \end{pmatrix} \tag{163}$$

where the three Euler angles are the three elemental rotations defined by the sequence shown in fig.24, and the inverse transformation is

$$\begin{pmatrix} v_X \\ v_Y \\ v_Z \end{pmatrix} = \begin{bmatrix} C_\theta C_\psi & S_\phi S_\theta C_\psi - C_\phi S_\psi & C_\phi S_\theta C_\psi + S_\phi S_\psi \\ C_\theta S_\psi & S_\phi S_\theta S_\psi + C_\phi C_\psi & C_\phi S_\theta S_\psi - S_\phi C_\psi \\ -S_\theta & S_\phi C_\theta & C_\phi C_\theta \end{bmatrix} \begin{pmatrix} v_x \\ v_y \\ v_z \end{pmatrix} \tag{164}$$

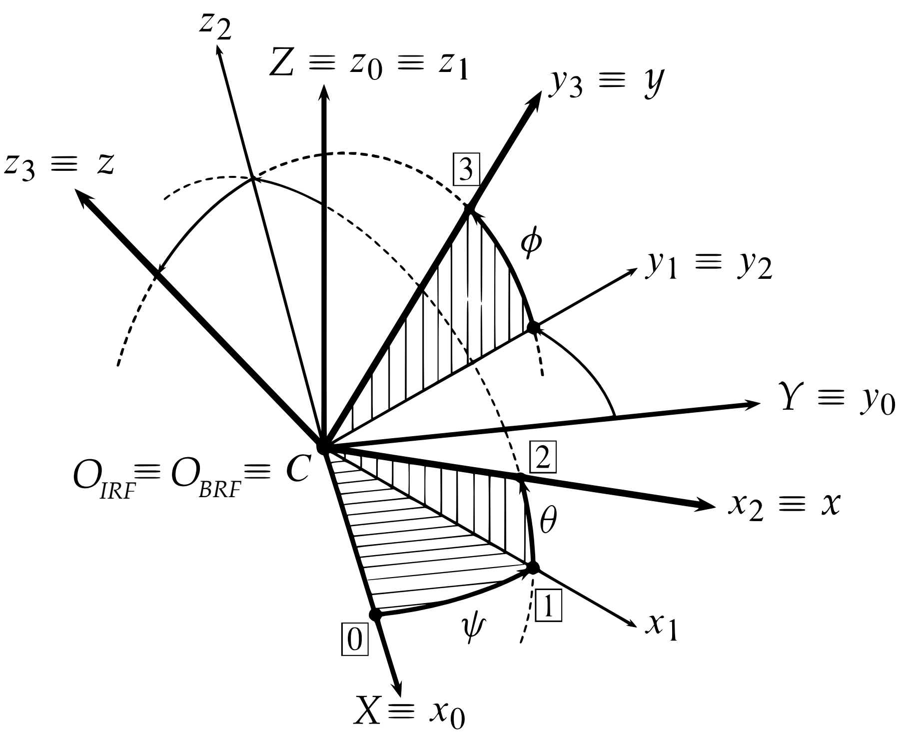

Figure 24: Sequence of the Euler angles rotations from X, Y, Z to x, y, z (Reproduced from [13] with modifications)

The two matrices are often called $[T_{I\rightarrow B}]$ and $[T_{B\rightarrow I}]$ where the indices I stands for inertial and B for body.

At each time-step, when the position of the BRF has to be calculated, the integration of the known velocity vector in the IRF has to be carried out, while the attitude in terms of the Euler angles could be calculated through the integration of the rate of variation of the Euler angles, given by the formula,

$$\begin{pmatrix} \dot{\phi} \\ \dot{\theta} \\ \dot{\psi} \end{pmatrix} = \begin{bmatrix} 1 & \frac{S_\phi S_\theta}{C_\theta} & \frac{C_\phi S_\theta}{C_\theta} \\ 0 & C_\phi & -S_\phi \\ 0 & \frac{S_\phi}{C_\theta} & \frac{C_\phi}{C_\theta} \end{bmatrix} \begin{pmatrix} p \\ q \\ r \end{pmatrix} \tag{165}$$

The presence of the C_θ at the denominator in the matrix generates a singularity when $\theta \rightarrow \frac{\pi}{2}$ or $\theta \rightarrow -\frac{\pi}{2}$, moreover the non-linearity in the elements of the matrix increases the computational effort, hence a transformation based on quaternions will be used in the current development of the method.

The Eulero-Rodrigues quaternion parameters are based on the Euler's rotation theorem, which states that any BRF attitude can be expressed by one angle (μ) and a corresponding axis of rotation (defined by the versor $\underline{e}$), so the quaternion components are defined as follows,

$$\begin{pmatrix} q_0 \\ q_x \\ q_y \\ q_z \end{pmatrix} = \begin{pmatrix} \cos\frac{\mu}{2} \\ e_x \sin\frac{\mu}{2} \\ e_y \sin\frac{\mu}{2} \\ e_z \sin\frac{\mu}{2} \end{pmatrix} \tag{166}$$

and as it is shown in [13], the rate of variation of quaternion components is related to the angular velocities in the BRF through the following linear set of equations,

$$\begin{pmatrix} \dot{q_0} \\ \dot{q_x} \\ \dot{q_y} \\ \dot{q_z} \end{pmatrix} = \frac{1}{2} \begin{bmatrix} 0 & -p & -q & -r \\ p & 0 & r & -q \\ q & -r & 0 & p \\ r & q & -p & 0 \end{bmatrix} \begin{pmatrix} q_0 \\ q_x \\ q_y \\ q_z \end{pmatrix} \tag{167}$$

where $p = 0$ and $r = 0$ for symmetrycal motion, and this formulation can be integrated to evaluate the attitude of the BRF in terms of the quaternion components and then transformed back into the Euler angles, that can be used in the transformation matrices.

The velocity of the origin of the BRF with respect to the IRF, in BRF coordinates are obtained through the following transformation,

$$\begin{pmatrix} u \\ v \\ w \end{pmatrix} = [\mathsf{T}_{\mathrm{I}\to\mathrm{B}}] \begin{pmatrix} U \\ V \\ W \end{pmatrix} \tag{168}$$

where $V = 0$ for symmetrycal motion.

Grid generation

The process that leads to the generation of a lattice of vortex-rings on the wing follows the same steps of the steady vortex lattice method grid generation. The right-hand side of the wing is divided into M rows and N columns, so the total amount of panels is $m = M \times N$. The leading-edge of the vortex-rings are placed on the panel $\frac{1}{4}$ chordwise length, and the collocation points are at $\frac{3}{4}$ of the same length. An example of the arrangement of the vortex-lattice for the UVLM is given in fig.25, which is similar to fig.19, but a new reference frame is present (in which the two velocities U and W are defined) and the wake is modelled by a similar set of vortex-rings.

Once the wing has been modelled, since we are dealing with unsteady motion, the wake becomes time-dependent and a shedding procedure has to be addressed. The physical condition that has to be satisfied is the unsteady extension to the steady Kutta's condition, that means the circulation at the trailing edge should vanish somehow. At the first time step the m bound vortex-rings have m unknown strengths and no wake is shed. At the second time-step the circulation of the m bound vortex rings from the previous time-step is known and we can apply the equivalent of Kutta's condition for unsteady methods.

A new row of wake vortex-rings is shed from the trailing-edge of the wing lattice, as it can be seen in fig.26, at each time-step t_i following these rules:

- The wake-shedding procedure scans all columns ($j = 1 : N$) to create one wake panel for each column.

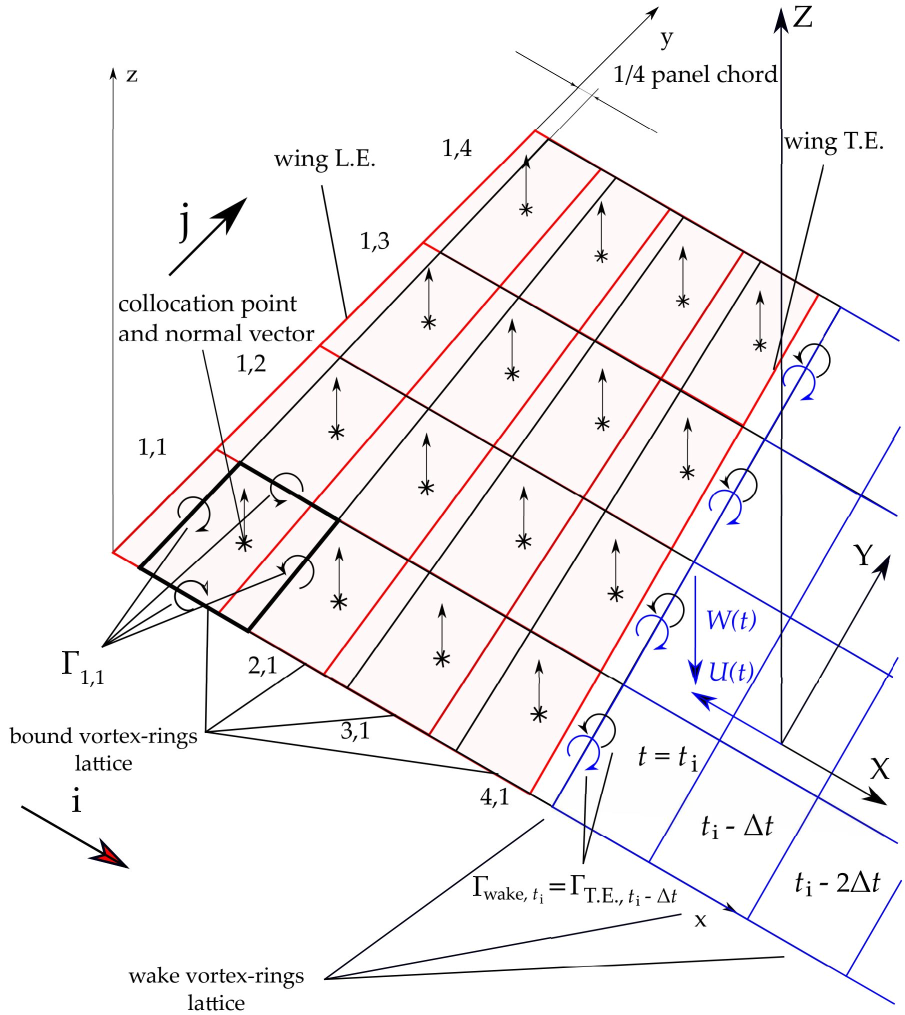

Figure 25: Right-hand side semi-wing vortex-rings arrangement for UVLM

- The leading-segment corner points of a wake vortex-ring with index j as column index, correspond to the corner points of the trailing-segment of the last row bound vortex-ring, with index j indicating the column, at the current time step (t_i).
- At the second time step (t_2) the trailing-segment corner points of a wake vortex-ring with index j as column index, correspond to the corner points of the trailing-segment of the last row bound vortex-ring, with the same index j, at the first time step (t_1).
- At any other time step (t_i) the trailing-segment corner points of a wake vortex-ring correspond to the corner points of the leading-segment of the last row of wake vortex-rings, with the same index j, at the previous time step (t_{i-1}).
- The length of the wake panels is related to the space travelled by the wing during the time-step interval, $c_{wake,p} = Q_{\infty}\Delta t$.
- The strength of the wake vortex-rings at the current time step is equal to the strengths of the corresponding column last row of bound vortex-rings, $\Gamma_{wake,\mathtt{textitt}_i} = \Gamma_{wake,\mathtt{textitt}_{i-1}}$.

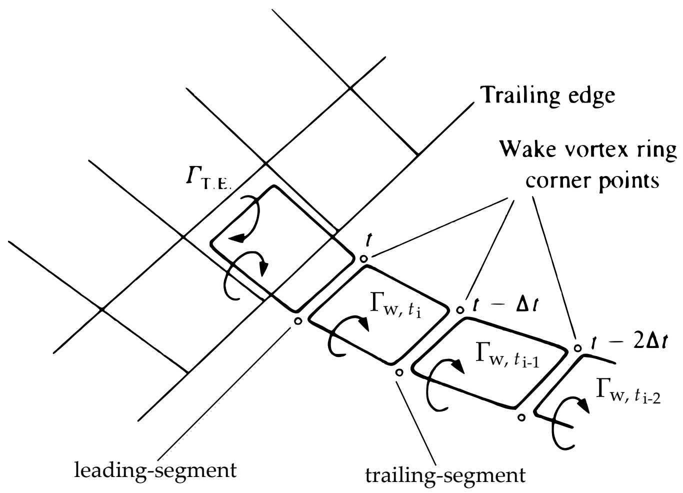

Figure 26: Example of wake shedding (Reproduced from [9] with modifications)

Influence coefficients

The aerodynamic influence matrix (AIM) and the corresponding elements called aerodynamic influence coefficients (AIC), namely the velocity inductions on each collocation point when $\Gamma = 1$ for each bound vortex-ring, can be calculated by the same formulas obtained in the steady VLM. From eq.106, when the vortex-rings are the only singularities in the flow-field, ensuring the Neumann condition of no normal flow on the m collocation points means that we calculate the

self-induction of the wing, the wake induction and the relative velocity of the wing with respect to the fluid.
The wake induction and the relative velocity at each time-step are known quantities because the wake strengths are fixed with the Kutta condition and the flight path is prescribed. The self-induction of the wing, when the geometry is fixed, only depends on the m unknown strengths. Therefore the AIM (filled by the coefficients of self-induction) can be calculated once before the time-stepping loop begins.

Once again, two scanning procedures loop for each collocation point and for each self-induction of the vortex-rings composing the wing model, hence the influence of the vortex-ring L on the collocation point K is computed through,

$$a_{K\,L} = (u,\ v,\ w)_{K\,L} \cdot \underline{\mathrm{n}}_K \tag{169}$$

where the velocity induction is obtained through the same routines,

$$(u_\mathrm{R},\ v_\mathrm{R},\ w_\mathrm{R})_{11} = \mathit{func\_voring}\ (x,\ y,\ z,\ i=1,\ j=1,\ \Gamma=1.0)$$

$$(u_\mathrm{L},\ v_\mathrm{L},\ w_\mathrm{L})_{11} = \mathit{func\_voring}\ (x,\ -y,\ z,\ i=1,\ j=1,\ \Gamma=1.0)$$

$$(u,\ v,\ w)_{11} = (u_\mathrm{R},\ v_\mathrm{R},\ w_\mathrm{R})_{11} + (u_\mathrm{L},\ -v_\mathrm{L},\ w_\mathrm{L})_{11}$$

The influence coefficients for the induced downwash, obtained through the trailing vortex segments, are calculated as follows,

$$b_{11} = (u,\ v,\ w)^*_{11} \cdot \underline{\mathrm{n}}_1 \tag{170}$$

where $(u,\ v,\ w)^*_{11}$ takes account of the trailing vortices induction.

RHS

In the unsteady extension of the vortex-lattice method, the Neumann's condition, which allows the computation of pressures and loads on the surface of the body, has to be updated at each time-step. The RHS vector represents the known quantities in the discretized form of the zero normal velocity boundary condition applied to the $M \times N$ collocation points.
The total induction at the time-step $t = t_\mathrm{i}$ on an arbitrary collocation point K is

$$\Big\{(u,\ v,\ w)_{K1}\Gamma_1 + (u,\ v,\ w)_{K2}\Gamma_2 + \cdots + \ (u,\ v,\ w)_{Km}\Gamma_m + \\ + \Big[\Big(u(x,y,z,t_\mathrm{i}),\ v(x,y,z,t_\mathrm{i}),\ w(x,y,z,t_\mathrm{i})\Big) + (u,\ v,\ w)_{wake}\Big]\Big\} \cdot \underline{\mathrm{n}}_K = 0 \tag{171}$$

where $(u(t_i),\ v(t_i),\ w(t_i))$ is the kinematic velocity at the collocation point defined by the coordinates (x, y, z), expressed in the BRF, calculated as follows,

$$\begin{pmatrix} u(x,y,z,t_i) \\ v(x,y,z,t_i) \\ w(x,y,z,t_i) \end{pmatrix} = \left[\mathsf{T}_{I \to B}\right]_{t_i} \begin{pmatrix} U(t_i) \\ V(t_i) \\ W(t_i) \end{pmatrix} + \begin{pmatrix} -q(t_i)z + r(t_i)y \\ -r(t_i)x + p(t_i)z \\ -p(t_i)y + q(t_i)x \end{pmatrix} \tag{172}$$

and $(u,\ v,\ w)_{wake}$is the wake total-induction on the collocation point, that can be calculated with a loop on the wake vortex-rings, since their strengths are known.
Consequently a right-hand side is defined by the formula

$$\begin{aligned} \mathsf{RHS}_K(t_i) = -\Big\{ &\Big[u(x,\ y,\ z,\ t_i),\ v(x,\ y,\ z,\ t_i),\ w(x,\ y,\ z,\ t_i)\Big] + \\ &+ (u,\ v,\ w)_{wake}\Big\} \cdot \underline{\mathrm{n}}_K \end{aligned} \tag{173}$$

Solver

When the geometry of the wing is fixed the AIM coefficients don't change at each time-step, hence only the RHS vector needs to be updated, finally the algebraic set of equations can be solved, and it leads to the computation of the unknown strength ΓK of the bound vortex-rings.

At each time step a new the set of equation is

$$\begin{pmatrix} a_{11}, & a_{12}, & \dots, & a_{1m} \\ a_{21}, & a_{22}, & \dots, & a_{2m} \\ \vdots & \vdots & & \vdots \\ a_{m1}, & a_{m2}, & \dots, & a_{mm} \end{pmatrix} \begin{pmatrix} \Gamma_1(t_i) \\ \Gamma_2(t_i) \\ \vdots \\ \Gamma_m(t_i) \end{pmatrix} = \begin{pmatrix} \mathsf{RHS}_1(t_i) \\ \mathsf{RHS}_2(t_i) \\ \vdots \\ \mathsf{RHS}_m(t_i) \end{pmatrix} \tag{174}$$

where the matrix inversion(of order m), to calculate the coefficients that solve the system, is provided only once at the first-time step.

Pressure and loads

The forces evaluation is based on the unsteady form of Bernoulli's equation, that, in terms of the local pressure, is

$$\frac{p_{\mathrm{ref}} - p}{\rho} = \frac{Q^2}{2} + \frac{\partial \Phi}{\partial t} - \frac{{q_{\mathrm{ref}}}^2}{2} \tag{175}$$

where $\underline{q}_{\mathrm{ref}} = -(u(x,y,z,t_{\mathrm{i}}),\ v(x,y,z,t_{\mathrm{i}}),\ w(x,y,z,t_{\mathrm{i}}))$ is the local kinematic velocity, $\underline{Q}$ is the local total velocity of the fluid and p_{ref} is a reference pressure.
When the body is modelled by a thin surface, therefore the force acting on the panels is given by the pressure gap between the two surfaces, eq.175 can be re-written considering the difference of the pressure on the upper and lower faces (Δp) of the panels as follows,

$$\Delta p = p_{\mathrm{low}} - p_{\mathrm{up}} = \rho \left[\left(\frac{Q_{\mathrm{t}}^2}{2} \right)_{\mathrm{up}} - \left(\frac{Q_{\mathrm{t}}^2}{2} \right)_{\mathrm{low}} + \left(\frac{\partial \Phi}{\partial t} \right)_{\mathrm{up}} - \left(\frac{\partial \Phi}{\partial t} \right)_{\mathrm{low}} \right] \tag{176}$$

where the subscript 't' stands for *tangential* and the tangential velocity is found from

$$Q_{\mathrm{t,up},\,k} = \Big[(u,\ v,\ w)\ + (u,\ v,\ w)_{wake} \Big]_k \cdot \underline{\tau}_k + \frac{\partial \Phi}{\partial \tau_k} \tag{177}$$

$$Q_{\mathrm{t,low},\,k} = \Big[(u,\ v,\ w)\ + (u,\ v,\ w)_{wake} \Big]_k \cdot \underline{\tau}_k + \frac{\partial \Phi}{\partial \tau_k} \tag{178}$$

where $\underline{\tau}_k$ is the tangential vector of the k vortex-segment and the tangential derivative of the potential Φ, from the thin airfoil potential theory, is

$$\left(\frac{\partial \Phi}{\partial \tau_k} \right)_{\mathrm{up}} \approx \frac{\Gamma_k}{2\ \Delta l_k} \tag{179}$$

$$\left(\frac{\partial \Phi}{\partial \tau_k} \right)_{\mathrm{low}} \approx -\frac{\Gamma_k}{2\ \Delta l_k} \tag{180}$$

where l_k is the length of the k vortex-segment. The tangential velocity due to the wing vortices will have two components for each $i,\ j$ panel, in the two directions $i,\ j$ of the vortex-segments, and it can be approximated as

$$\pm \frac{\partial \Phi}{\partial \tau_i} \approx \pm \frac{\Gamma_{i,\,j} - \Gamma_{i-1,\,j}}{2\ \Delta c_{i,\,j}} \tag{181}$$

$$\pm \frac{\partial \Phi}{\partial \tau_j} \approx \pm \frac{\Gamma_{i,\,j} - \Gamma_{i,\,j-1}}{2\ \Delta b_{i,\,j}} \tag{182}$$

$$\tag{183}$$

where $\pm$ represents the upper and lower surfaces, respectively, and $\Delta c_{i,\,j}$ and $\Delta b_{i,\,j}$ are the panel lengths in the i_{th} and j_{th} directions, respectively.

The velocity-potential derivative is obtained considering that for the vortex ring model $\Delta\Phi = \Gamma$, then

$$\pm\frac{\partial \Phi_{i,\,j}}{\partial t} = \pm\frac{\partial}{\partial t}\frac{\Gamma_{i,\,j}}{2} \tag{184}$$

$$\tag{185}$$

A discretized form of the pressure difference for the $i,\ j$ panel is

$$\begin{aligned}\Delta p_{i,\,j} =& \rho\Bigg[(u+u_w,\ v+v_w,\ w++w_w)_{i,\,j}\cdot \underline{\tau}_i\ \frac{\Gamma_{i,\,j}-\Gamma_{i-1,\,j}}{2\ \Delta c_{i,\,j}} + \\ &+\ (u+u_w,\ v+v_w,\ w++w_w)_{i,\,j}\cdot \underline{\tau}_j\ \frac{\Gamma_{i,\,j}-\Gamma_{i,\,j-1}}{2\ \Delta b_{i,\,j}} + \frac{\partial}{\partial t}\Gamma_{i,\,j}\Bigg]\end{aligned} \tag{186}$$

The force generated by each panel is then

$$\Delta \underline{F} = -(\Delta p\ \Delta S)_{i,\,j}\underline{n}_{i,\,j} \tag{187}$$

And the total force is obtained by adding all the contribution of the panels.

Wake Roll-up

The vortex-rings modelling the wake must satisfy another physical condition at each time step. Since they represent a force-free surface they must move according to the local stream velocity, which is the sum of the inductions of the singularities and the free stream velocity. A scanning procedure takes each wake vortex-ring corner point, calculate the induction, and then performs the motion of the wake vortex-rings.

First the induction on the corner point indicated by the counter l is computed with the same routine used in the influence coefficients calculation,

$$
\begin{aligned}
(u_{\mathrm{R}},\ v_{\mathrm{R}},\ w_{\mathrm{R}})_l =& \sum_{i=1}^{M}\sum_{j=1}^{N} func\_voring\ (x,\ y,\ z,\ i,\ j,\ \Gamma_{i,\ j})+\\
&+\sum_{K=1}^{N_w} func\_voring\ (x,\ y,\ z,\ i_w,\ j_w,\ \Gamma_w)\\
(u_{\mathrm{L}},\ v_{\mathrm{L}},\ w_{\mathrm{L}})_l =& \sum_{i=1}^{M}\sum_{j=1}^{N} func\_voring\ (x,\ -y,\ z,\ i,\ j,\ \Gamma_{i,\ j})+\\
&+\sum_{K=1}^{N_w} func\_voring\ (x,\ -y,\ z,\ i_w,\ j_w,\ \Gamma_w)\\
(u,\ v,\ w)_l =&(u_{\mathrm{R}},\ v_{\mathrm{R}},\ w_{\mathrm{R}})_l + (u_{\mathrm{L}},\ -v_{\mathrm{L}},\ w_{\mathrm{L}})_l
\end{aligned}
$$

then this velocity allows the calculation of the space travelled in a time-step, obtained by the formula,

$$(\Delta x,\ \Delta y,\ \Delta z)_l = (u,\ v,\ w)_l \Delta t \tag{188}$$

2.2 UNSTEADY METHOD IMPLEMENTATION

In this section the implementation of the current unsteady vortex-lattice method in Matlab scripting language is carried out. This implementation is based on the unsteady development of the method presented in the previous section.
A brief review of the main features of the method is presented here,

- The wing is modeled by placing vortex rings on the non-planar surface. Variations in twist angle and airfoil shape is taken into account by rotation of the normal vector of the panels.
- An unlimited number of wing's segments can be modeled, each segment is defined by 6 parameters : span length, taper ratio, sweep angle, dihedral angle, root twist angle and tip twist angle.

The algorithm flow is shown in fig.27, where the names of the scripts employed in the method are on the right-hand side of the blocks.

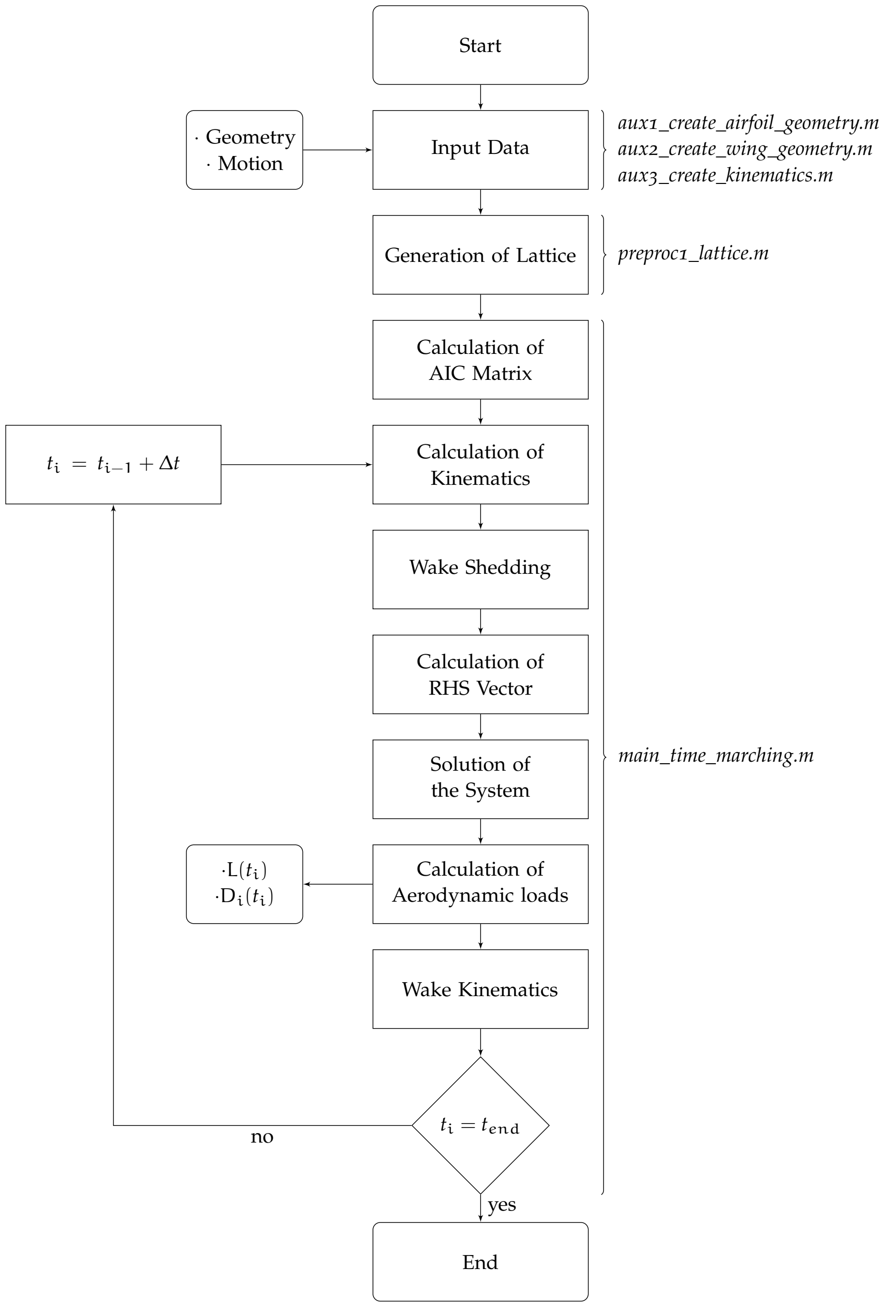

Figure 27: Simplified algorithm of UVLM

2.2.1 *Airfoil Geometry*

The script *'aux1_create_airfoil_geometry.m'* loads the geometry data of the airfoil from a *.txt* or *.dat* file including the coordinates of the lower and upper surfaces of the airfoil and converts the information into the output needed to take account of the camber line effect on wing aerodynamic properties. In the script the actual boundary conditions on the cambered surface are shifted on the chord line of a flat wing. This is a common thin-wing approximation [14] and in our case it is used to prevent surface intersections at the hinges when the wing has a dihedral angle.Only one airfoil can be used for the whole wing, and the thickness of the airfoil has no impact on the calculations.
The script creates **K** new X coordinates using a cosine law spaced mesh, valid for the upper and lower surfaces to calculate **K** camber line's Y coordinates and **K** curvatures of camber line.

The output are then

- the camber line Y coordinates
- the curvature of the camber line
- new cosine-law spaced mesh

Two examples of how the airfoil data input is converted and the plots generated by the script are given below with $\mathbf{K} = 100$.

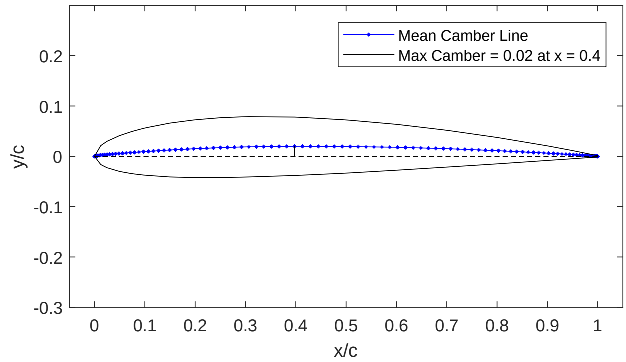

(a) Airfoil surfaces and camber line

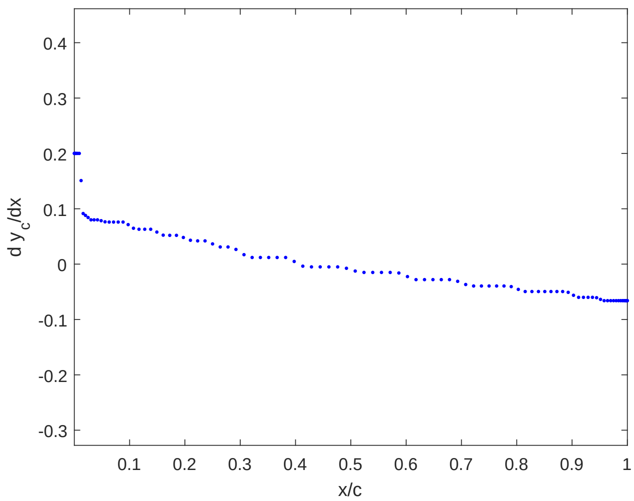

(b) Curvature of camber line

Figure 28: NACA 2412 airfoil geometry (*Matlab*)

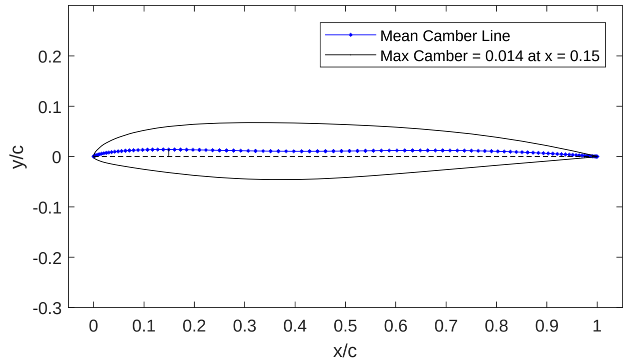

(a) Airfoil surfaces and camber line

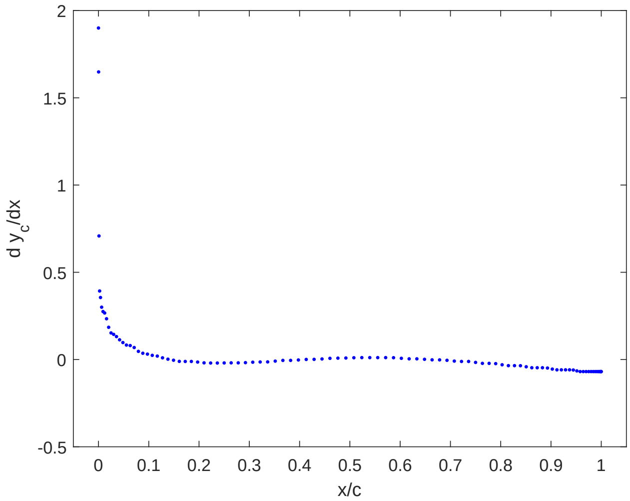

(b) Curvature of camber line

Figure 29: Boeing BACXXX airfoil geometry (*Matlab*)

2.2.2 *Wing Geometry*

The script *'aux1_create_wing_geometry.m'* loads the geometry of the wing from a *.txt* or *.dat* file containing the information of the semi-wing in terms of

- span-wise length
- chord length
- sweep angle
- dihedral angle
- twist angle

and the semi-wing can be divided in any number of *segments* with different geometrical properties.
The script then creates the other symmetrical semi-wing and stores the information in structs called *'patches'* .

An example of how the wing geometry is plotted by the script is presented here:

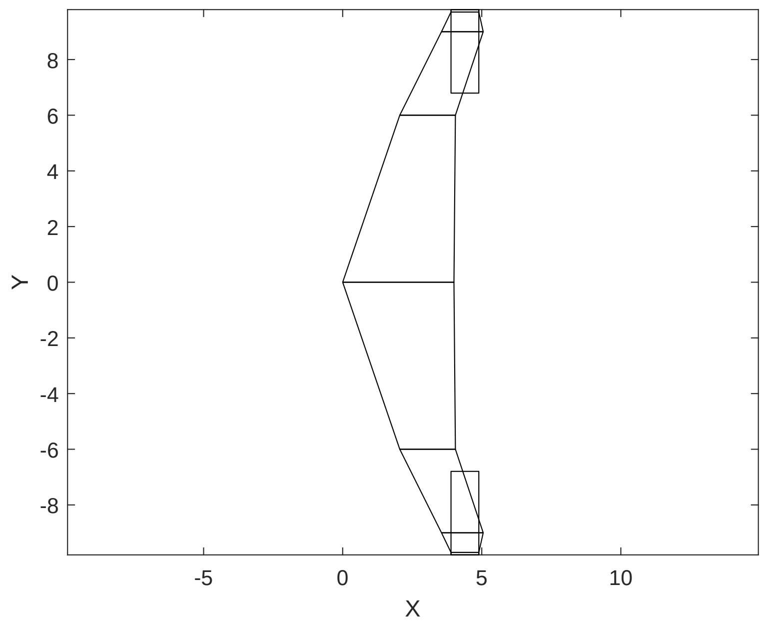

(a) 2D view

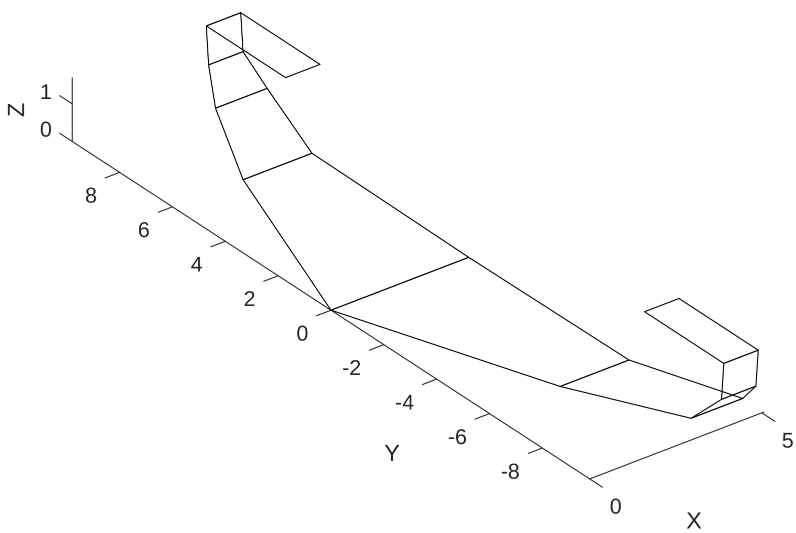

(b) 3D view

Figure 30: Wing geometry (*Matlab*)

2.2.3 *Kinematics Input*

The script *'aux3_create_kinematics.m'* contains the kinematics of the wing and stores it for the analysis.
Only symmetrical motion can be processed by the program due to the restrictions of the application of the method of images.
The kinematics is given in terms of time histories of the linear velocities in the inertial reference frame (IRF), U, W, and the angular velocity in the body reference frame (BRF) q (these velocities are shown in figure 23). It is also possible to add a time history of the twist angle at the wing tip, in such case the twist angle increases linearly from 0 at the wing root to the wing tip prescribed value. The final time of the simulation needs to be chosen in this file as well. It must be reminded that the initial condition is always at rest (all velocities are 0) and the wing starts to move at the first time step.

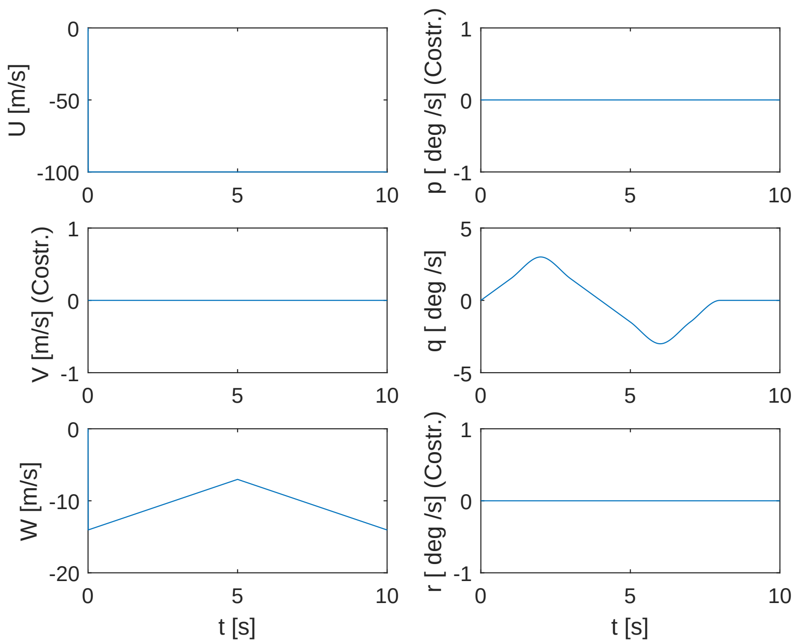

Figure 31: Example of Kinematics time histories (*Matlab*)

2.2.4 *Discretization and Vortex Lattice Creation*

The script '*preproc1_lattice.m*' creates the vortex-rings lattice on the wing parts created by the execution of '*aux1_create_wing_geometry.m*'. The panelling procedure requires as inputs the number of span-wise divisions N_i for each segment of the semi-wing and the number of chord-wise divisions M, that is the same for all segments.

The total number of panels m for a semi-wing, i. e. the total number of vortex-rings, is:

$$m = \sum_{i=1}^{N_{segments}} N_i \cdot M \tag{189}$$

The output of the script is a collection of vortex-rings structs, 4-sided plane shapes which cover the surface of the wing.
A vortex-ring struct contains the following information:

- The X, Y, Z BRF coordinates of the 4 corner points
- The X, Y, Z BRF coordinates of the collocation point, the mid-point of the panel
- Panel's area S
- Panel's normal vector $\underline{n}$
- Panel's twist θ

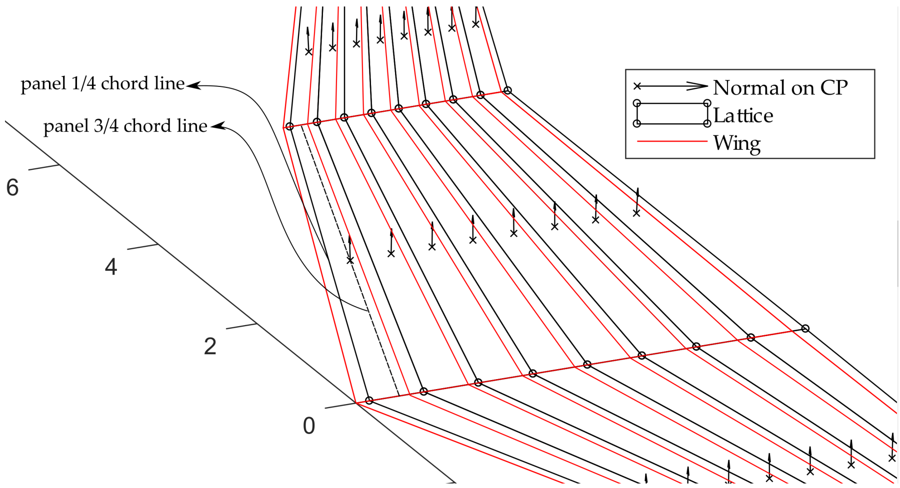

Figure 32: Panelling on the wing of fig.30 with LE zoom (*Matlab*)

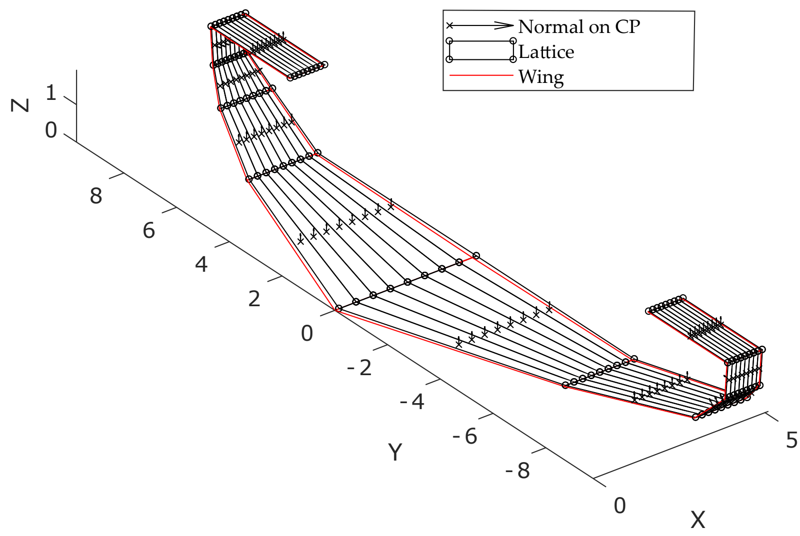

Figure 33: Vortex lattice on the wing of fig.30 with $M = 8$ and $N_i = 1$ for each segment (*Matlab*)

The script takes account of the curvature due to the airfoil shape by rotating the normal vector $\underline{\mathbf{n}}$ of the panels [14], as shown in figure fig.34 .

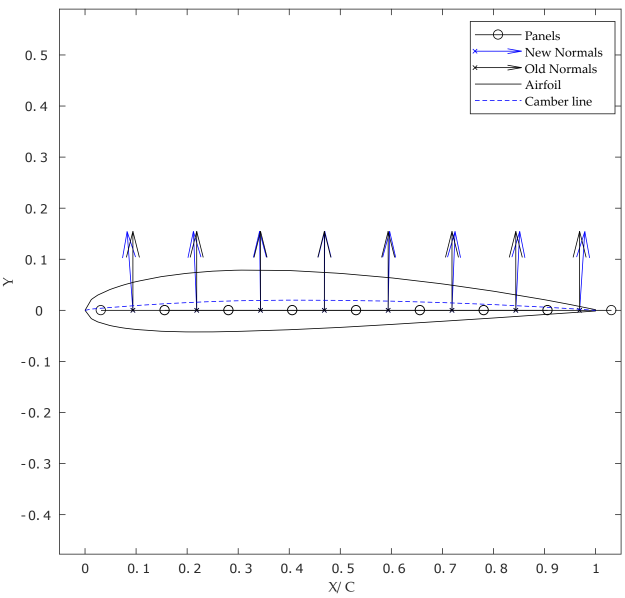

Figure 34: Rotation of the normals due to the curvature of NACA 2412 airfoil (*Matlab*)

2.2.5 *Simulation Settings*

Before starting a simulation the settings must be chosen in the script *'main_time_marching.m'*. They are called *'flags'* and can be set on ON or OFF.

The flag is listed below:

- **Wake roll-up flag** activates the routine that calculates the velocities induced by the singularities in the flow-field on the wake and move the corner points of the wake vortex-rings.
- **Vortons flag** activates the routine that transforms wake vortex-rings into vortons.

2.2.6 *Aerodynamic Influence Matrix*

The computation of the AIM is performed once, by the function *'func_AIM.m'*. At this point the self-induction coefficients fulfill the $\underline{\underline{AIM}}$ and the trailing-vortices inductions fulfill another matrix called $\underline{\underline{TV\_AIM}}$.

2.2.7 *Time Stepping Procedure*

The script *'main_time_marching.m'* takes the airfoil and wing geometry, the kinematics and the vortex lattice properties as inputs and simulate the potential, unsteady flow field through a time stepping technique. Firstly the time step is calculated forcing the chord of the wake panels $c_{wake,p}$ to be homogeneous to the wing panels' chordwise length $c_{wing,p}$ (shown in fig. 35) as stated in [15], [23] and reproduced here through the formulas:

$$c_{wing,p} \approx c_{wake,p} \tag{190}$$

$$c_{wing,p} = \frac{c_{ref}}{M} \tag{191}$$

$$c_{wake,p} = Q_{\infty,ref} \cdot \Delta t \tag{192}$$

$$\Delta t = \frac{c_{ref}}{M \cdot Q_{\infty,ref}} \tag{193}$$

where c_{ref} is the mean geometrical chord, M is the number of chordwise divisions and $Q_{\infty,ref}$ is the mean velocity of the wing computed through a time average of the modulus of the velocity vector $\underline{Q} = \{U,\ V,\ W\}$.

As a consequence of the calculation of the time step through the formula 193, the number of time steps in which the simulation is divided (N_t) depends on the vortex lattice settings.

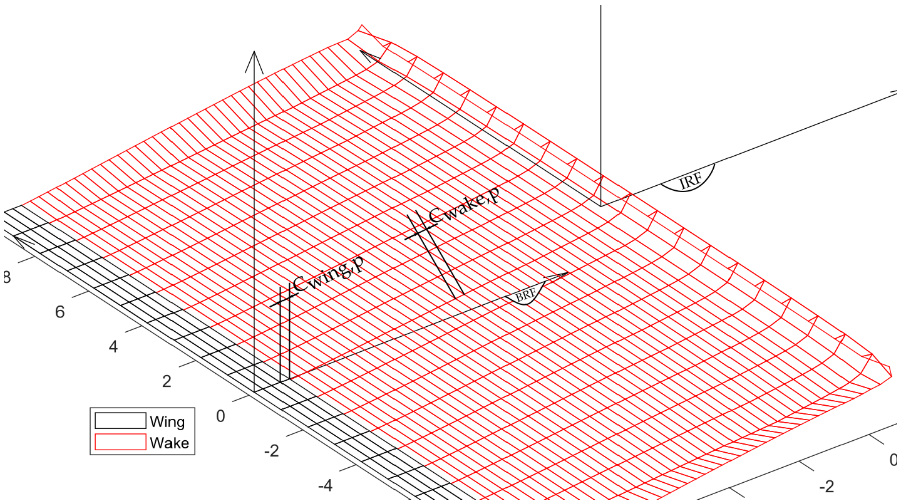

Figure 35: Wing and wake panels' chords

$$N_t = \frac{t_{fin}}{\Delta t} \tag{194}$$

Once the time-step has been calculated the loop starts at $t = \Delta t$. We recall that at $t = 0$ the origins and the three directions of the BRF and the IRF coincide and the wing is considered at rest.
At each time-step the script updates the wing attitude in the IRF through the auxiliary kinematic eq.s 167 and a scanning-procedure on each vortex-ring moves the corner points according to the BRF velocity $(U,\ V,\ W)$ of a quantity expressed by the vector $(\Delta X,\ \Delta Y,\ \Delta Z)$, obtained as

$$(\Delta X,\ \Delta Y,\ \Delta Z) = (U,\ V,\ W)\Delta t \tag{195}$$

If the current time-step is the first, the script doesn't shed any vortex-ring at the trailing edge and skips to the calculation of the RHS and the solution of the set of equations.
From the second time-step until the end of the time loop, at each time-step, the shedding procedure adds a row of wake vortex-ring at the trailing edge, following the rules presented in the previous section.
Then the core-function *'func_proc_solver.m'* calculates the RHS and solves the set of equations which returns the singularities strength vector $\Gamma_k(t_i)$ at each time-step. The calculation of the RHS needs the kinematic velocities of the fluid at the CPs, given by eq.172 and the wake inductions, performed through the routine *'func_voring.m'* applied to the wake vortex-rings.
The output in terms of the forces acting on the lifting-surface is carried out through eq.186.
Finally the wake roll-up routine moves the wake vortex-rings corner points.

2.2.8 *Vortons Wake Model Implementation*

As we stated in the previous chapter the vortons can be employed to represent the vorticity in the flow-field. In the current implementation of the unsteady vortex lattice method we can choose to use vortons instead of vortex-rings to model the wake shed by the wing at the trailing-edge.

The vorton wake model implementation procedure contemplates

1. The conversion of the wake vortex-rings into vortons
2. The convection of the vortons
3. The vorticity stretching that changes the vortons strength and orientation

The conversion of the wake vortex-rings into vortons is performed through the following steps

1. The scheme presented in fig.36 is used to represent the vortex-rings wake as vortons
2. The circulation of the vortex-rings is integrated to calculate the vorticity of the vortons

The position $\underline{r}_p(t)$ of a vorton in time is given by

$$\underline{r}_p(t+1) = \underline{r}_p(t) + \underline{Q}(r_p(t), t)\Delta t \tag{196}$$

while its strength is uptaded as follows,

$$\underline{\alpha}_p(t+1) = \underline{\alpha}_p(t) + \underline{\alpha}_p(t) \cdot \nabla\underline{Q}(r_p(t), t)\Delta t \tag{197}$$

When the vorton wake model is activated the wake consists of two distributions of singularities, the near wake vortex-rings and the far-wake vortons. The near wake is composed by the first row of wake panels, attached to the trailing-edge, where the Kutta condition is applied in the same way of the vortex-rings wake model and a second row of vortex-rings which is going to be converted into vortons. At each time-step, after the second row of wake vortex-rings is shed, that is after the second time-step, the conversion from near-wake vortex-rings to far-wake vortons is accounted for.
The strength $\underline{\alpha}_p(t)$ of each vorton is computed by integrating the strength of the vortex line segments between adiacent panels, as follows,

$$\underline{\alpha}_p(t) = \int \Gamma \underline{ds} \tag{198}$$

that for the current scheme is discretized as follows,

$$\begin{aligned}\underline{\alpha}_j(t_k) =& 0.5\underline{t}^j{}_1(-\Gamma^{k-1}{}_{j-1} + \Gamma^{k-1}{}_j) + \underline{t}^j{}_2(\Gamma^{k-1}{}_j - \Gamma^{k-2}{}_j) + \\ &+ 0.5\underline{t}^j{}_3(\Gamma^{k-1}{}_j - \Gamma^{k-1}{}_{j+1})\end{aligned} \tag{199}$$

where the quantities $\underline{t}^j{}_1, \underline{t}^j{}_2, \underline{t}^j{}_3$ and the circulations are presented in fig.36.

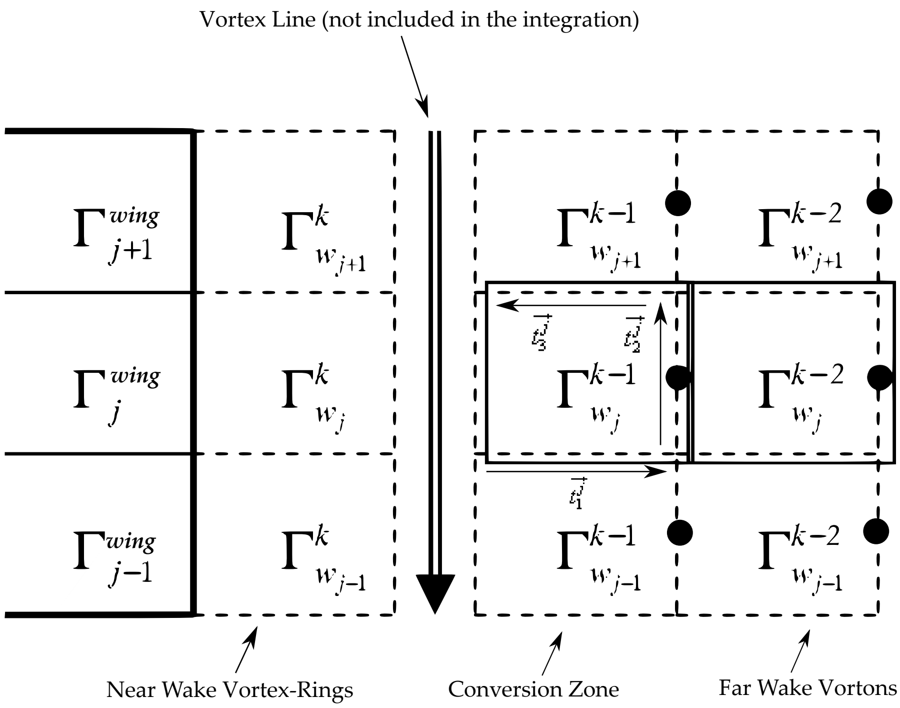

Figure 36: Scheme for vortex-rings to vortons conversion

Finally we need to choose a core-radius for the regularization function. A common choice in the literature is to fix the core-radius to the space travelled in a time-step by the body, that is $\sigma = kQ_\infty \Delta t$, therefore as shown in [11] we apply this condition with $k = 2$.

3

VALIDATION AND RESULTS

In this chapter the current method is validated with respect to analytical and computational methods available in the literature. First the steady method calculation of lift and drag has been carried out and the results compared with the *lifting line* theory with a correction for the wings shapes proposed by Jones as shown in [17].
Then the distribution of loads has been compared to that calculated through a VLM in [9] to check the effects of taper ratio and sweep angle.
Then the UVLM calculation of lift and drag have been validated in the case of a sudden acceleration, and plunging periodic oscillations.

3.1 LIFT COEFFICIENT AND POLARS

The steady VLM has been tested to check the correct calculation of the lift and drag. A flat plate with varying Æ undergoing different angles of attack generated the lift coefficient curves of fig.37 and fig.38. Three different discretizations have been tested to show the influence of the number of panels on the calculations.

The three discretizations tested are

1. $M = 4$ $N = 10$
2. $M = 4$ $N = 20$
3. $M = 4$ $N = 40$

The reference lift coefficient's curves are obtained from lifting line's theory with the correction for non-elliptical spanwise load distributions, as follows

$$C_L(\alpha) = 2\pi \frac{Æ}{2(1+\tau) + EÆ}\alpha \tag{200}$$

where Jones' correction parameter is $E = \frac{p}{Æ}$, p is the perimeter of the semi-wing and τ is a function of the Æ and λ.

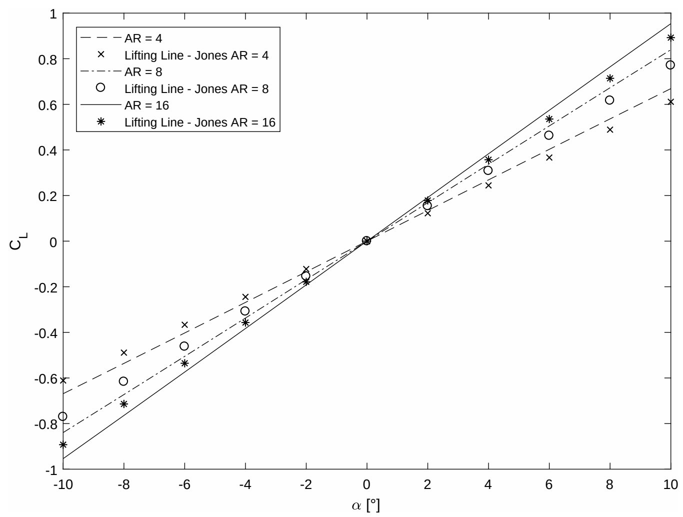

(a) $M = 4$ $N = 10$

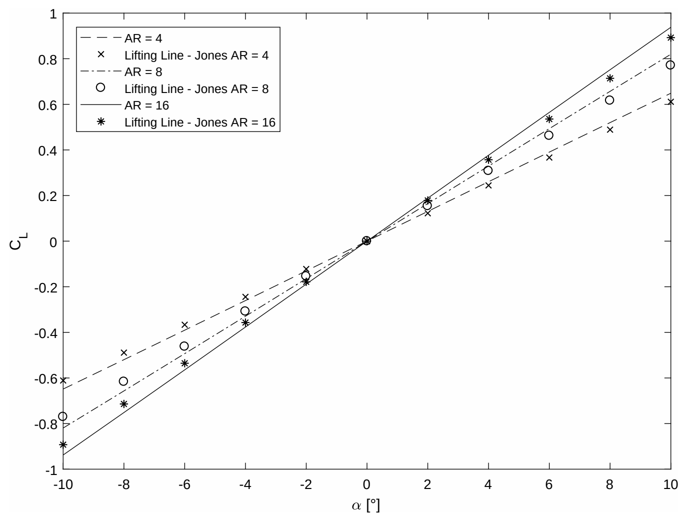

(b) $M = 4$ $N = 20$

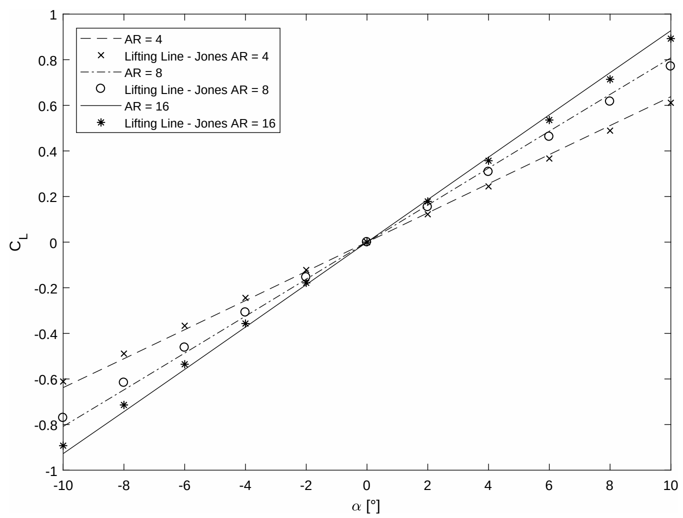

(c) $M = 4$ $N = 40$

Figure 37: $C_L - \alpha$ curves generated by the VLM for Æ = 4, Æ = 8, Æ = 16 and comparison with lifting line theory results (*Matlab*)

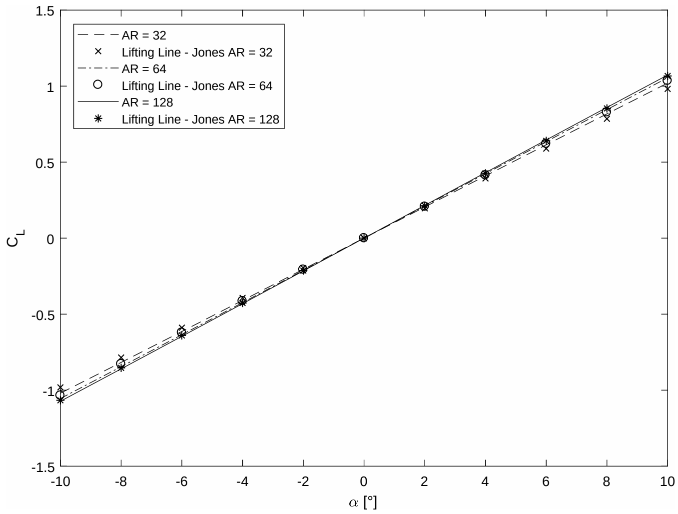

(a) $M = 4$ $N = 10$

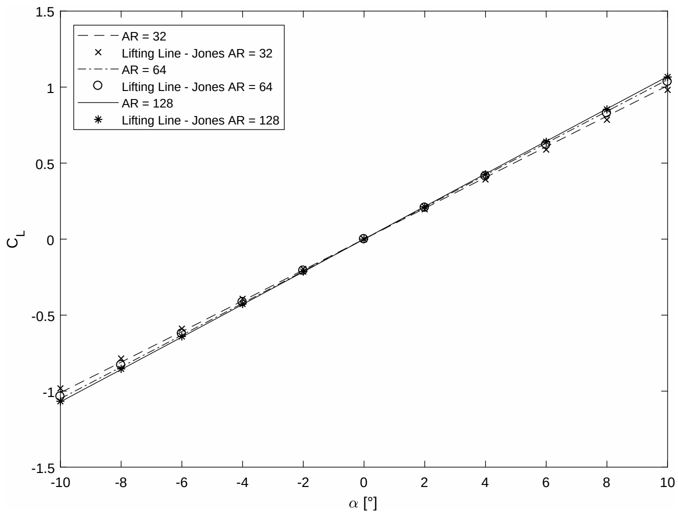

(b) $M = 4$ $N = 20$

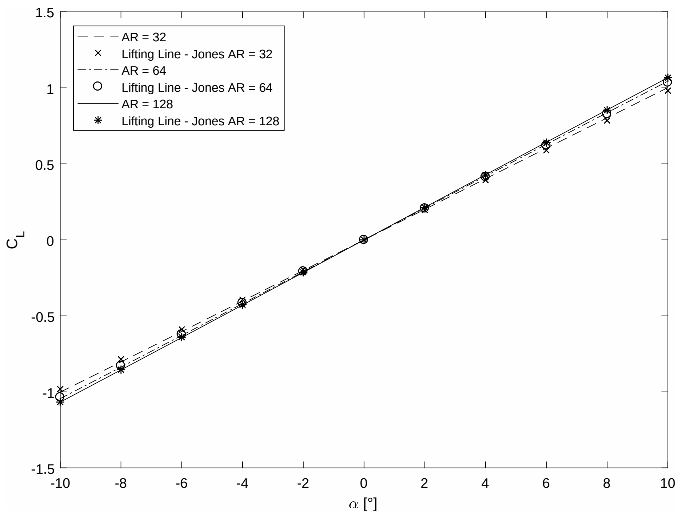

(c) $M = 4$ $N = 40$

Figure 38: $C_L - \alpha$ curves generated by the VLM for Æ = 32, Æ = 64, Æ = 128 and comparison with lifting line theory results (*Matlab*)

The slope of the lift coefficient curves C_{L_α} calculated through the VLM is shown w.r.t AR and compared to the one calculated with the lifting line theory.

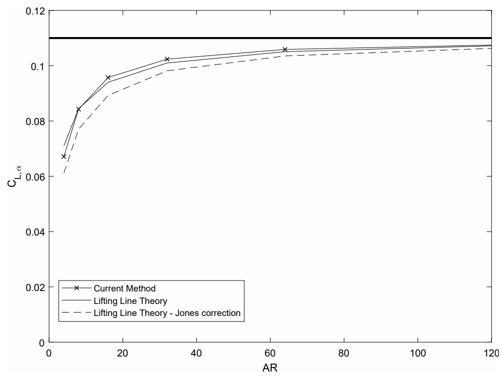

(a) $M = 4$ $N = 10$

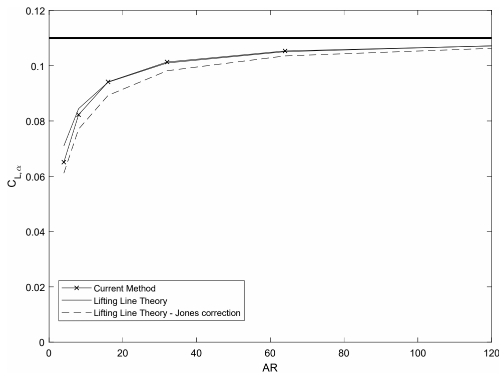

(b) $M = 4$ $N = 20$

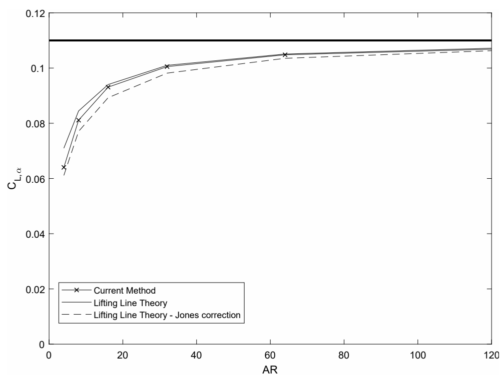

(c) $M = 4$ $N = 40$

Figure 39: C_{L_α} - AR curves and comparison with lifting line theory results (*Matlab*)

The induced drag coefficient polars are obtained through the VLM, while the reference values are obtained from lifting line's theory with the correction for non-elliptical spanwise load distributions K, that is $C_{D_i}(C_L) = K\dfrac{{C_L}^2}{\pi AR}$.

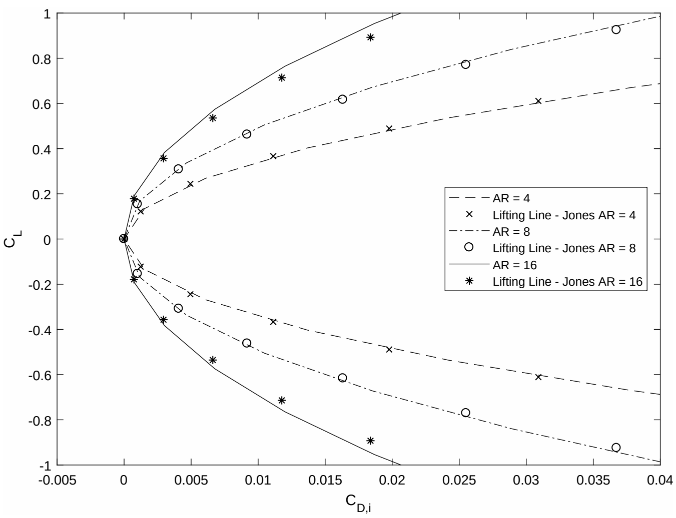

(a) $M = 4$ $N = 10$

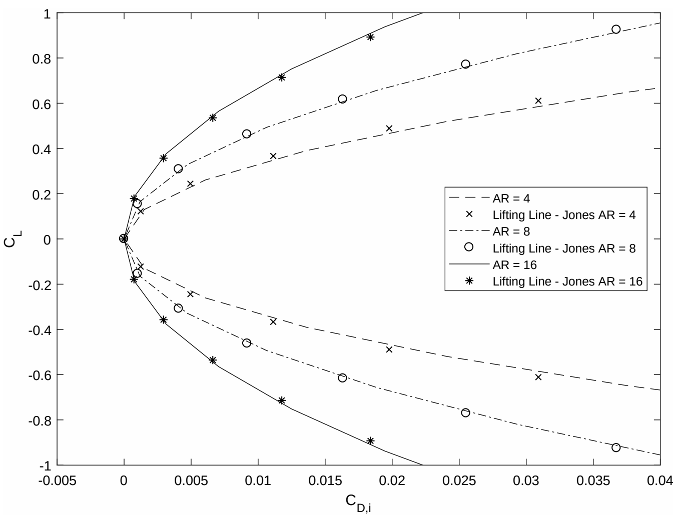

(b) $M = 4$ $N = 20$

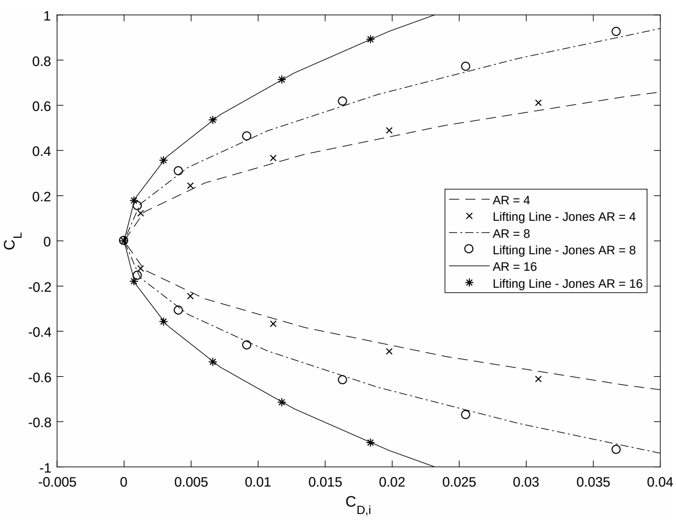

(c) $M = 4$ $N = 40$

Figure 40: $C_L - C_{D_i}$ curves generated by the VLM for Æ = 4, Æ = 8, Æ = 16 and comparison with lifting line theory results (*Matlab*)

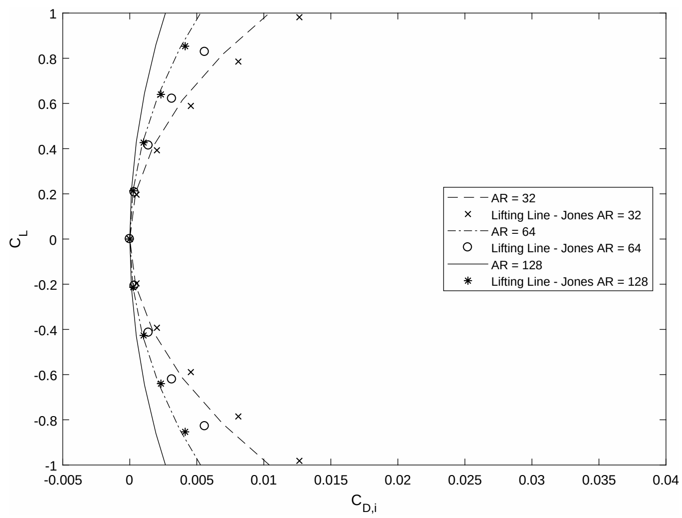

(a) $M = 4$ $N = 10$

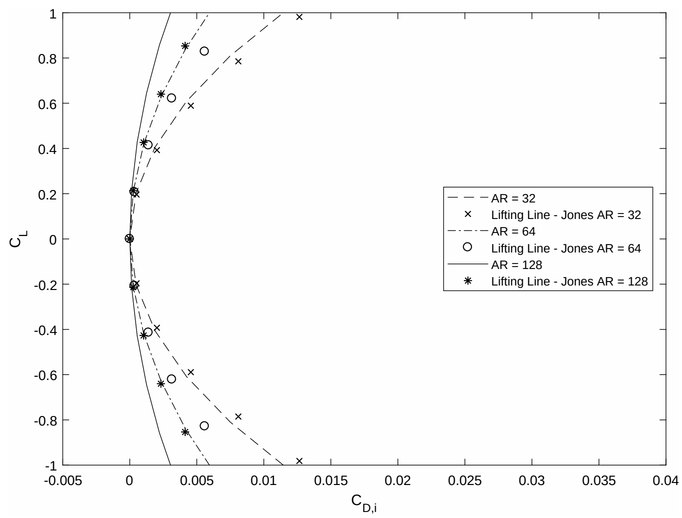

(b) $M = 4$ $N = 20$

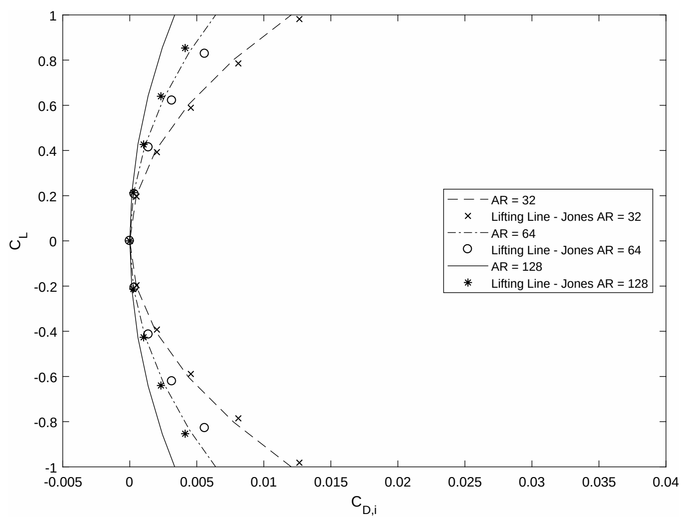

(c) $M = 4$ $N = 40$

Figure 41: $C_L - C_{D_i}$ curves generated by the VLM for Æ = 32, Æ = 64, Æ = 128 and comparison with lifting line theory results (*Matlab*)

3.2 TAPER RATIO EFFECT ON LOADS

The effects of taper ratio, namely the ratio between the root chord and the tip chord of a wing $\lambda = \frac{c_{root}}{c_{tip}}$, on span-wise loads have been investigated with the current VLM. The loads distribution used as a reference has been calculated through a VLM found in [9]. The load calculated by the VLM is $C_l(\eta) = \frac{2\Gamma(\eta)}{cV_\infty}$. In the current calculations the wing is a flat plate with $AR = 7.28$ and $\lambda = 0.4$.

Wing Properties			
Airfoil	Flat Plate	AR	7,28
b/2	2,55 m	Λ	0°
c_{root}	1 m	λ	0,4
Γ	0°	M x N	4 x 20

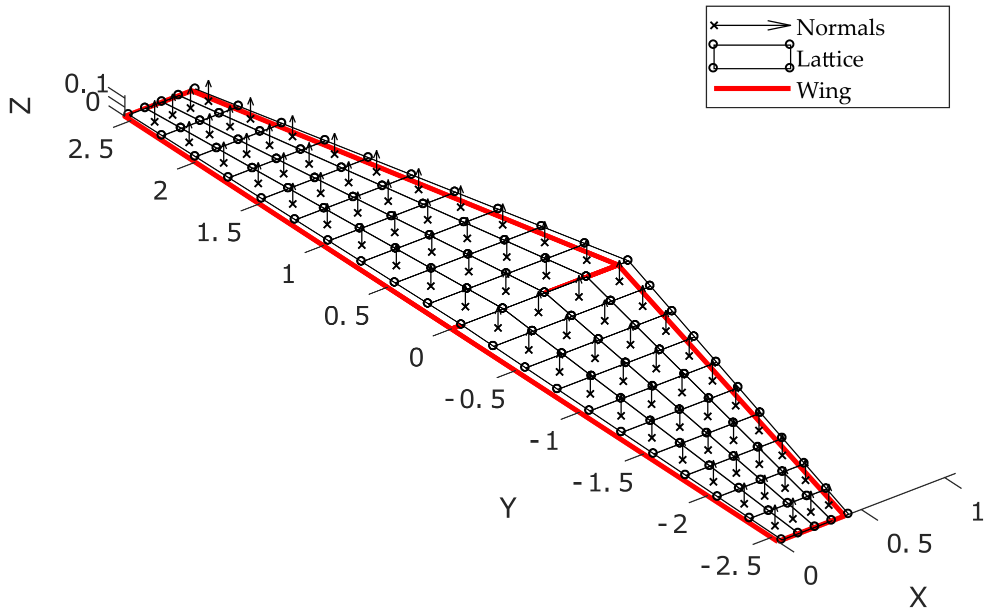

Figure 42: Wing properties and discretization (*Matlab*)

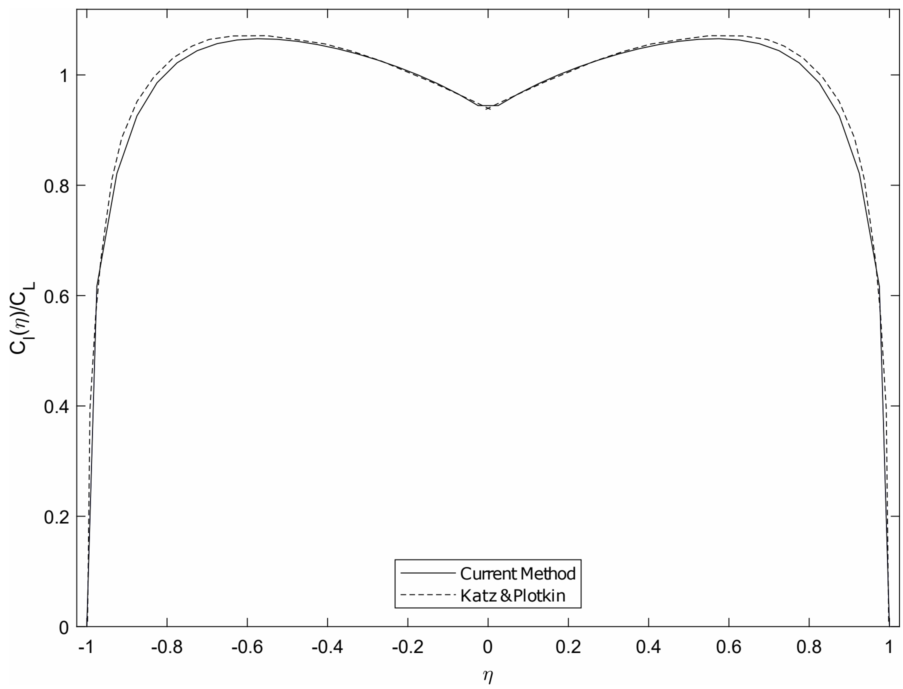

Figure 43: Loads distribution generated by the VLM for $AR = 7.28$, $\lambda = 0.4$, $M = 4$ $N = 40$, and comparison with [9] (*Matlab*)

3.3 SWEEP ANGLE EFFECT ON LOADS

The effects of sweep angle on span-wise loads have been investigated with the current VLM. The loads distribution used as a reference has been calculated through a VLM found in [9].The load calculated by the VLM is $C_l(\eta) = \dfrac{2\Gamma(\eta)}{cQ_\infty}$. In the current calculations the wing is a flat plate with $Æ = 4$ and $\Lambda = 0°, 45°, -45°$.

Wing Properties			
Airfoil	Flat Plate	Æ	4
b/2	2 m	Λ	$0°\|+45°\|-45°$
c_{root}	1 m	λ	1
Γ	0°	M x N	4 x 20

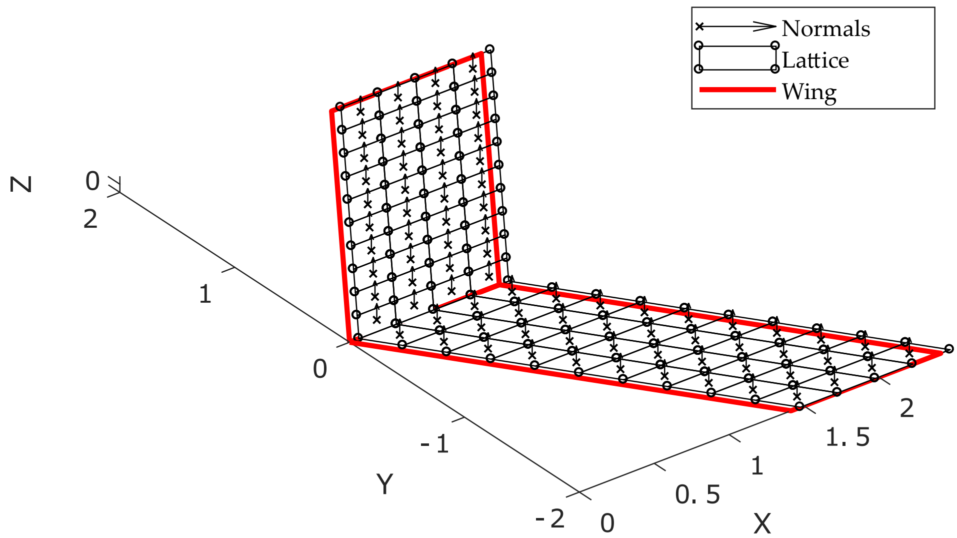

Figure 44: Wing properties and discretization ($\Lambda = +45°$) (*Matlab*)

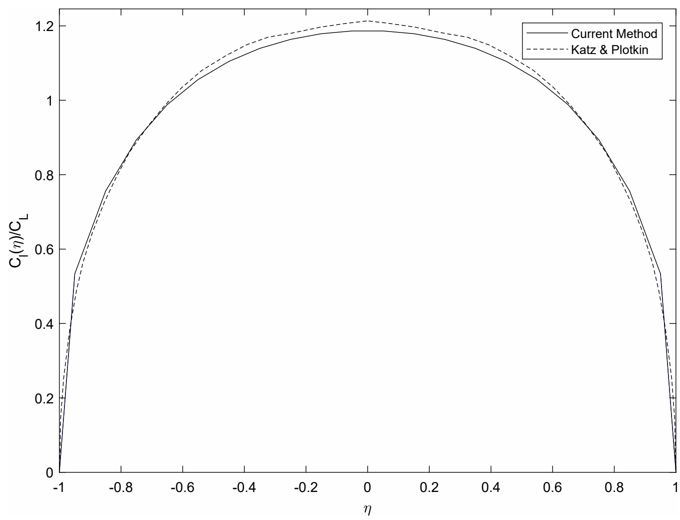

(a) $\Lambda = 0°$

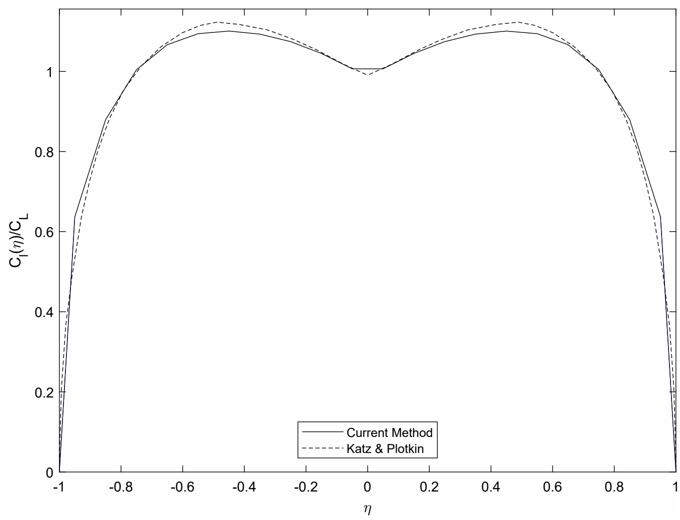

(b) $\Lambda = 45°$

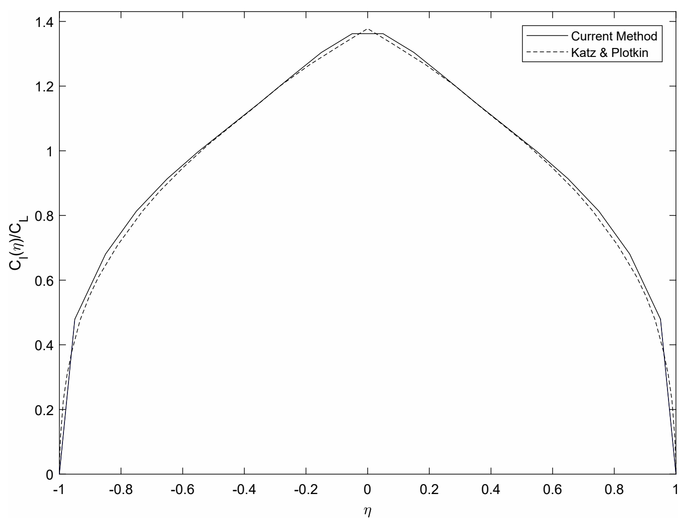

(c) $\Lambda = -45°$

Figure 45: Loads distribution generated by the VLM for Æ $= 4$, $M = 4$ $N = 20$, and comparison with [9] (*Matlab*)

3.4 CURVATURE OF CAMBER-LINE EFFECT ON LOADS

The effects of non-zero curvature of the camber-line on chord-wise loads have been investigated with the current VLM. The pressure coefficient difference distribution used as a reference has been calculated through the program *Xfoil*. In the current calculations the airfoil used is a NACA 2404 and the wing has $\text{Æ} = 200$ and $\lambda = 1$, $\Lambda = 0°$. The $\Delta C_p(x/c)$ is calculated in the proximity of the axis of symmetry of the wing to avoid 3-D aerodynamic phenomena.

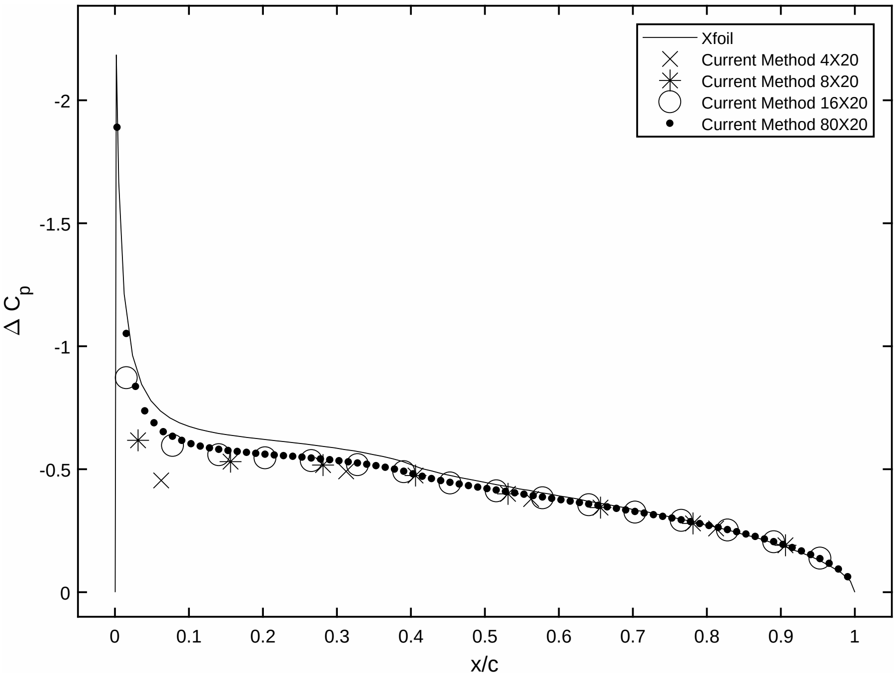

Figure 46: Loads distribution generated by the VLM and comparison with *Xfoil* (*Matlab*)

3.5 SUDDEN ACCELERATION

The first test case for the UVLM is the sudden acceleration, in which the wing starts from being still at t = 0 and undergoes an acceleration in the first time step that leads it to the steady motion in which the angle of attack is equal to 5°. The results of a similar UVLM in [9] is taken as a reference. The reference chose a $M = 4, N = 6$ mesh and a non-dimensional time-step $\Delta\tau = \frac{1}{16}$. This non-dimensional time is defined as $\tau = \frac{tQ_{\infty,ref}}{c_{ref}}$.

The wings used in this test case are rectangular wings with different AR and the time-step is $\tau = \frac{1}{16}$. The lift coefficient history shows a transient due to the acceleration (that is the derivative of the potential function $\frac{\partial\Phi}{\partial t}$) and a steady-state value due to the non-zero angle of attack. The agreement between the two methods is good, nonetheless the differences in the calculations at the beginning of the motion can be explained by the different mesh, [9] uses a coarser mesh, and the different approach to the wake-panels shedding.

Osservations found in [15] suggests to choose a span-wise panelling that leads to a AR of the single panels (defined as $AR_{panel} = {b_{panel}}^2/S_{panel}$) smaller than 3, while in the cases below this condition is matched in the first simulation only (AR = 4).

Wings Properties	
Airfoil	Flat Plate
AR	4 | 8 | 12 | 20
$b/2$	2 | 4 | 6 | 10 m
λ	1
c_{root}	1 m
Λ	0°
Γ	0°

Simulation Config.	
M	16
N	12 | 24
Motion	See fig.47
α	5°
U	1 m/s
τ_{fin}	10
Wake Model	Vortex Rings - Roll-up

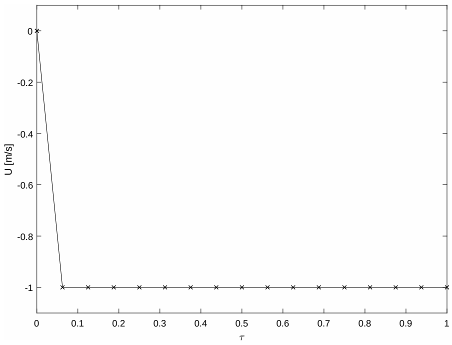

(a) U

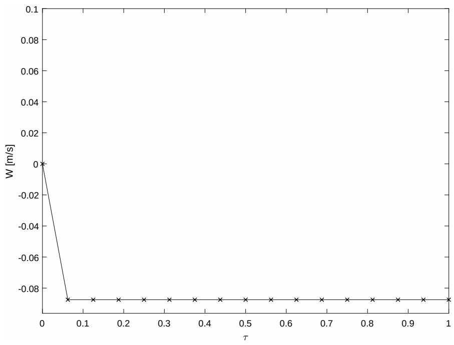

(b) W

Figure 47: Sudden acceleration kinematics zoomed in the range $[0, 1]\ \tau$ (*Matlab*)

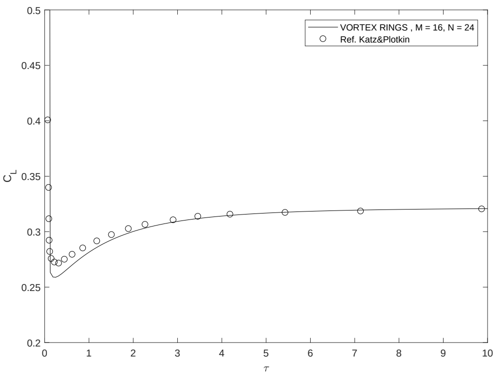

(a) Æ= 4

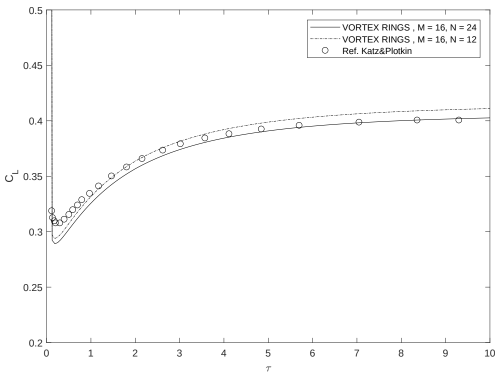

(b) Æ= 8

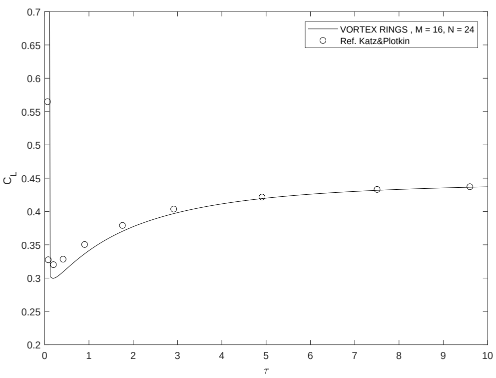

(c) Æ= 12

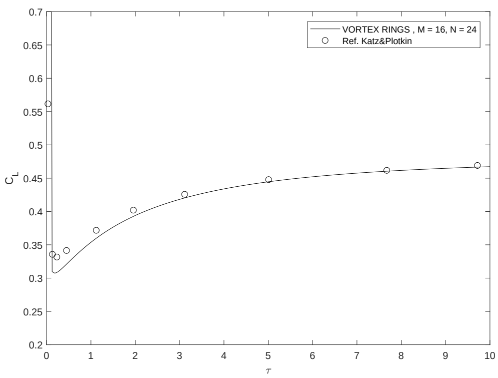

(d) Æ= 20

Figure 48: Lift coefficient generated by the UVLM for a sudden acceleration, and comparison with [9] (*Matlab*)

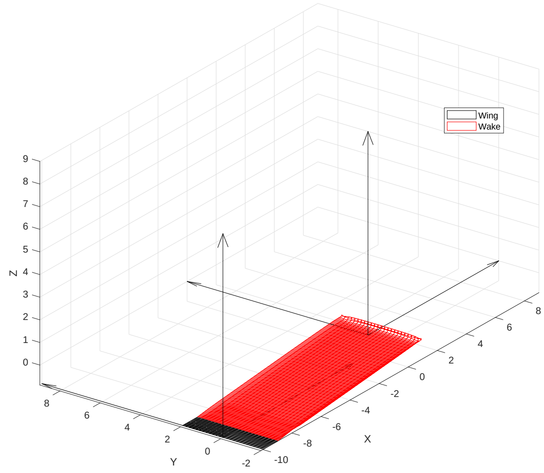

Figure 49: 3-D view of a rectangular wing with Æ = 4 undergoing sudden acceleration (*Matlab*)

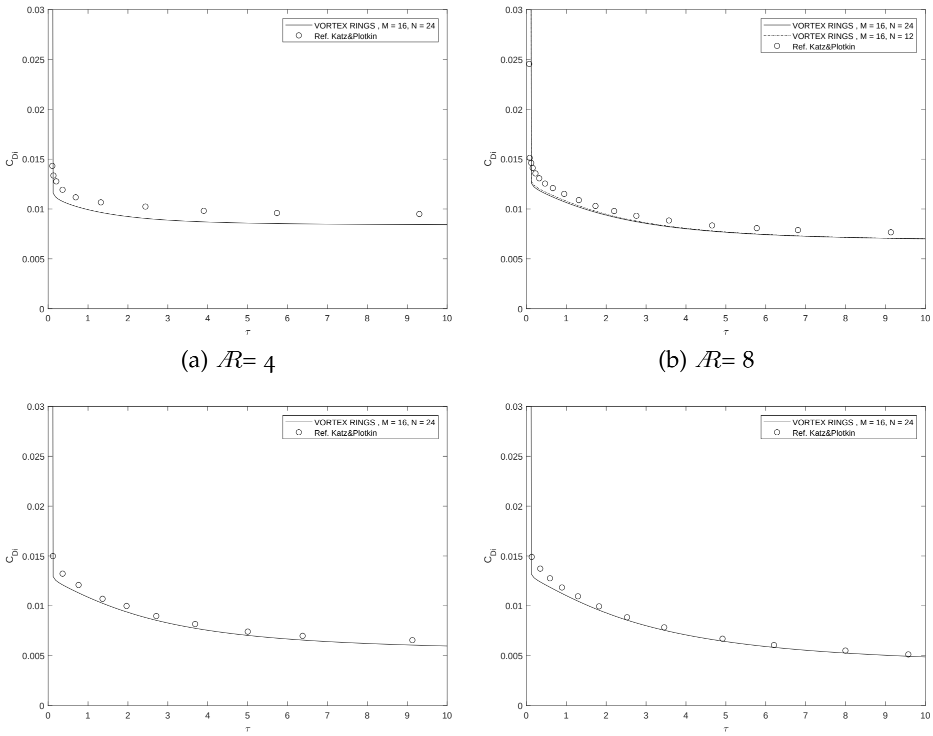

(a) Æ= 4

(b) Æ= 8

(c) Æ= 12

(d) Æ= 20

Figure 50: Drag coefficient generated by the UVLM for a sudden acceleration, and comparison with [9] (*Matlab*)

3.6 CONVERGENCE OF STEADY-STATE VALUES

In this test case we focus on the transient that leads to the steady-state value of the lift and drag coefficients when a rectangular wing of $\mathcal{R} = 20$ undergoes two different sudden accelerations with $\alpha = 2°$ and $\alpha = 8°$. We evaluate the convergences to the steady-state value in terms of the percentage of the final values reached in the simulations. The test-case shows that the convergence to a steady-state value is independent of the angle of attack both for lift coefficient and induced drag coefficient, but in the case of the induced drag coefficient the final value is reached later in time.
The results are shown in fig.51.

Wings Properties	
Airfoil	Flat Plate
$\mathcal{R}$	20
λ	1
$b/2$	10 m
c_{root}	1 m
Λ	$0°$
Γ	$0°$

Simulation Configurations	
M	4
N	12
Motion	Sudden Acceleration
α	$2°$ | $8°$
U	100 m/s
τ_{fin}	50
Wake Model	Vortex Rings - No Roll-up

3.7 STEADY-STATE VALUES

The steady-state values of lift and drag coefficients of the previous test-cases have been plotted with respect to the angle of attack, hence we obtain the lift coefficient curves and induced drag polars in fig.52.

Wings Properties	
Airfoil	Flat Plate
$\mathcal{R}$	20
λ	1
$b/2$	10 m
c_{root}	1 m
Λ	$0°$
Γ	$0°$

Simulation Configurations	
M	8
N	12
Motion	Sudden Acceleration
α	$0° - 16°$
U	$1 m/s$
τ_{fin}	30
Wake Model	Vortex Rings - No Roll-up

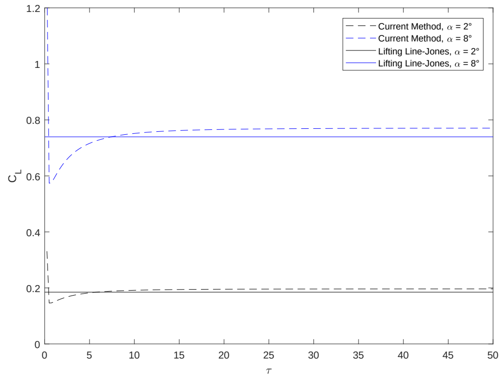

(a) C_L

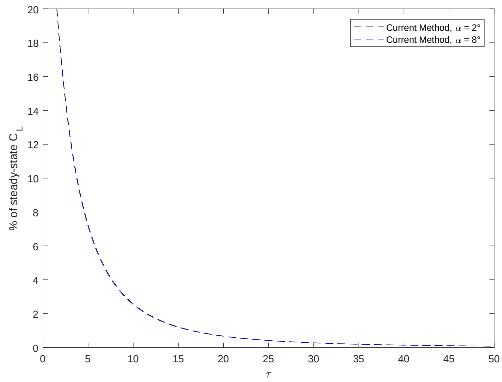

(b) C_L - Convergence

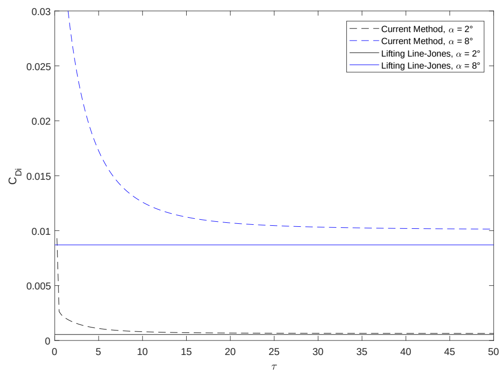

(c) C_{D_i}

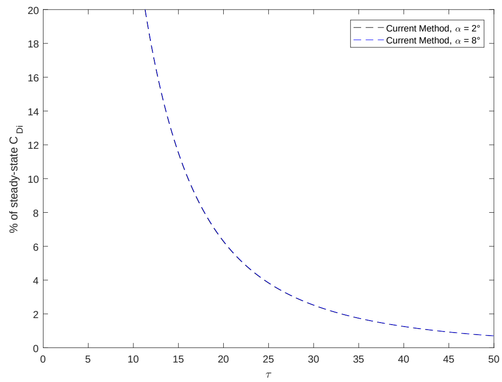

(d) C_{D_i} - Convergence

Figure 51: Convergence of lift and drag coefficients generated by the UVLM for a sudden acceleration, and comparison with results of lifting-line theory's results (*Matlab*)

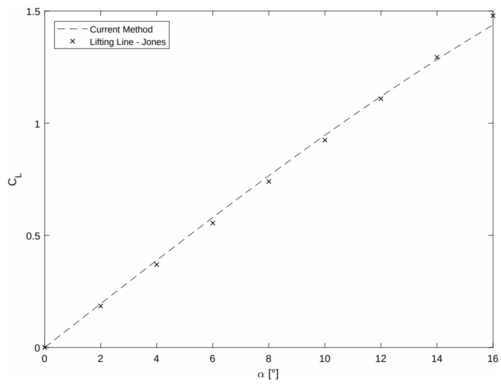

(a) C_L

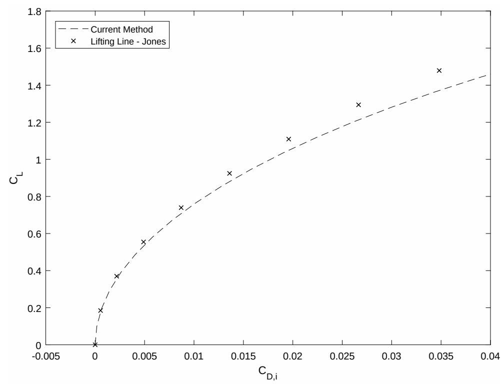

(b) C_{D_i}

Figure 52: Steady-state values of lift and drag coefficients generated by the UVLM, and comparison with results of lifting-line theory's results (*Matlab*)

3.8 PERIODIC MOTION

The validation of the unsteady VLM is performed through the comparison with the analytical solutions of 2-D aerofoils in inviscid flow. Theodorsen theory's for aerofoils undergoing harmonic small amplitude plunging motion provides a solution for inviscid flows and the calculation of lift coefficient that can be compared to the results of the UVLM when the aspect ratio is large enough, say $AR = 100$, and the 3-D effects are negligible.
The plunging motion is described by the function $h = h_0 \sin(\omega t)$, where ω is the frequency, which generates harmonic oscillations along the Z axis, and a uniform X axis velocity.
We analyse the aerodynamic beahviour of the wing undergoing different reduced frequencies motions, where the reduced frequency is defined as $k = \dfrac{\omega c}{2Q_\infty}$.
The span-wise panelling in the current method has not being increased to ignore the 3-D effects at the wing-tip, while the chord-wise mesh should be dense enough in order to obtain a small Δt to catch the unsteadiness of the motion.

Wings Properties	
Airfoil	Flat Plate
AR	100
λ	1
b/2	50 m
c_{root}	1 m
Λ	0°
Γ	0°

Simulation Configurations	
M	See fig.s 53,55,57
N	See fig.s 53,55,57
Motion	Periodic Motion
U	1 m/s
h(t)	$-0.1 \sin(\omega t)$ m
k	0.25 | 0.50 | 0.75
t_{fin}	4 T
Wake Model	Vortex Rings - No Roll-up

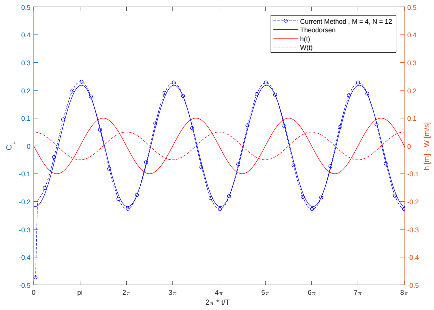

(a) $M = 4$ $N = 12$

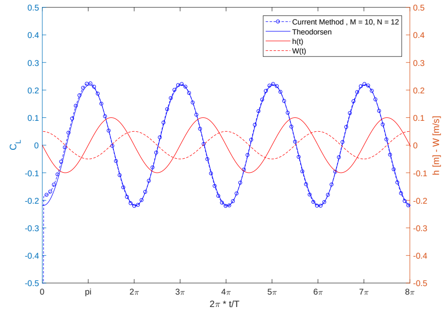

(b) $M = 10$ $N = 12$

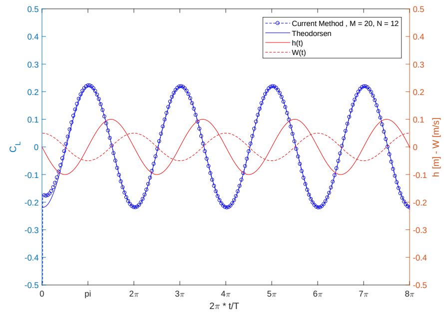

(c) $M = 20$ $N = 12$

Figure 53: $C_L - 2\pi\frac{t}{T}$ curves generated by the UVLM for a periodic motion with **k = 0.25**, and comparison with results of Theodorsen theory's results (*Matlab*)

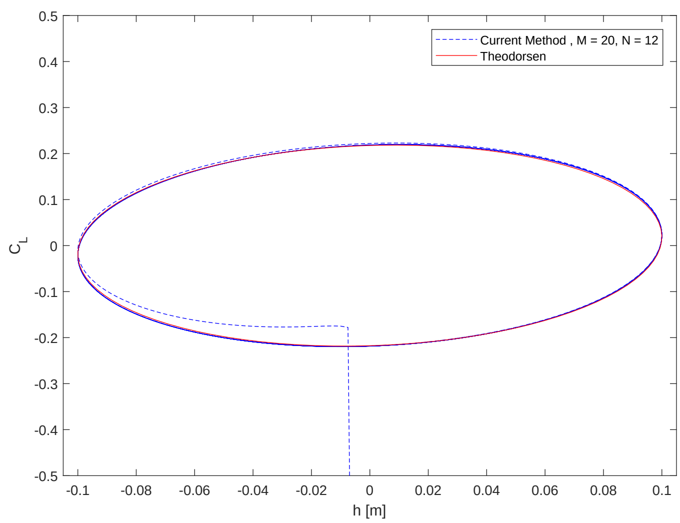

Figure 54: $C_L - h$ curve generated by the UVLM for a periodic motion with **k = 0.25**, and comparison with results of Theodorsen theory's results (*Matlab*)

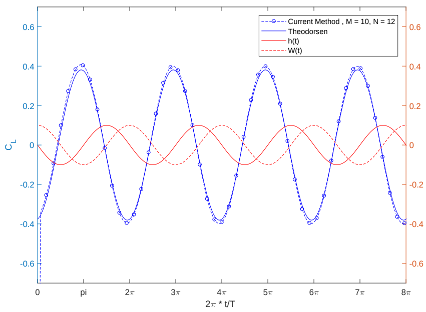

(a) $M = 10$ $N = 12$

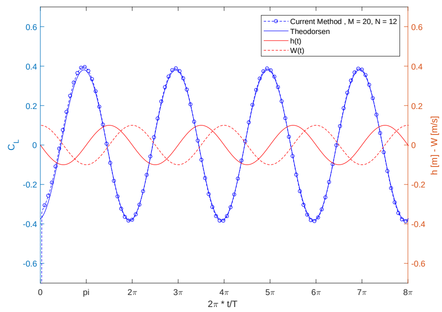

(b) $M = 20$ $N = 12$

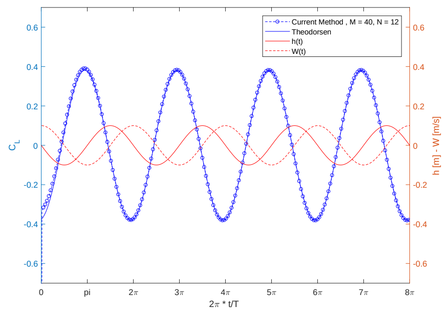

(c) $M = 40$ $N = 12$

Figure 55: $C_L - 2\pi\frac{t}{T}$ curves generated by the UVLM for a periodic motion with **k = 0.50**, and comparison with results of Theodorsen theory's results (*Matlab*)

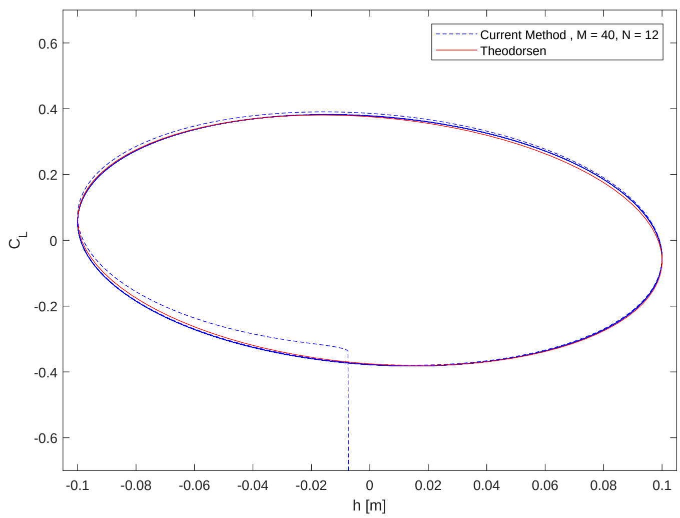

Figure 56: $C_L - h$ generated by the UVLM for a periodic motion with **k = 0.50**, and comparison with results of Theodorsen theory's results (*Matlab*)

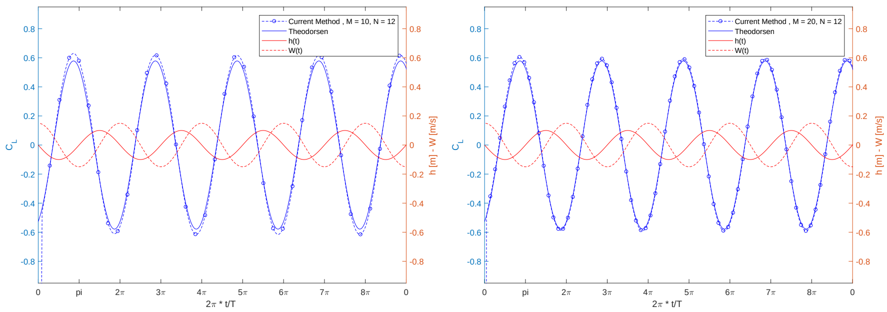

(a) $M = 10$ $N = 12$ (b) $M = 20$ $N = 12$

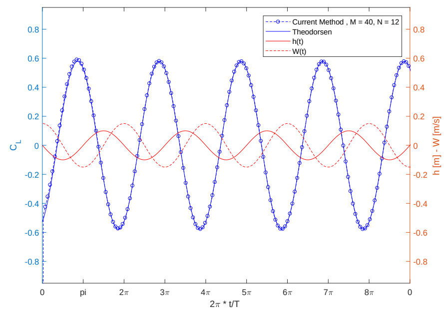

(c) $M = 40$ $N = 12$

Figure 57: $C_L - 2\pi\frac{t}{T}$ curves generated by the UVLM for a periodic motion with **k = 0.75**, and comparison with results of Theodorsen theory's results (*Matlab*)

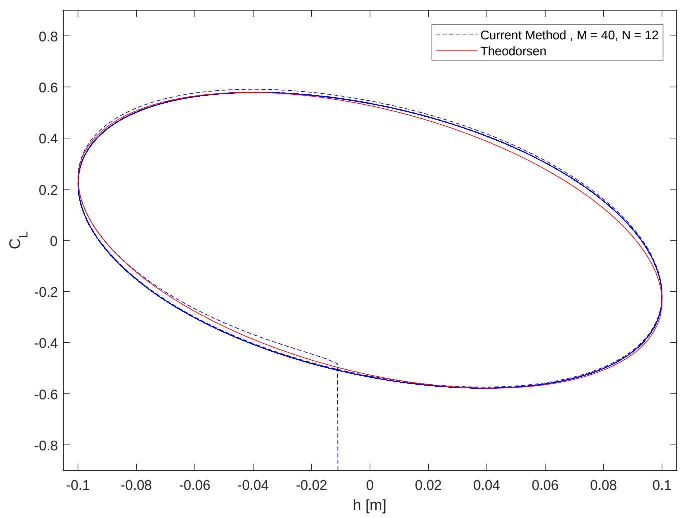

Figure 58: $C_L - h$ curve generated by the UVLM for a periodic motion with **k = 0.75**, and comparison with results of Theodorsen theory's results (*Matlab*)

3.9 RESULTS FOR VORTONS WAKE MODEL AND COMPARISON

Once the vortex-rings wake model has been tested, we test the conversion to vortons of the wake. The validation test cases are the sudden acceleration and the periodic plunging motion. The setting of the simulations are shown in the tabs.
The sudden acceleration test cases show that the number of spanwise divisions heavily influences the results, therefore a thicker mesh is needed when the Æ is bigger to avoid a coarse model of the vorticity in the wake. The vorton wake model shows differences in the evaluation of lift for Æ $= 4$, this could be due to the effects of vortons stretching, which is stronger in the starting vortex and in the wing-tip vortices.
The plunging periodic motion is shown in fig.62, where the chordwise mesh has been chosen with the criterion explained in [15].

Wings Properties	
Airfoil	Flat Plate
Æ	4 | 8 | 12 | 20
$b/2$	2 | 4 | 6 | 10 m
λ	1
c_{root}	1 m
Λ	$0°$
Γ	$0°$

Simulation Config.	
M	16
N	12 | 24
Motion	See fig.47
α	$5°$
U	1 m/s
τ_{fin}	10
Wake Model	Vortex Rings - Roll-up | Vortons - Roll-up
σ	$2Q_{\infty}\Delta t$

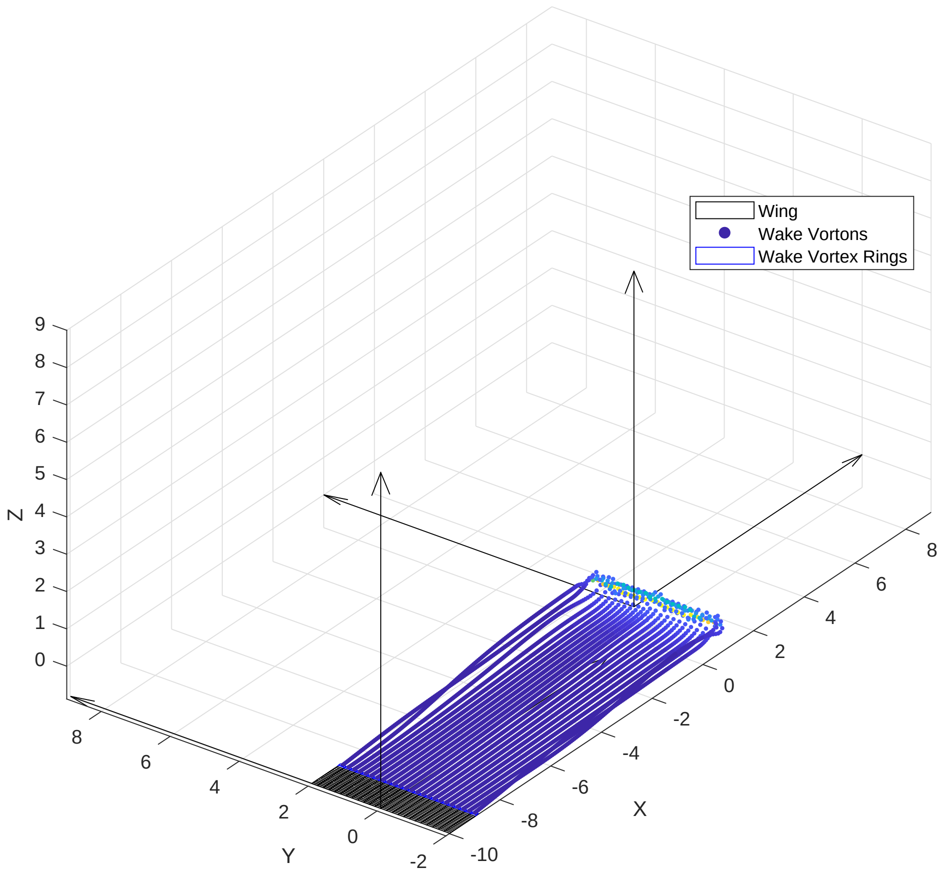

Figure 59: 3-D view of a rectangular wing with Æ = 4 undergoing sudden acceleration, vortons wake model (*Matlab*)

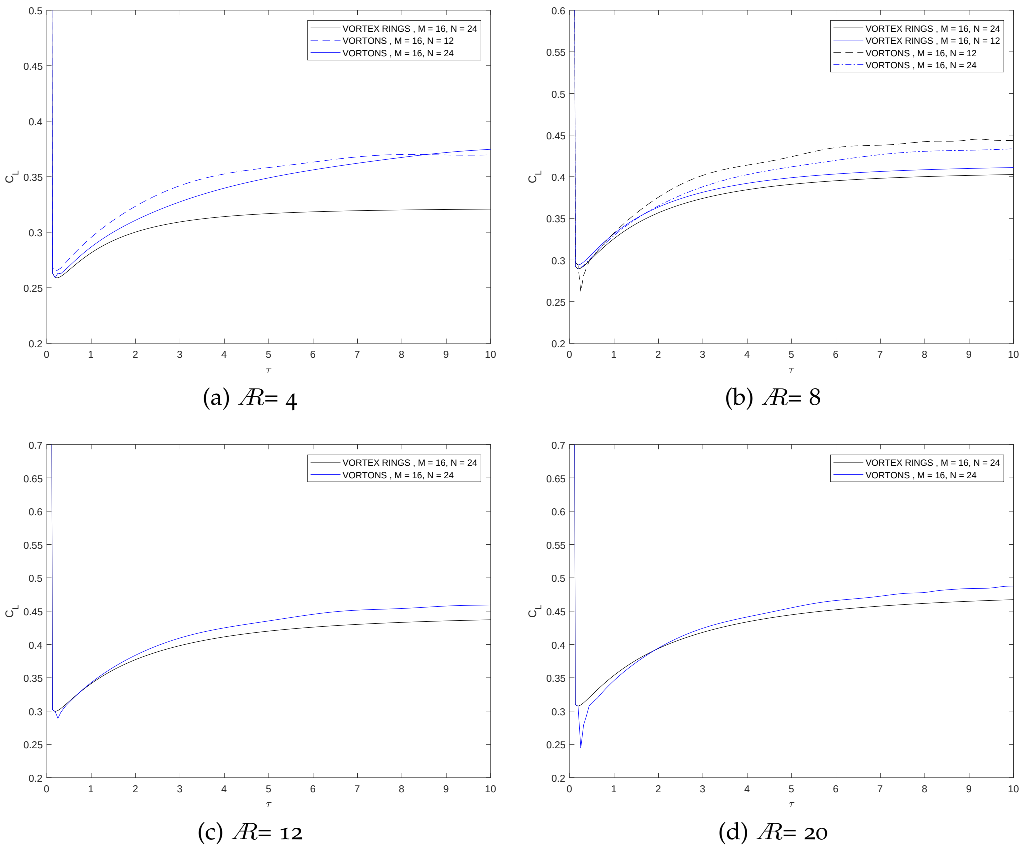

(a) Æ= 4 (b) Æ= 8

(c) Æ= 12 (d) Æ= 20

Figure 60: Lift coefficient generated by the UVLM for a sudden acceleration, and comparison with [9] (*Matlab*)

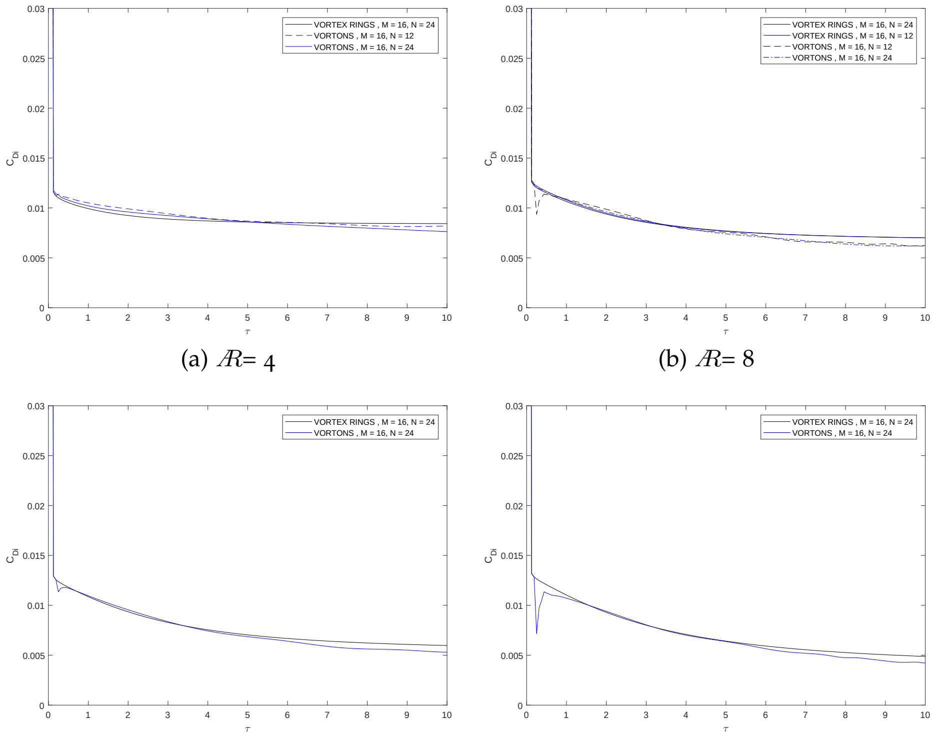

(a) Æ= 4

(b) Æ= 8

(c) Æ= 12

(d) Æ= 20

Figure 61: Drag coefficient generated by the UVLM for a sudden acceleration, and comparison with [9] (*Matlab*)

Wings Properties	
Airfoil	Flat Plate
$\mathcal{R}$	100
λ	1
$b/2$	50 m
c_{root}	1 m
Λ	$0°$
Γ	$0°$

Simulation Configurations	
M	See fig.62
N	48
Motion	Periodic Motion
U	1 m/s
$h(t)$	$-0.1\sin(\omega t)$ m
k	0.25 | 0.50 | 0.75
t_{fin}	2 T
Wake Model	Vortons - No Roll-up

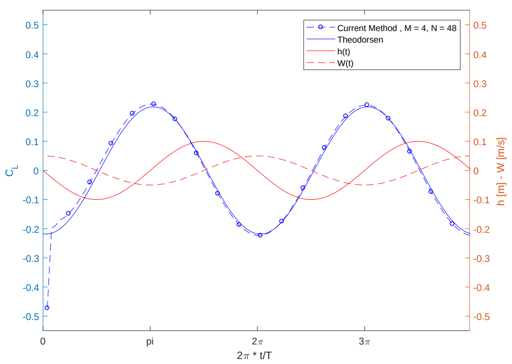

(a) k = 0.25

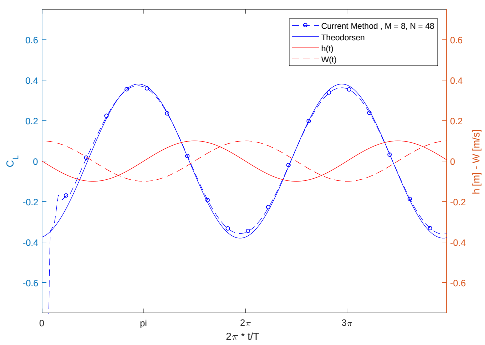

(b) k = 0.50

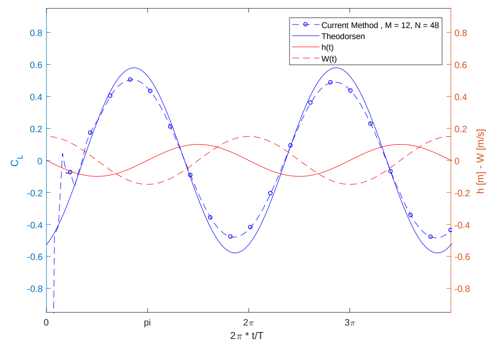

(c) k = 0.75

Figure 62: $C_L - 2\pi\frac{t}{T}$ curves generated by the UVLM for a periodic motion, and comparison with results of Theodorsen theory's results (*Matlab*)

3.10 CONCLUSIONS

As shown in this chapter the current method tries to avoid the phyisical inconsistency of the arbitrary constant used in some methods for the wake vortex-rings shedding while obtaining encouraging results for the evaluation of lift and drag of lifting surfaces undergoing unsteady motion. The validation test-cases carried out in this thesis have shown good agreement with analytical and numerical results available in the literature, and both vortex-rings and vortons can be used as a wake-model.

When the current method is employed it should be reminded that particular attention must be given to the following parameters

- The discretization of the wing, in terms of chord-wise and span-wise ($M \times N$) mesh influences the quality of the results, in particular the chord-wise panels are related to the time-step of the simulation and, as a consequence of it, to the capability of catching the unsteadiness of the phenomena.
- A thicker span-wise discretization is needed when the wake model is made by vortons, as the vortons represent the vorticity in the wake in a somehow different way from vortex-rings.

Nonetheless this newly developed method is a fast and reliable tool for preliminary design of lifting surfaces.

3.11 FUTURE DEVELOPMENTS

Being built on a modular set of *Matlab* scripts and functions, the current method could well represent a starting point for different applications or integrations. Some of them are listed below

- Unsteady asymmetrical motion can be accounted for with a loss on the speed of the simulations.
- A script or function can be included to evaluate moments.
- Fluid-structure interaction integrated tools can be built using the current method for the evaluation of forces on the surfaces.
- The aerodynamic analysis can be extended to other lifting surfaces in the domain to account for multi-body fluid interaction.

a

APPENDIX A : INPUT FILES FORMATS

A.1 AIRFOIL GEOMETRY INPUT FILE

An example of how the input airfoil file must be written is given below:

```
1.0000     0.0013
0.9500     0.0114
0.9000     0.0208
0.8000     0.0375
0.7000     0.0518
0.6000     0.0636
0.5000     0.0724
0.4000     0.0780
0.3000     0.0788
0.2500     0.0767
0.2000     0.0726
0.1500     0.0661
0.1000     0.0563
0.0750     0.0496
0.0500     0.0413
0.0250     0.0299
0.0125     0.0215
0.0000     0.0000
0.0125     -0.0165
0.0250     -0.0227
0.0500     -0.0301
0.0750     -0.0346
0.1000     -0.0375
0.1500     -0.0410
0.2000     -0.0423
0.2500     -0.0422
0.3000     -0.0412
0.4000     -0.0380
0.5000     -0.0334
0.6000     -0.0276
0.7000     -0.0214
0.8000     -0.0150
0.9000     -0.0082
0.9500     -0.0048
1.0000     -0.0013
```

On the first column there are the X coordinates and on the second column there are the Y coordinates.
The file shows that the coordinates start from the trailing edge of the upper surface and end at the trailing edge of the lower surface. The upper surface matches the lower surface at the leading edge in the middle of the listing of coordinates.

A.2 WING GEOMETRY INPUT FILE

An example of how the input wing file must be written is given below:

```
% WING GEOMETRY INPUT DATA(N PARTS PER SEMI-SPAN) ,ALL MEASURES IN METRES AND DEGREES ,SPACE
     IS THE DIVIDER ,POINT IS THE DECIMAL SEPARATOR
% MIND THAT CHORD_OUT MUST BE EQUAL TO CHORD_IN WHEN THE PARTS ARE SUBSEQUENT
% MIND THAT TWIST_ANGLE_INNER MUST BE EQUAL TO TWIST_ANGLE_IN WHEN THE PARTS ARE SUBSEQUENT
% INNER-MOST PART DATA FIRST (NEAREST TO AXIS OF SIMMETRY) THEN OTHER PARTS DATA
```

SPAN_LENGTH	SWEEP_ANGLE	DIHEDRAL_ANGLE	TWIST_ANGLE_IN	TWIST_ANGLE_OUT	CHORD_IN	CHORD_OUT
6	20	0	0	0	4	2
3	30	0	0	0	2	1.5
1	20	45	0	0	1.5	1
1	0	85	0	0	1	1
3	0	180	0	0	1	1

BIBLIOGRAPHY

[1] Hiroshi Uchihori Akira Sakurai. "Unsteady Vortex Lattice Calculation of the Flow Around a Slender Delta Wing." Japan Aerospace Exploration Agency. 1990.

[2] John J. Bertin and Russell M. Cummings. *Aerodynamics for Engineers*. Ed. by Pearson Prentice-Hall. Pearson Education International, 2009.

[3] Paolo Caccavale. "Un Moderno Metodo a Potenziale per Analisi Fluidodinamiche." PhD thesis. Università di Napoli Federico II, Facoltà di Ingegneria, 2006.

[4] Gregory W. Reich Darrel K. Robertson James J. Joo. "Vortex Particle Aerodynamic Modelling of Perching Manoeuvres and with Micro and Air Vehicles." In: *51st AIAA/ASME/ASCE/AHS/ASC Structures, Structural Dynamics, and Materials Conference
 18th AIAA 2010-2825*. 2010.

[5] A. Leonard G.S. Winckelmans. "Contributions to Vortex Particle Methods for the Computation of Three-Dimensional Incompressible Unsteady Flows." In: *Journal of Computational Physics* 109 (1993), pp. 247–273.

[6] Jack A. Geoghegan. "Application of an Unsteady Vortex Lattice Method to Rotating Lifting Surfaces with One-Dimensional Aeroelastic Coupling." MA thesis. The University of Sidney, 2014.

[7] Henrik Hesse and Rafael Palacios. "Reduced-Order Aeroelastic Models for Dynamics of Maneuvering Flexible Aircraft." In: *AIAA Journal* 52.8 (2014), pp. 1717–1732. DOI: 10.2514/1.j052684.

[8] Yoshikazu Hirato, Minao Shen, Sachin Aggarwal, Ashok Gopalarathnam, and Jack R. Edwards. "Initiation of Leading-Edge-Vortex Formation on Finite Wings in Unsteady Flow." In: *53rd AIAA Aerospace Sciences Meeting*. American Institute of Aeronautics and Astronautics (AIAA), 2015. DOI: 10.2514/6.2015-0546.

[9] Allen Plotkin Joseph Katz. *Low-Speed Aerodynamics*. Ed. by Joseph Katz. Cambridge University Press, 2001.

[10] P. Konstandinopoulos, D. F. Thrasher, D. T. Mook, A. H. Nayfeh, and L. Watson. "A vortex-lattice method for general, unsteady aerodynamics." In: *Journal of Aircraft* 22.1 (1985), pp. 43–49. DOI: 10.2514/3.45078.

[11] Sidney Lebental. “Optimization of the Aerodynamics of Small-Scale Flapping Aircraft in Hover.” PhD thesis. Duke University, 2008.

[12] Lyle N. Long and Tracy E. Fritz. “Object-Oriented Unsteady Vortex Lattice Method for Flapping Flight.” In: *Journal of Aircraft* 41.6 (2004), pp. 1275–1290. DOI: 10.2514/1.7357.

[13] Domenico P. Coiro Agostino de Marco. *Elementi di Dinamica e SImulazione di Volo*. Università di Napoli Federico II, Dipartimento di Ingegneria Industriale. 2016.

[14] Tomas Melin. “A Vortex Lattice MATLAB and Implementation for Linear Aerodynamic Wing Applications.” MA thesis. Royal Institute of Technology (KTH), 2000.

[15] Joseba Murua. “Flexible Aircraft Dynamics with a Geometrically-Nonlinear Description of the Unsteady Aerodynamics.” PhD thesis. Imperial College London, 2012.

[16] NASA. *Vortex-Lattice Utilization SP-405*. Tech. rep. NASA Langley Research Center, 1976.

[17] Carlo de Nicola. *Appunti per un corso di Aerodinamica degli Aeromobili*. 2014-2015. Università degli Studi di Napoli "Federico II". 2014.

[18] Kiran Ramesh, Ashok Gopalarathnam, Kenneth Granlund, Michael V. Ol, and Jack R. Edwards. “Discrete-vortex method with novel shedding criterion for unsteady aerofoil flows with intermittent leading-edge vortex shedding.” In: *Journal of Fluid Mechanics* 751 (2014), pp. 500–538. DOI: 10.1017/jfm.2014.297.

[19] John E. Lamar Richard J. Margason. *Vortex-Lattice Fortran Program for Estimating Subsonic Aerodynamic Characteristics of Complex Planforms*. Tech. rep. Hampton, Va. 23365: NASA Langley Research Center, Feb. 1971.

[20] Bruno A. Roccia, Sergio Preidikman, Julio C. Massa, and Dean T. Mook. “Modified Unsteady Vortex-Lattice Method to Study Flapping Wings in Hover Flight.” In: *AIAA Journal* 51.11 (2013), pp. 2628–2642. DOI: 10.2514/1.j052262.

[21] Raffaele Savino Rodolfo Monti. *Aerodinamica*. Ed. by Liguori Editore. Liguori Editore, 1998.

[22] Robert J. S. Simpson, Rafael Palacios, and Joseba Murua. “Induced-Drag Calculations in the Unsteady Vortex Lattice Method.” In: *AIAA Journal* 51.7 (2013), pp. 1775–1779. DOI: 10.2514/1.j052136.

[23] Carlos de Souza, Roberto Gil da Silva, and Carlos Cesnik. "Nonlinear Aeroelastic Framework Based on Vortex-Lattice Method and Corotational Shell Finite Element." In: *53rd AIAA/ASME/ASCE/AHS/ASC Structures, Structural Dynamics and Materials Conference,20th AIAA/ASME/AHS Adaptive Structures Conference, 14th AIAA* (2012). DOI: 10.2514/6.2012-1976.